

Rodrigo Arredondo Parra

## **Operation, Commissioning and Installation of a High-Speed Lithium Pellet Injector in the ASDEX Upgrade Fusion Reactor**

**IPP 2017-06**  
**Oktober 2017**



NTech  
Lehrstuhl für  
Nukleartechnik

Technische Universität München 

## Master Thesis

from cand. Ing. Rodrigo Arredondo Parra  
Registration no. 03650701

# Operation, Commissioning and Installation of a High-Speed Lithium Pellet Injector in the ASDEX Up- grade Fusion Reactor

**Director TUM:** Prof. Dr. Rafael Macián-Juan

**Director IPP:** Prof. Dr. Rudolf Neu

**Issued:** 15.11.2014

**Submitted:** 15.05.2015

# Erklärung

Hiermit versichere ich, die vorliegende Arbeit selbstständig und ohne Hilfe Dritter angefertigt zu haben. Gedanken und Zitate, die ich aus fremden Quellen direkt oder indirekt übernommen habe, sind als solche kenntlich gemacht. Diese Arbeit hat in gleicher oder ähnlicher Form noch keiner Prüfungsbehörde vorgelegen und wurde bisher nicht veröffentlicht.

Ich erkläre mich damit einverstanden, dass die Arbeit durch den Lehrstuhl für Nukleartechnik der Öffentlichkeit zugänglich gemacht werden kann.

München, den 15. Mai, 2015

Rodrigo Arredondo Parra

# Acknowledgments

I would first like to thank my friends and family for their support, and for bearing with me these past few months as I rambled on about plasmas. This applies doubly to my girlfriend Carolin, my first proofreader, who's had to move or cancel her plans because of me more than once and more than twice. It's a wonder how she puts up with me at times.

A thesis is not only about producing something of worth, it's about learning, and there's a great deal I've learned. On that note I'd like to thank Prof. Cardella for introducing me to the world of nuclear fusion, Prof. Neu, my director at the Max Planck and Prof. Macián, my director at the TUM. There are always stories about thesis directors giving their students a hard time. Both of mine were as far from this image as one can possibly be.

From the university I would also like to thank Frau Franke for her help and kind support, and from the IPP, the many who have helped me along the way. This applies especially to the members of my work group: Michael Beck and Wolfgang Weisbart for their assistance and jokes. Mathias Dibon for all the questions and input in our office. Of course Bernhard Plöck and Peter Lang for their patience, their explanations and their insight. Lastly, I can't forget my friend and colleague Rubén Moreno Quicios, who went above and beyond the call of duty in his internship. His priority was always to help me, it wouldn't be fair to say that this project isn't a little bit his as well.

Quite a few invitations from my friends have gone unanswered these past few months. For that I wish to apologize. I was working on something, a machine. The next few pages can explain it better. There are pictures.



# Abstract

Operation, Commissioning and Installation of a High-Speed Lithium Pellet Injector in the ASDEX Upgrade Fusion Reactor

Encouraging results with respect to plasma performance have been observed earlier in several tokamak devices (TFTR, NSTX, etc) when injecting Lithium. Recently, a pedestal broadening resulting in an enhanced energy content during transient ELM-free H-mode phases was achieved in DIII-D. Experiments are also planned at ASDEX Upgrade, aiming to investigate the impact of Li in an all-metal wall tokamak and attempting to enhance the pedestal operational space. For this purpose, a Lithium pellet injector has been developed, capable of injecting pellets carrying a particle content ranging from  $1.82 \cdot 10^{19}$  atoms (0.21 mg) to  $1.64 \cdot 10^{20}$  atoms (1.89 mg). The maximum repetition rate is about 2Hz. Free flight launch from the torus outboard side without a guiding tube is envisaged. In such a configuration angular dispersion and speed scatter are low, and a transfer efficiency exceeding 90 % was achieved in the test bed. Pellets will be accelerated in a gas gun; hence special care must be taken to avoid deleterious effects by the propellant gas pulse. Therefore, the main plasma gas species must be applied as propellant gas, leading to speeds ranging from  $420 \text{ m/s}$  to  $700 \text{ m/s}$ . In order to minimize the residual amount of gas to be introduced into the plasma vessel, a large expansion volume equipped with a cryopump is added in to the flight path. In view of the planned experiments, an optimal propellant gas pressure of 50 bar was chosen for operation, since at this pressure maximum efficiency and low propellant gas flux coincide. This leads to pellet speeds of  $585 \text{ m/s} \pm 32 \text{ m/s}$ .

Currently, the injector is under commissioning in a test bed expected to be installed and operational at ASDEX Upgrade by the end of May 2015.

# Kurzfassung

Aufbau, Konditionierung und Betrieb eines Hochgeschwindigkeits Lithiuminjektors für das Plasmaexperiment ASDEX Upgrade

In verschiedenen Fusionsexperimenten (TFTR, NSTX, DIII-D, EAST usw.) wurden ermutigende Ergebnisse in Bezug auf die Plasmaeigenschaften durch die der Injektion von Lithium (Li) beobachtet. Dabei wurde zum Beispiel in DIII-D und NSTX eine Verbreiterung der Rand-Transportbarriere beobachtet die zu einem verbesserten Energieeinschluss während transienter ELM-freier H-Mode Phasen führt. Während der Kampagne 2015/16 sind nun auch am Plasmaexperiment ASDEX Upgrade Versuche mit Li im Plasma geplant. Deren Ziel ist es, die Wirkung von Li in einem Tokamak mit einer vollständigen Metallwand zu untersuchen mit dem Ziel, auch hier einen verbesserten Energieeinschluss zu erzielen. Zu diesem Zweck wurde ein Li-Pellet Injektor entwickelt mit dem es möglich ist Pellets mit einem Teilcheninhalt von  $1.82 \cdot 10^{19}$  Atomen (0.21 mg) bis  $1.64 \cdot 10^{20}$  Atomen (1.89 mg) in das Plasma einzuschiessen. Die bislang erzielte maximale Repetitionsrate beträgt dabei 2 Hz. Der Einschuss wird direkt ohne Führungsrohr von der Torusaussenseite her erfolgen. In dieser Konfiguration gelingt es, Winkel- und Geschwindigkeitsstreuung der Pellets gering zu halten. Im Labor-Testbetrieb konnten Transfereffizienten von mehr als 90% erreicht werden. Die Pellets werden durch einen Treibgaspuls beschleunigt. Um einen möglichen negativen Einfluss dieses Treibgaspulses auf das Plasma zu minimieren, mussten besondere vakuumtechnische Vorkehrungen getroffen werden. So wurden ein grosses Expansionsgefäß und eine Kryopumpe in das System integriert. Auch

kann nur die hauptsächliche Plasmakomponente Deuterium (D) als Treibgas verwendet werden, was verschiedene sicherheitstechnische Vorkehrungen nötig machte. Durch die Verwendung von D erreicht man Einschussgeschwindigkeiten von  $420 \text{ m/s}$  bis  $700 \text{ m/s}$ . Das gesamte Injektionssystem wurde in Labortests konditioniert und charakterisiert. Für den Einsatz wurde als optimaler Treibgasdruck 50 bar gewählt, da hier maximale Effizienz bei geringender Treibgaslast korrelieren. Die entsprechende Pelletgeschwindigkeit trägt  $585 \text{ m/s} \pm 32 \text{ m/s}$ . Gegenwärtig wird das System an ASDEX Upgrade angebaut und in das Kontroll- und Sicherheitssystem integriert. Voraussichtlich wird es Ende Mai 2015 betriebsbereit installiert sein und bereits für Experimente am unmittelbaren Beginn der Experimentkampagne zur Verfügung stehen.

# Contents

<b>Erklärung</b>	<b>ii</b>
<b>Acknowledgments</b>	<b>iii</b>
<b>Abstract</b>	<b>iv</b>
<b>Kurzfassung</b>	<b>vi</b>
<b>Table of Contents</b>	<b>xi</b>
<b>List of Figures</b>	<b>xiv</b>
<b>List of Tables</b>	<b>xvi</b>
<b>1 Introduction</b>	<b>1</b>
1.1 Current and future global energy demand . . . . .	1
1.2 Environmental advantages of nuclear fusion . . . . .	2
1.3 Current research on nuclear fusion reactors . . . . .	6
1.4 Lithium injection at ASDEX Upgrade . . . . .	9
<b>2 Theoretical principles</b>	<b>11</b>
2.1 What is a plasma? . . . . .	11
2.2 Nuclear fusion reactions . . . . .	12
2.3 The Lawson criterion . . . . .	13

2.4	Magnetic confinement . . . . .	16
2.4.1	Introduction to magnetic confinement . . . . .	16
2.4.2	Toroidal magnetic confinement . . . . .	16
2.4.3	Tokamak design . . . . .	17
2.4.4	H-mode . . . . .	17
2.4.5	ELMs . . . . .	19
2.5	The effect of Lithium in other tokamaks . . . . .	19
2.6	Important pellet parameters . . . . .	20
2.7	Gas pulse pellet injection . . . . .	21
2.8	Propellant gas flux . . . . .	23
<b>3</b>	<b>Experimental set-up</b>	<b>25</b>
3.1	Working principle of the lithium injector . . . . .	25
3.1.1	Mechanical operation . . . . .	25
3.1.2	Gas injection system and pneumatics . . . . .	27
3.1.3	Electronic firing mechanism . . . . .	31
3.2	Experimental test bed set-up . . . . .	32
3.2.1	Equivalent expansion volume . . . . .	32
3.2.2	Required vacuum pumps and valves . . . . .	34
3.2.3	Support structure . . . . .	35
3.2.4	Lithium manipulation & extrusion . . . . .	37
3.2.5	Design of the lithium injector characterization tests . . . . .	38
3.2.5.1	Angular scatter measurements . . . . .	38
3.2.5.2	Pellet speed and speed scatter measurements . . . . .	39
3.2.5.3	Pellet transfer rate measurements . . . . .	43
3.2.5.4	Propellant gas flux measurements . . . . .	44
3.3	Design of the lithium injector installation in ASDEX Upgrade . . . . .	46
3.3.1	Commissioning of the CAD models . . . . .	46

3.3.1.1	Expansion vessel . . . . .	46
3.3.1.2	Shielding tube . . . . .	48
3.3.1.3	Required vacuum pumps and valves . . . . .	49
3.3.1.4	Standardized connection parts and support structure . . . . .	50
3.3.2	Pressurized gas and cooling water lines . . . . .	51
3.3.3	Remote control electronics . . . . .	52
<b>4</b>	<b>Experimental procedure</b>	<b>55</b>
4.1	Pellet transfer rate . . . . .	55
4.2	Angular scatter . . . . .	55
4.3	Pellet speed and speed scatter . . . . .	56
4.4	Propellant gas flux . . . . .	57
4.5	Replacement fast valve characterization . . . . .	59
<b>5</b>	<b>Evaluation of the experimental results</b>	<b>60</b>
5.1	Pellet transfer rate tests . . . . .	60
5.2	Angular scatter measurements . . . . .	61
5.3	Pellet speed and speed scatter measurements . . . . .	62
5.4	Propellant gas flux measurements . . . . .	63
5.4.1	Expansion volume . . . . .	64
5.4.2	Vacuum tank . . . . .	65
5.5	Replacement fast valve characterization tests . . . . .	66
5.5.1	Amount of gas . . . . .	66
5.5.2	Gas evacuation time . . . . .	67
<b>6</b>	<b>Conclusion</b>	<b>69</b>
<b>A</b>	<b>Test results</b>	<b>71</b>
A.1	Propellant gas flux tests . . . . .	71

A.2	Replacement fast valve characterization tests . . . . .	73
A.3	Transfer rate . . . . .	75
A.4	Angular scatter . . . . .	75
A.5	Speed and speed scatter . . . . .	75
<b>B</b>	<b>Calculation of uncertainty</b>	<b>76</b>
B.1	Angular scatter . . . . .	76
B.2	Pellet speed . . . . .	77
<b>C</b>	<b>Lithium loading procedure</b>	<b>79</b>
<b>D</b>	<b>Vacuum</b>	<b>82</b>
D.1	Vacuum system at ASDEX Upgrade . . . . .	82
D.2	pump specifications . . . . .	84
<b>E</b>	<b>Lithium injector drafts</b>	<b>86</b>
E.1	Injector . . . . .	86
E.2	Pneumatics . . . . .	86
E.3	Diagnostics . . . . .	86
E.4	Extrusion . . . . .	86
<b>F</b>	<b>Electronics</b>	<b>94</b>
F.1	Fast valve trigger sequence . . . . .	94
F.2	Lithium Injector SIMATIC control system . . . . .	96
F.3	Light barrier electronics . . . . .	111



# List of Figures

1.1	EIA World energy consumption forecast . . . . .	2
1.2	EIA world energy-related CO <sub>2</sub> yearly emissions forecast[UEIA11]	3
1.3	Comparison of fission- and fusion-generated nuclear waste activities and decays[MPIfP] . . . . .	4
1.4	Computer model of ITER. Source: [ITE14d] . . . . .	8
1.5	Inside view of the ASDEX Upgrade tokamak [Upg14] . . . . .	9
2.1	Binding energy per nucleon, weighed by atomic mass number [Gar14] . . . . .	13
2.2	Triple product and temperature of fusion reactors and power plant conditions [fP14] . . . . .	15
2.3	Helical field lines and tokamak design [MPIfP] . . . . .	18
2.4	Sketch of H-mode profile and pedestal . . . . .	18
3.1	Lithium injector revolver plate [Ale11] . . . . .	26
3.2	Lateral cut of the lithium injector [Ale11] . . . . .	26
3.3	3D model of the lithium injector [Ale11] . . . . .	27
3.4	Propellant gas injection system . . . . .	28
3.5	Swangelok Nupro SS-HBS6-C shut-off valve [www.swangelok.com] . . . . .	28
3.6	Power source output and valve opening of a five pellet firing sequence at 2 Hz . . . . .	29

3.7	Lithium injector test bed . . . . .	33
3.8	Standardized bars of length 250, 353, 500, 707 and 1000 <i>mm</i> and MERO ball [Ale11] . . . . .	36
3.9	Complete vacuum system support structure . . . . .	36
3.10	Lithium extruder and extrusion nozzles. . . . .	38
3.11	Lithium pellet catching box design . . . . .	39
3.12	Catching box with paper for angular scatter measurement and catching box position inside the vacuum system . . . . .	40
3.13	Light barrier structure [Ale11] . . . . .	41
3.14	Light barrier arrays. Left: first diode chamber. Right: Second diode chamber [Ale11] . . . . .	42
3.15	Light barrier electronic box . . . . .	42
3.16	Oscilloscope readout of pellet flight . . . . .	43
3.17	Complete injector and vacuum system test bed, showing the position of both pressure gauges . . . . .	45
3.18	Space limitations in the S16 Bo port . . . . .	47
3.19	View of the central expansion vessel . . . . .	48
3.20	Lithium pellet flight dispersion cone and shielding tube . . . . .	49
3.21	Lithium pellet injector installation in ASDEX Upgrade . . . . .	51
3.22	Shielding tube support structure . . . . .	52
3.23	Visual representation of the lithium injector with the WINCC control program . . . . .	54
4.1	Nylon aperture . . . . .	58
5.1	Pellet transfer rates with propellant gas pressure . . . . .	61
5.2	Pellet scattering angle with propellant gas pressure . . . . .	62
5.3	Pellet flight speed and speed scatter with propellant gas pres- sure . . . . .	63

5.4	Peak amount of gas in the lithium injector expansion volume with pressure . . . . .	64
5.5	In tank amount of gas with pressure . . . . .	65
5.6	Expansion tank gas with pressure . . . . .	67
5.7	Gas evacuation time with pressure . . . . .	68
E.1	Lithium injector barrel draft [MPIfP] . . . . .	87
E.2	Lithium injector revolver plate draft [MPIfP] . . . . .	88
E.3	Lithium injector pneumatic system . . . . .	89
E.4	Lithium pellet catching box draft . . . . .	90
E.5	Lithium injector extruder, $\phi$ 6 mm to $\phi$ 2.5 mm . . . . .	91
E.6	Lithium injector extruder, $\phi$ 2.5 mm to $\phi$ 1.5 mm . . . . .	92
E.7	Lithium injector extrusion nozzles, $\phi$ 1.5 mm to $\phi$ 0.4 mm . . . .	93

# List of Tables

2.1	Available pellet sizes . . . . .	20
4.1	Resistance and operating voltage of the fast valves . . . . .	59
A.1	Propellant gas flux results for the “Normal” scenario . . . . .	71
A.2	Propellant gas flux results for the “Aperture” scenario . . . . .	72
A.3	Propellant gas flux results for the “Cryopump” scenario . . . . .	72
A.4	Propellant gas flux results for the “Aperture + Cryopump” scenario . . . . .	72
A.5	Propellant gas flux results for the “Previously” scenario . . . . .	73
A.6	Results for the fast valve currently in use . . . . .	73
A.7	Results for the replacement valve A . . . . .	73
A.8	Results for the replacement valve B . . . . .	73
A.9	Transfer rate results . . . . .	74
A.10	Angular scatter results . . . . .	74
A.11	Speed and speed scatter results . . . . .	75
B.1	Angular scatter uncertainty . . . . .	77
B.2	Pellet speed uncertainty . . . . .	78
D.1	Specifications of the Leybold Trivac D30A vacuum pump [Vac]	85
D.2	Specifications of the Leybold Turbovac 360 turbopump [Vac04]	85

D.3 Specifications of the Cryo-Torr 8 cryopump [CC] . . . . .	85
---	----

# Chapter 1

## Introduction

### 1.1 Current and future global energy demand

There is consensus among both industry and the scientific community that finding an adequate and sustainable mid- and long-term energy plan is one of the key challenges of the 21st century. This complex issue is strongly tied to matters of economic and population growth, and of course to important environmental issues, such as climate change. Global energy demand is steadily on the rise, a trend expected to continue especially in non-OECD countries (see fig. 1.1), where fossil fuels are the most common energy source.[UEIA11, G<sup>+</sup>06]

This in turn leads to a rise in CO<sub>2</sub> emissions, the leading greenhouse gas, as seen in fig. 1.2[UEIA11, G<sup>+</sup>06]

Within this context, if the imperative to reduce carbon dioxide emissions is to be addressed, it is clear that CO<sub>2</sub>-free energy sources<sup>1</sup> must be widely used. The two currently employed options are nuclear fission energy and renewable energies. However, nuclear fusion provides a number of key advantages to both of these, which would make it an ideal energy source.

---

<sup>1</sup>Denoting CO<sub>2</sub>-free energy sources as those that do not incur in CO<sub>2</sub> emissions during energy production, or are considered CO<sub>2</sub> neutral

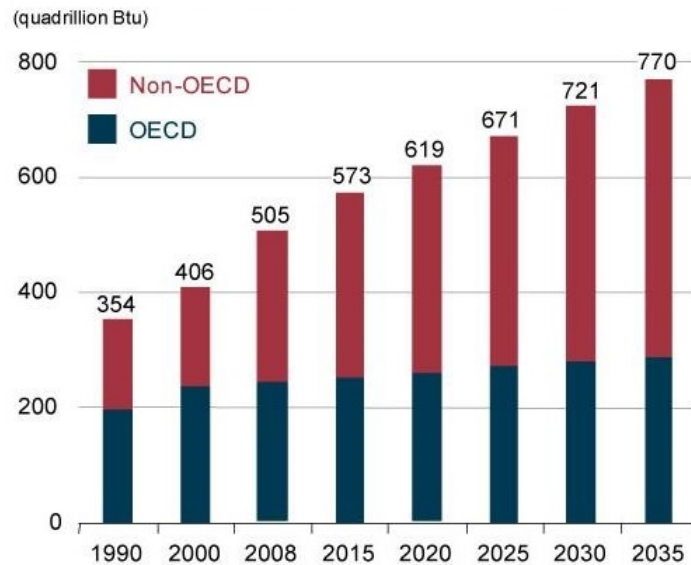


**Figure 1.1:** EIA World energy consumption forecast. Units given in BTu (British Thermal unit.  $1 \text{ BTu} \approx 1055 \text{ J}$ ) [UEIA11]

## 1.2 Environmental advantages of nuclear fusion

Nuclear fission is well established as a  $\text{CO}_2$ -free, very high capacity factor energy source, accounting for 13% of electricity production in 2012 [Age12]. It is currently growing, notably with China set to triple its output over the following six years, reaching 58 GWe by 2020 [WNN14]. Furthermore, total economically recoverable fuel supplies are believed to last 670 years with present reactor technology, according to the OECD and NEA. Breeder and fast reactor technology would in turn push this figure up to 160,000 years[AA12].

However, nuclear fission is also the cause of a series of public concerns. The chief among these is the generation of long-lived nuclear waste, which poses problems both for post-use waste management and storage, and for accident situations. Although nuclear fusion also produces nuclear waste, originating primarily from structural materials activation by high-energy neutrons, these

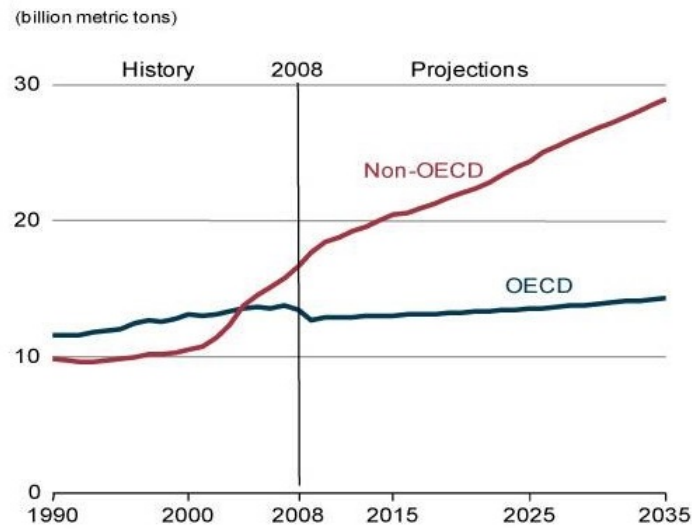


**Figure 1.2:** EIA world energy-related CO<sub>2</sub> yearly emissions forecast[UEIA11]

are much lower in total volume and activity, decaying within 100 years to activity levels allowing for recycling and re-utilization, with 30-40% reaching free-release limits within 50 years [IPP14]. In comparison, nuclear fission produces more waste both in volume and activity, with decay times to admissible levels in the range of tens of thousands of years [Bod06], as seen in fig. 1.3, where coal ash refers to the non-combustible residue of coal burnt in commercial power plants.

Moreover, fusion is also deemed highly resistant to nuclear proliferation attempts, since all efforts to harness either tritium or the strong fast neutron flux to breed weapons grade fuels would prove either easily detectable or easily preventable through adequate detection measures [GGR13].

Thirdly, another major concern with nuclear fission is the potentially catastrophic consequences of a severe accident, as occurred in Chernobyl in 1986 or in Fukushima Daiichi in 2011. This problem is in a possible fusion power plant in practice non-existent, or in a worst-case scenario severely limited, since given the nature of a controlled nuclear fusion reaction, temperature, pressure and magnetic field must be precisely controlled for the reaction to



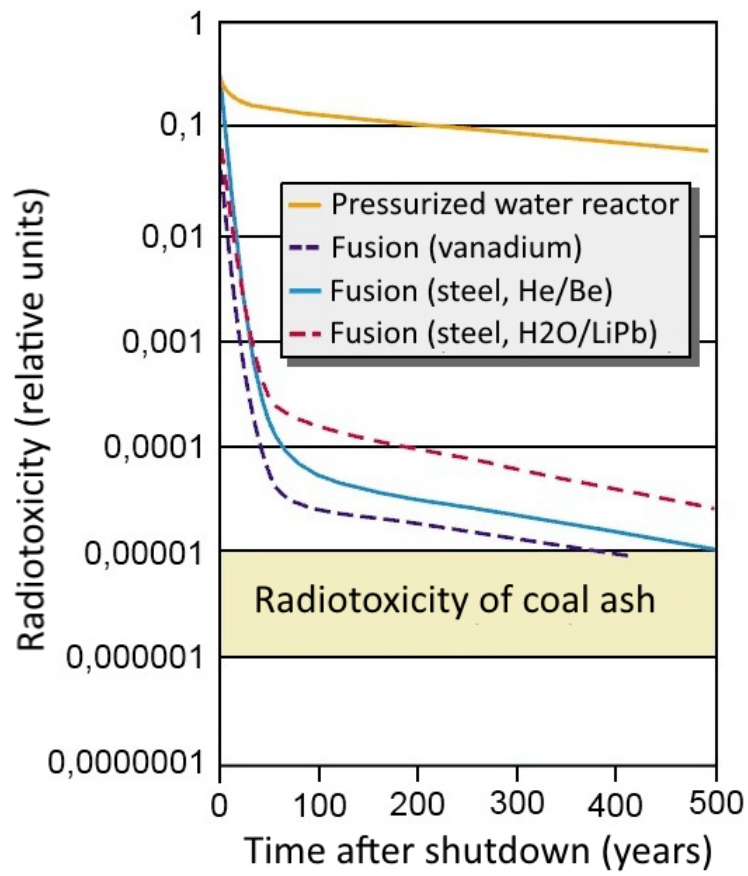


**Figure 1.3:** Comparison of fission- and fusion-generated nuclear waste activities and decays[MPIfP]

take place and produce a net energy gain. Any disruption of these parameters would effectively terminate the reaction, unlike in a fission power plant, where the reaction can continue to be self-sustained without any exterior intervention. Additionally, the fuel present at any given time within the fusion reactor is burnt up within seconds and amounts to a very low energy content, in comparison to a fission reactor, which typically contains at any given time enough fuel to power the reaction for several months. Lastly, fusion reactors do not suffer from significant decay heat, as is the case in fission reactors, which continue to generate heat for months after shutdown from beta-decay.[MS12, Dul09]

Renewable energies produce very little greenhouse gas emissions during their lifetimes, and are expected to grow strongly in the following years, especially in OECD countries [UEIA11]. However, those with most room for growth (solar and wind power) are dependent on the weather for their energy output, making their widespread use for base load supply a challenge [Age07]. This would prove an important advantage for nuclear fusion energy, not as a competitor, but as complementary to renewable energy, since the nuclear fusion process would make it best suited for base load power supply.

Lastly, deuterium<sup>2</sup> in seawater is estimated to last for billions of years. Lithium, which is projected to be used in the tritium<sup>3</sup> breeding process, is estimated to last for 3000 years from known reserves, and would last for millions of years if it were extracted from seawater [AMBF10, OVO00]. This would make nuclear fusion a practically limitless energy source, proving a sustainable long-term solution, especially in comparison to fossil fuels, whose resources are estimated to last for another 40 years in the case of oil, 70 for natural gas, and 200 years for coal. [S<sup>+</sup>09]

---

<sup>2</sup>An isotope of hydrogen, consisting of one proton and one neutron, and nuclear fusion's main fuel

<sup>3</sup>Another isotope of hydrogen, consisting of one proton and two neutrons

## 1.3 Current research on nuclear fusion reactors

Nuclear fusion research for energy production has been ongoing since the 1940s, with the first patent for a nuclear fusion device being published in 1946 in the UK [TB46]. Since then, different fusion principles and devices have developed, with two main concepts dominating within the fusion community: inertial confinement and magnetic confinement.

Inertial confinement consists on compressing and heating the fuel via an imploding shell. Compression ratios of the order of 30 times its solid density must be produced. This can be achieved either through laser blasts hitting the target directly (direct drive) or through these laser blasts hitting a structure, known as *hohlraum*, which in turn emits x-ray radiation capable of compressing the fuel more uniformly than through direct drive. This second process is known as indirect drive [Pfa06].

Inertial confinement has been predominantly developed in the U.S.A., tied in part to nuclear weapons research. The largest device in this field is the National Ignition Facility (NIF), at the Lawrence Livermore National Laboratory in Livermore, California [Lab14].

Magnetic confinement is based on having the fuel in the form of a plasma<sup>4</sup>. The plasma is heated to fusion conditions and magnets are used to create strong magnetic fields. Due to the single particles of the plasma being charged, they will move following the magnetic field lines, thereby being confined by them and not impacting on the walls of the device, which would terminate the plasma discharge, as well as damage the device.

Within magnetic confinement, the most advanced concept is known as toroidal magnetic confinement, where the magnetic field lines are arranged in the shape of a torus, thereby closing on themselves. This concept has been

---

<sup>4</sup>Plasma is a state of matter in which atoms in a gas-like state have been fully or partly ionized, so that nuclei and electrons are moving freely. As a result, plasmas are electric conductors

most developed in devices known as tokamaks, with the second most advanced devices being the stellarators. Toroidal magnetic confinement is the main fusion research focus in Europe, with devices such as JET<sup>5</sup> in the U.K. or ASDEX<sup>6</sup> Upgrade in Germany; though research is also being performed in North America and Asia with devices such as DIII-D, JT-60, EAST or KSTAR [lis14].

The next step in tokamak research is ITER in France (seen in fig. 1.4), a multinational project which aims to be the first nuclear fusion reactor capable of achieving a substantial power amplification of 10, reaching a fusion power of 500 MW in 1000 second pulses, with plasma experiments planned to start in 2020 [ITE14a, ITE14c].

Most current experiments are now operating in what is known as H-mode<sup>7</sup>. In this operational regime, discovered in the ASDEX tokamak in 1982, additional heating leads to drastically improved confinement, and H-mode is considered crucial for commercial fusion power [ITE14b]. However, plasma edge instabilities known as ELMs<sup>8</sup> appear in H-mode plasmas, and can prove hazardous both to plasma operation and overall integrity of the plasma facing components. ELM suppression or mitigation is for that reason a currently active field of research [ITE14e].

Introduction of lithium into the plasma has shown strongly enhanced plasma confinement parameters and has delayed the onset and diminished the frequency of ELMs in various reactors, such as DIII-D, NSTX<sup>9</sup> or EAST<sup>10</sup> [J<sup>+</sup>14].

---

<sup>5</sup>Joint European Torus

<sup>6</sup>Axial Symmetric Divertor Experiment

<sup>7</sup>Short for High-confinement mode

<sup>8</sup>Short for Edge Localized Modes

<sup>9</sup>National Spherical Torus Experiment in the Princeton Plasma Physics Laboratory

<sup>10</sup>Experimental Advanced Superconducting Tokamak in Hefei, China

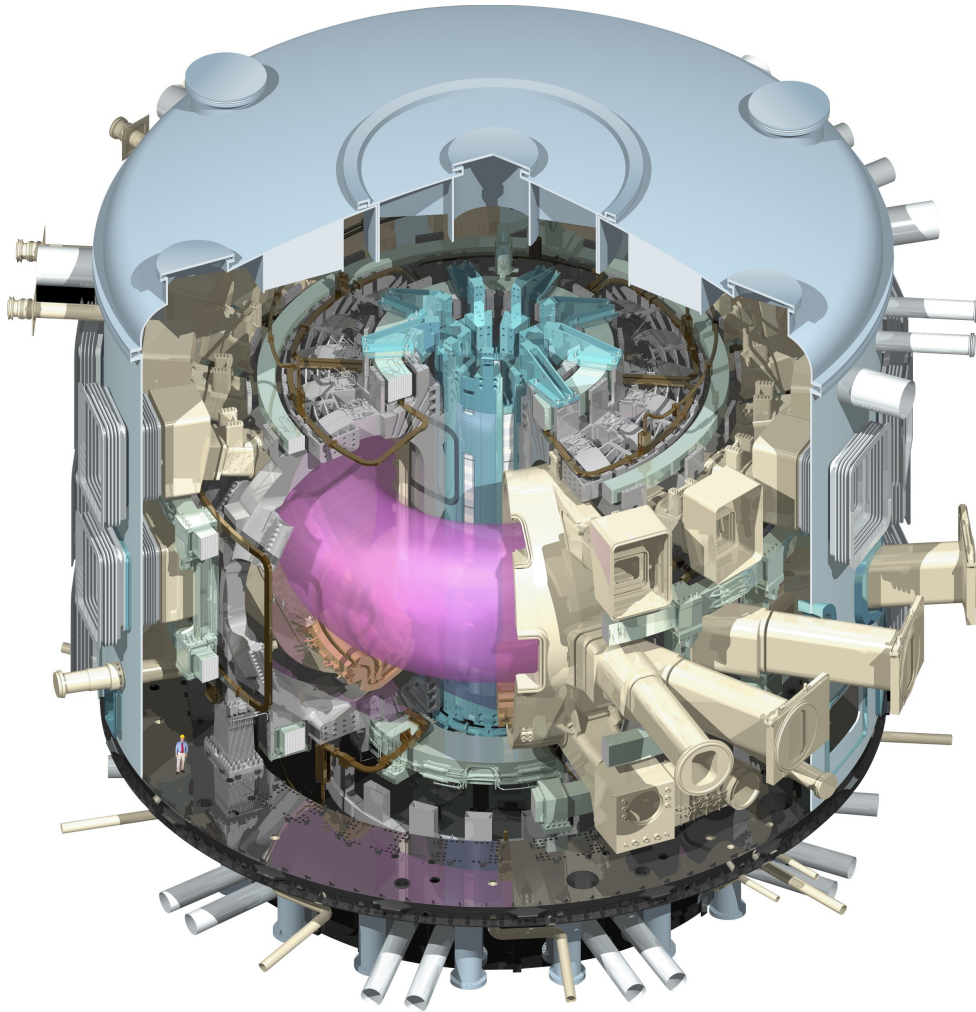


**Figure 1.4:** Computer model of ITER. Source: [ITE14d]

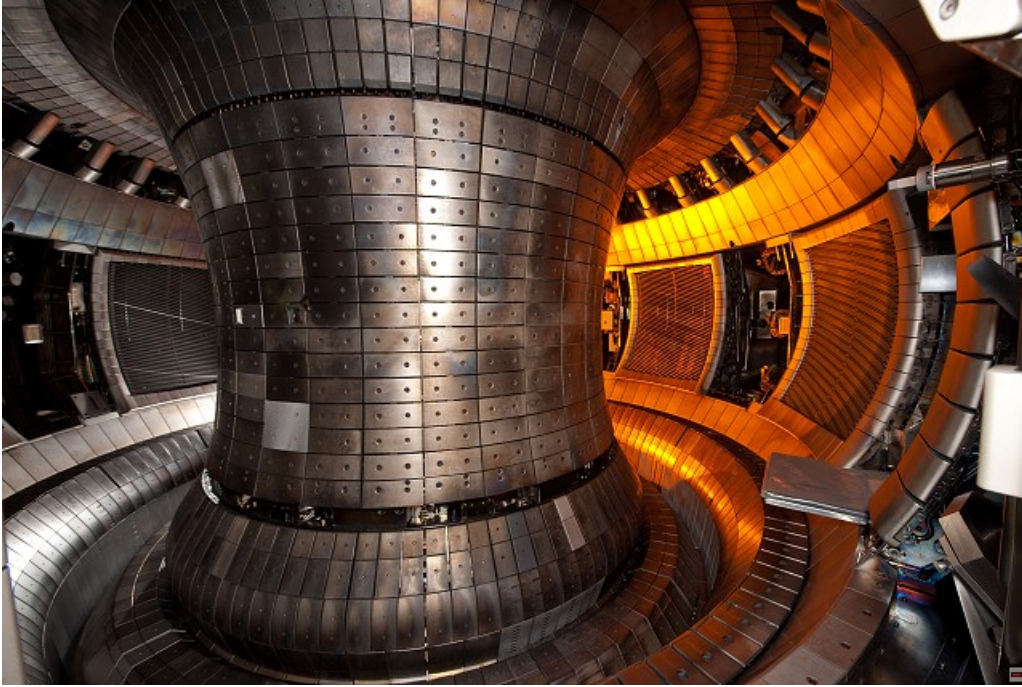


**Figure 1.5:** Inside view of the ASDEX Upgrade tokamak [Upg14]

## 1.4 Lithium injection at ASDEX Upgrade

The Max Planck IPP's<sup>11</sup> tokamak ASDEX Upgrade (fig. 1.5), located in Garching bei München is currently the only reactor with an all-tungsten wall. As already shown, lithium holds promise for improving operation in tokamak devices [J<sup>+</sup>14], and so holds special relevance for ITER-like scenarios. However, it has up to date never been tested on ITER-like walls. Since it has been shown that lithium doping affects plasma wall interaction parameters, it is of direct interest to investigate the effect of lithium in an all-tungsten wall reactor.

The ASDEX Upgrade team designed and built a room temperature solid pellet injector for use with lithium, which was extensively tested and characterized by Christoph Münther in his Diploma<sup>12</sup> thesis in 2001 [Mün01]. Ultimately, the device was not used for research into the plasma, and was shelved

---

<sup>11</sup>MPI für Plasmaphysik

<sup>12</sup>Equivalent to a present Master's degree

for ten years. In 2011 and 2012 Athanasios Alexiou and Chengis Demirtas characterized the pellet injector for use with other materials and studied the gas outflow rates in their bachelor theses, respectively [Ale11, Dem12].

The injector is capable of propelling pellets of up to 2 mg in weight at high speeds into the plasma, with high transfer efficiencies and low speed and angular scatter. A pressurized gas is used to propel the pellet, with special care being taken to ensure that the lowest achievable amount of gas enters the plasma chamber.

The machine is now planned for use in lithium injection testing at ASDEX Upgrade in the summer campaign, starting end of May.

As charged with the operation, conditioning and installation of the lithium injector, I was responsible for a series of tasks, which are covered within this thesis.

- Design and modeling of the injector vacuum system for use in the torus hall, to ensure minimal propellant gas flow into the reactor
- Training with the lithium injector for operation, reparation and maintenance work
- Installation of the machine in a test bed, verification of C. Münther's results and testing of the previously designed in-torus vacuum system

In the following chapters, I will explain the physical principles that guide this work (chapter 2), the concrete steps taken to ensure the system works as required (chapter 3), the experimental procedure for the tests (chapter 4), the results thereof (chapter 5) and the final conclusions of this work (chapter 6).

# Chapter 2

## Theoretical principles

### 2.1 What is a plasma?

Plasma can be called the fourth state of matter. It consists on an overall roughly electrically neutral medium, composed partly or totally of positively and negatively charged particles, typically positively charged ions and electrons<sup>1</sup>. This state can be achieved through heating of a gas, an electrical current, or the use of electromagnetic waves to excite the electrons or nuclei of an atom. The particles within the plasma are unbound, but their movement can generate electrical currents with associated magnetic fields. Plasma particles are affected by each others fields, governing the whole plasma's collective behavior [Stu94].

Due to the presence of positive and negative charge carriers, plasmas are electrically conductive. Unlike gases, the fact that plasmas respond to electromagnetic fields lets them form macroscopic structures such as double layers.[WM87]

---

<sup>1</sup>In the case of deuterium or tritium plasmas, since hydrogen atoms and its isotopes only posses one electron, these are formed by deuterium or tritium nuclei and electrons



## 2.2 Nuclear fusion reactions

Nuclear fusion reactions hinge on Albert Einstein's famous equation (2.1) [Ein05], and the concept of binding energy.

$$E = m * c^2 \quad (2.1)$$

To understand this concept, it is helpful to present the previous equation as:

$$\Delta E = \Delta m * c^2 \quad (2.2)$$

In light of this equation, a net change in mass can lead to a very strong change in energy, given the large value of the speed of light [Pen04].

$$c = 299,792,458 \text{ m/s} \quad (2.3)$$

Given the masses of a proton, a neutron and a deuterium nucleus, it is clear to see that the mass of a deuterium nucleus is in fact lower than the sum of the masses of its constituents. This mass defect is released as energy, which is known as binding energy [Gar14]. This concept is not unlike that of enthalpy of formation in chemistry.

$$\left\{ \begin{array}{l} m_p = 1.0073 \text{ u} = 1.67 \cdot 10^{-27} \text{ kg} \\ m_n = 1.0087 \text{ u} = 1.68 \cdot 10^{-27} \text{ kg} \\ m_d = 2.0141 \text{ u} = 3.34 \cdot 10^{-27} \text{ kg} \\ m_{Difference} = 0.0014 \text{ u} \rightarrow B_E = 1.3041 \text{ MeV} \end{array} \right. \quad (2.4)$$

<sup>2</sup>, <sup>3</sup>

In comparison, chemical reactions are typically in the range of 2 – 5 eV [oNSWSoP14]. Nuclear reactions are consequently more energetic by 5-6 orders of magnitude.

<sup>2</sup>u: unified atomic mass unit. 1 u = 1.660538921 \* 10<sup>-27</sup> kg

<sup>3</sup>10<sup>6</sup>electron volts. 1 electron volt (eV) = 1.60217657 \* 10<sup>-19</sup> joules

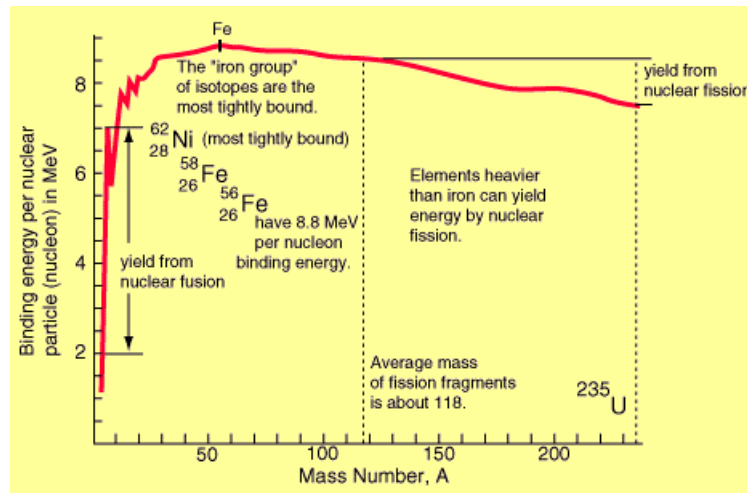
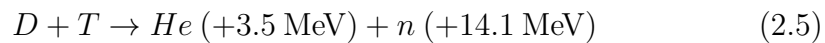


**Figure 2.1:** Binding energy per nucleon, weighed by atomic mass number [Gar14]

If binding energy is weighed by atomic mass number, relative atom stability can be seen, as well as possible energy yields from fusion and fission reactions, since reactions that lead to a greater binding energy will be energetically favorable.

Nuclear fusion reactions are therefore reactions in which two or more nuclei combine or “fuse” to form at least one particle heavier than any of the initial ones. This occurs only when both particles are in close proximity, of the order of a nuclear radius [Pfa06], and as shown in fig. 2.1, this process can yield significantly higher energies per particle than nuclear fission reactions. Currently, the main reaction to be used in nuclear fusion power is:



## 2.3 The Lawson criterion

Unlike nuclear fission reactions in commercial power plants, which can occur at room temperature and do not require thermodynamic equilibrium, nuclear fusion reactions such as the one presented in 2.5 require certain conditions

in order to occur.

Both interacting nuclei must come into close proximity in order for the strong nuclear force to bind them, thus releasing energy. However, since both nuclei are positively charged<sup>4</sup>, the electromagnetic force will repel them. This does not happen in fission reactors, where neutrons interact with heavy nuclei, because neutrons have no electric charge. As a consequence, in a fusion reaction the nuclei must possess enough energy to overcome this repelling force (known as Coulomb barrier) [GSUA14]. Also, energy is required in order to confine the nuclei to distances where the reaction can occur.

Fusion can only be energetically viable if more energy is gained from the fusion reactions than that which is put into the process of overcoming the Coulomb barrier and confinement. Three parameters describe the fusion reaction: fuel temperature  $T$  (a measure of the overall energy of the system), fuel density  $n$  and confinement time<sup>5</sup>  $\tau_E$ .

The point at which the power generated from nuclear fusion reactions equals the power required to maintain the fuel within fusion conditions is known as breakeven. Achieving breakeven fusion is however insufficient for a commercial fusion power plant, since no net power is being produced. The point at which heating from the fusion reactions is sufficient to compensate for heat losses and maintain the overall fuel temperature without the need for external heating is called ignition. Ignition is not necessarily required for commercial power plant operation, since external heating can be supplied so long as it is considerably less than the serviceable energy supplied by the fusion reaction. In spite of this, ignition conditions are considered an adequate design benchmark for fusion reactors. The Lawson criterion is the minimum value of the “triple product” of temperature, density and confinement time which yields ignition conditions, and so is often used as a figure of merit.[H<sup>+</sup>00].

---

<sup>4</sup>Atomic nuclei are formed by protons, with positive electric charge, and neutrons, with no electric charge

<sup>5</sup>The time it would take the fuel to lose all its energy to the environment

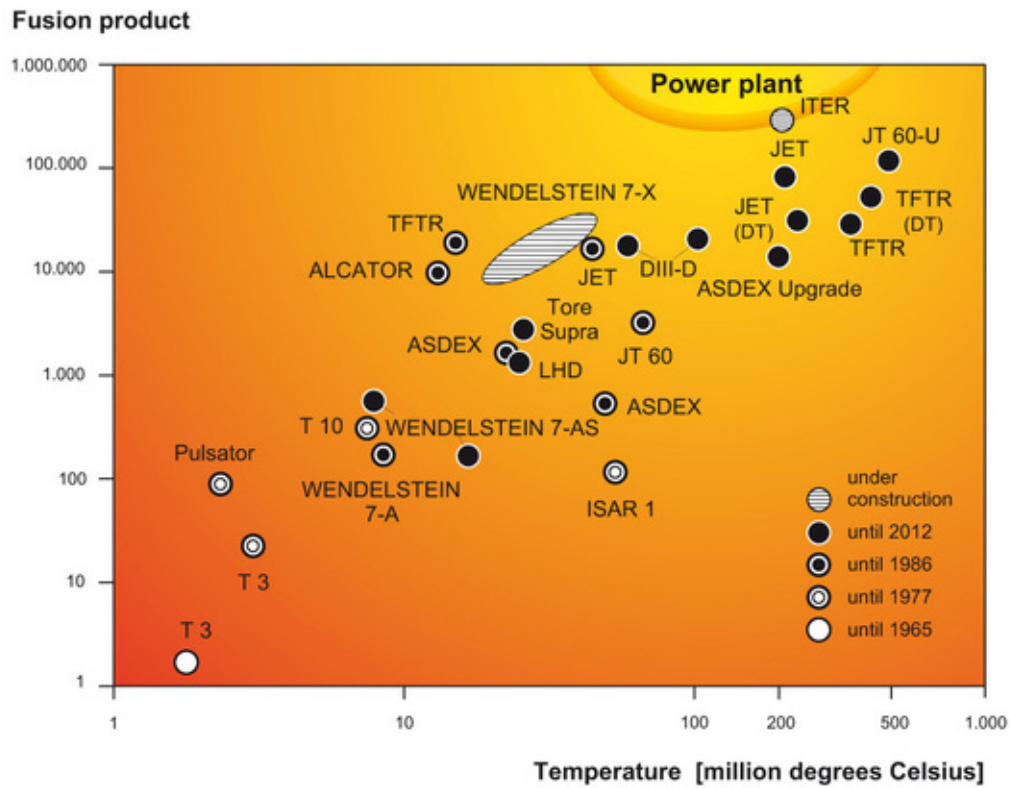


**Figure 2.2:** Triple product and temperature of fusion reactors and power plant conditions [fP14]

In the case of a deuterium - tritium reaction, this value minimizes at:

$$T = 14 \text{ keV} \approx 1.625 \cdot 10^8 \text{ K} \quad (2.6)$$

with a triple product of:

$$n \cdot \tau_E \cdot T \approx 3 \cdot 10^{21} \text{ keV} \cdot \text{s}/\text{m}^3 \quad (2.7)$$

Any reactor that achieves ignition conditions must attain a triple product factor above this value. Figure 2.2 shows the triple product values of different fusion reactors.

## 2.4 Magnetic confinement

### 2.4.1 Introduction to magnetic confinement

Three general conditions must be met for self-sustained fusion to occur:

- The fuel must be kept in a state of equilibrium, with acting forces being balanced.
- The state of equilibrium must be quasi-stable. The system must be able to revert to the equilibrium state when small disturbances are introduced, either on its own or through man-made means.
- The loss of mass and energy must remain relatively low. Self sustaining fusion requires that energy from the fusion reaction be in part retained to provide self heating for the fuel that has yet to react. Mass retention must be sufficient to ensure that a significant portion of the fuel reacts before it escapes the plasma.

In magnetic fusion reactors, the fuel is heated to a plasma state in order to reach fusion conditions, with temperatures of millions of degrees. In order to not damage the walls and cool the fuel, the hot plasma is confined via magnets. This inhibits massive interaction with the wall. Due to the electrical charge of the particles, Lorenz forces will act perpendicular to the magnetic field lines, so that charged particles within the plasma will follow them, gyrating around the field lines. [H<sup>+</sup>00]

For magnetic confinement to be effective at retaining plasma particles, these must be prevented from “leaking” out of the ends of the field lines. The most developed approach is through toroidal magnetic confinement.

### 2.4.2 Toroidal magnetic confinement

As the name suggests, magnets are placed creating a toroid, approximating a solenoid whose field lines close in on themselves and are contained within the

structure. Unlike the solenoid however, the field lines are not constant, since the magnetic field strength diminishes with the major toroidal radius and the field lines are curved. This induces a drift of the particles, which will tend to transport them to the torus wall. This drift must be compensated with the addition of a poloidal field (perpendicular to the toroidal field), thus giving way to helical field lines. This is done in all toroidal confinement schemes, the most advanced of which is the tokamak.

### **2.4.3 Tokamak design**

In the tokamak, the poloidal field is primarily created by inducing a current within the plasma, which is achieved by charging a central solenoid placed at the toroid's axis. Additionally, secondary poloidal field coils (also called equilibrium field coils or outer poloidal field coils) help to further control the poloidal field and define the shape of the plasma (see fig. 2.3). Control of heating and magnetic parameters within the coils will lead to different modes of plasma confinement and operation, the most used of which is currently the High-confinement mode.

### **2.4.4 H-mode**

In 1982, the High - confinement mode was discovered at the ASDEX tokamak of the Max Planck Institut für Plasmaphysik [ITE14b]. Provoked by supplying heating power above a characteristic threshold, energy confinement time within a H-mode increases significantly, typically by a factor of 2 [Kei87]. This is known as the H-factor. A pedestal is formed, a profile (for instance pressure) increase due to a narrow edge plasma region displaying enhanced profile gradients, with an edge transport barrier forming between the core and edge plasma regions (see fig. 2.4) [Tea89].

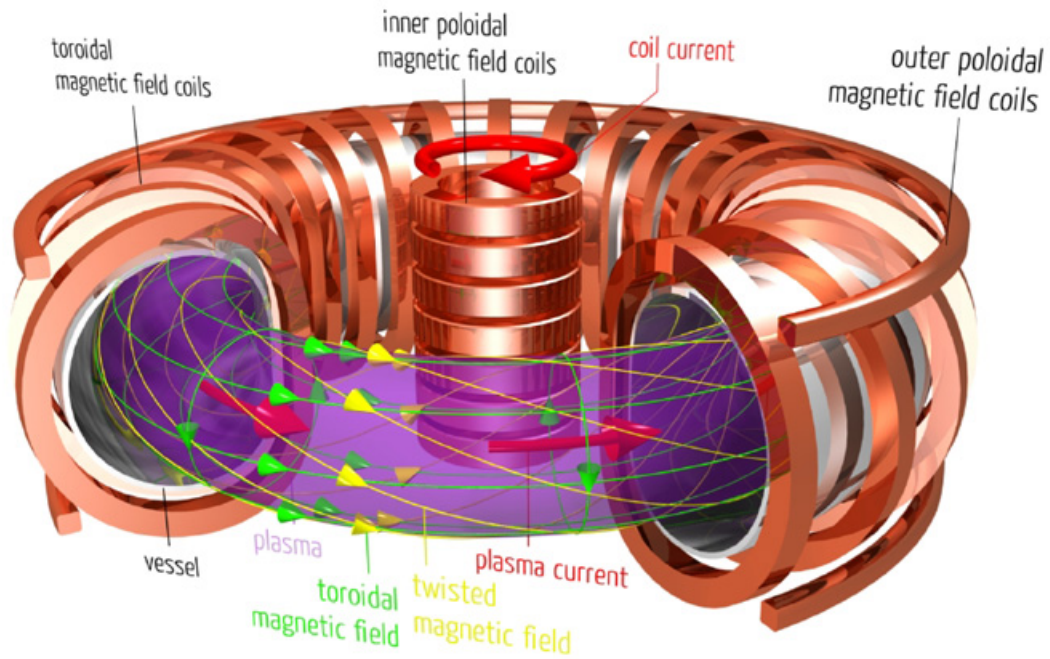


**Figure 2.3:** Helical field lines and tokamak design [MPIfP]

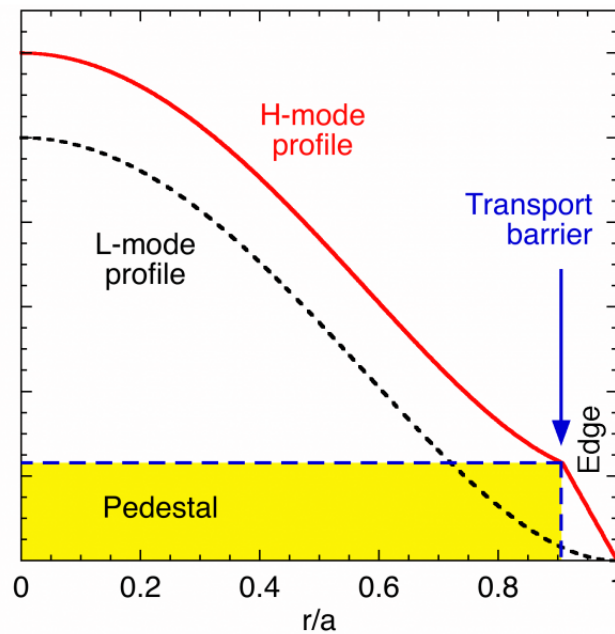


**Figure 2.4:** Sketch of H-mode profile and pedestal, showing density profile to relative radius in a plasma [CIE15]

### 2.4.5 ELMs

This steep edge gradient associated with H-modes produces a quasi-periodic sudden expulsion of particles and heat, known as ELMs, or Edge Localized Modes. These can easily prove detrimental to operation and machine lifetime, on occasion terminating the plasma, and are expected in ITER's standard operating scenario, making ELM mitigation a priority in ITER-relevant research [Zoh96, Wad09]

## 2.5 The effect of Lithium in other tokamaks

Lithium injection tests done on the DIII-D, NSTX and EAST tokamaks have yielded promising results, improving several key plasma parameters [Mai14, J<sup>+</sup>14]:

- A pedestal height and width increase, and consequently an overall H-factor increase, has been observed in DIII-D and NSTX.
- ELMs have been delayed or eliminated across all reactors.
- Plasma inventory recycling by the walls has been reduced in NSTX and EAST.

Additionally, an optimum lithium injection rate of  $15\text{mg/s}$  was found in DIII-D when injecting  $\mu\text{g}$ -sized Li granules at low speeds[Mai14].

The projected ASDEX Upgrade lithium injection experiments aim to test these findings on an all-metal wall device. If successful, the results will empower ASDEX Upgrade with a new tool capable of affecting pedestal height and width, potentially enabling the testing of new experimental scenarios for the reactor. The optimum lithium injection rate determined in DIII-D serves as an initial benchmark for the lithium injector at ASDEX Upgrade.



Pellet sizes	Volume	Mass	Atom count
2 mm · $\phi$ 0.5 mm	0.393 mm <sup>3</sup>	0.21 mg	$1.82 \cdot 10^{19}$
2 mm · $\phi$ 1 mm	1.571 mm <sup>3</sup>	0.84 mg	$7.28 \cdot 10^{19}$
2 mm · $\phi$ 1.5 mm	3.53 mm <sup>3</sup>	1.89 mg	$1.64 \cdot 10^{20}$

Table 2.1: Available pellet sizes

## 2.6 Important pellet parameters

The 15 mg/s benchmark determined in DIII-D must be scaled proportionately for ASDEX Upgrade. Three factors have been considered:

- Relative size of the reactor must be taken into account. ASDEX Upgrade possesses plasma volume of 13 m<sup>3</sup>, whereas DIII-D’s plasma volume is 24 m<sup>3</sup> [Mar15].
- Better recycling results are expected with ASDEX Upgrade’s all-metal wall in comparison to DIII-D’s carbon composite wall, as tungsten has been shown to provide significantly lower gas retention rates in comparison to graphitic wall components. This should lead to a lower lithium requirement [Age15].
- Increased lithium in-plasma deposition efficiency is expected, as pellet penetration depth increases with pellet size and speed. Whereas ASDEX Upgrade’s lithium injector utilizes a gas pulse injection, with injection speeds of 500 – 800 m/s and pellets in the mg range, DIII-D uses a dust dropping mechanism, with injection at very low speed and pellets in the  $\mu$ g range [Mai14, Mün01].

With these factors taken into consideration, an optimal lithium injection rate of 3 – 6 mg/s is envisaged for the ASDEX Upgrade fusion reactor.

Three pellet sizes (and corresponding masses) are available for use with the lithium injector, as documented in C. Münther’s 2001 master thesis (table 2.1).

Overall transfer efficiencies are expected to be high (above 90%), with a very low angular dispersion ( $\sigma_{cone} = 1^\circ$ ) and speed scatter ( $\sigma = 30 \text{ m/s}$ ).

The baseline pellet injection repetition rate is 0.07 Hz (one pellet each 14 seconds), which could be improved up to a hard limit of  $\sim 3 \text{ Hz}$  [Mün01].

A maximum reliable repetition rate of 2 – 2.5 Hz is expected. Within these conditions, the largest pellet size (1.89 mg) has been selected for use in experiments, as it is deemed the most suitable for reaching the 3 – 6 mg/s optimum injection rate estimated for ASDEX Upgrade.

Pellet injector loading is effectuated manually. Thus, since access to the ASDEX Upgrade torus hall is restricted during reactor operation, pellet inventory inside the injector is limited to 36 pellets per operation day, as this is the maximum pellet magazine size. As a consequence, lithium pellet injection experiments must be scheduled carefully in advance, including the number of pellets to be introduced during any given plasma discharge, so as to not plan past this hard limit.

## 2.7 Gas pulse pellet injection

A theoretical model is used to explain the end speed of propelled pellets, based on gas species and pressure used. As shown by C. Münther in his thesis, the gas drag model yields results which fit well with the experimental measurements [Mün01]. This model considers that solid pellets within a tube are, in the presence of a gas pulse, accelerated by the drag forces exerted by the fast moving gas as it expands. In the case of a straight tube, the maximum achievable velocity for the pellet is therefore the sound velocity of that gas, which will depend on the gas species and its temperature.

In the case of the lithium injector operation parameters, typically Reynolds numbers are of the order of  $10^5$ , thus propellant gas flux can be considered a turbulent phenomenon. With this in consideration, the following equation can be used [LS94]:

$$m \frac{dv}{dt} = c_d A \frac{\rho_G(x)}{2} (v_G(x) - v(x))^2 \quad (2.8)$$

Where  $m$ ,  $A$  and  $v$  represent the pellet mass, cross sectional area and velocity (these last two in the direction of flight), respectively. Similarly,  $c_d$ ,  $\rho_G$  and  $v_G$  are the turbulent gas drag coefficient, the gas density and the gas velocity along the flight trajectory.

By employing the transformation:

$$\frac{dv}{dt} = \frac{\partial v}{\partial t} + v \frac{\partial v}{\partial x} \quad (2.9)$$

And:

$$\frac{\partial v}{\partial t} = 0 \quad (2.10)$$

Equation 2.8 can be expressed as:

$$\frac{v}{(v_G(x) - v(x))^2} dv = c_d A \frac{\rho_G(x)}{2m} dx \quad (2.11)$$

Integrating for the whole acceleration process:

$$\int_{v^i}^{v^f} \frac{v}{(v_G(x) - v(x))^2} dv = \frac{c_d A}{2m} \int_0^L \rho_G(x) dx \quad (2.12)$$

Where  $v^i$  and  $v^f$  are the initial and final pellet speeds, and  $L$  is the length of the barrel. With the following approximations:

$$v_G(x) = \text{const}$$

$$\rho_G(x) = \text{const}$$

$$v^i = 0$$

$$v^f = v$$

The equation yields:

$$\ln\left(1 - \frac{v}{v_G}\right) + \frac{\frac{v}{v_G}}{1 - \frac{v}{v_G}} = \frac{c_d A \rho_G L}{2m} \quad (2.13)$$

Knowing the conditions of the gas (pressure, gas species, temperature), the geometry of the barrel and the characteristics of the pellet, the values for all the variables except  $v$  can be obtained. Eq. 2.13 can then be solved by iterating on  $v$ , thus yielding the expected pellet speed according to the gas drag model. This model predicts monotonously increasing pellet speeds with propellant gas pressure, with a sharp increase for lower pressures and a more flattened increase in the case of higher pressures, asymptotically approaching the speed of sound of the propellant gas at infinite pressure.

## 2.8 Propellant gas flux

As previously stated, a gas pulse is used to propel the lithium pellets into the plasma. However, the inclusion of this gas into the plasma could severely hamper confinement and plasma edge stability. Gas outflow rates were measured by C. Münther and C. Demirtas at different propellant gas pressures, with results ranging from  $100 \text{ mbar} \cdot \text{l}$  ( $2.416 \cdot 10^{21}$  molecules) at 20 bar to  $700 \text{ mbar} \cdot \text{l}$  ( $1.691 \cdot 10^{22}$  molecules) at 80 bar, approximately one order of magnitude greater than the atomic count of lithium injected per pellet. It was therefore deemed necessary to reduce these rates, and it was determined that only the main plasma gas can be used as propellant, as the addition of other species would behave like impurities within the plasma.

This is accomplished in part via the addition of an expansion tank. Whereas

the propelled pellet will pass through the tank in relatively unaffected free-flight, the gas will suffer an expansion within the tank, consequently slowing down. A newly added cryopump together with the preexisting turbomolecular pump will then remove this gas from the system, thereby diminishing the amount of gas to enter the torus. Also, a nylon aperture is used in order to further reduce gas outflow.

The newly formed expansion system has an inner volume of 30 l, while the previously used configuration held an inner volume of  $\sim 1$  l. Together with the increased extraction power and the use of the nylon aperture, the system was designed to provide gas outflow reductions 30 to 100 times lower than those originally measured. These results were confirmed by the measurements taken in the test bed, shown in chapter 5.3.

# Chapter 3

## Experimental set-up

### 3.1 Working principle of the lithium injector

#### 3.1.1 Mechanical operation

The lithium pellet injector mechanics were described in detail by C. Münther in his diploma thesis in 2001 [Mün01]. Its mechanical operation hinges on its revolver-type cylinder, consisting on a revolver plate outfitted with 36 equally spaced holes of a certain specified diameter, 0.5 mm, 1 mm or 1.5 mm (tab. 2.1), according to the desired pellet size (fig. 3.1). The plate rotates on its axis inside the injector via a check wheel operated by a push rod connected to a pneumatic piston. This mechanism ensures that the rotation of the revolver plate is  $10^\circ$ , constant with every piston upward stroke, which is calibrated by regulating the stroke length. Two openings within the injector are aligned with the revolver plate's holes. These are the pellet loading-port, used to load the holes with lithium; and the pellet chamber, into which propellant gas flows and from which the lithium pellet is propelled out of the injector. The lithium pellet extruder is attached to the injector at the pellet loading-port, thus permitting to load the injector by extruding lithium inside the revolver plate's hole and rotating the disk one position. This extruding and rotating process is repeated until all 36 holes are filled with lithium. The

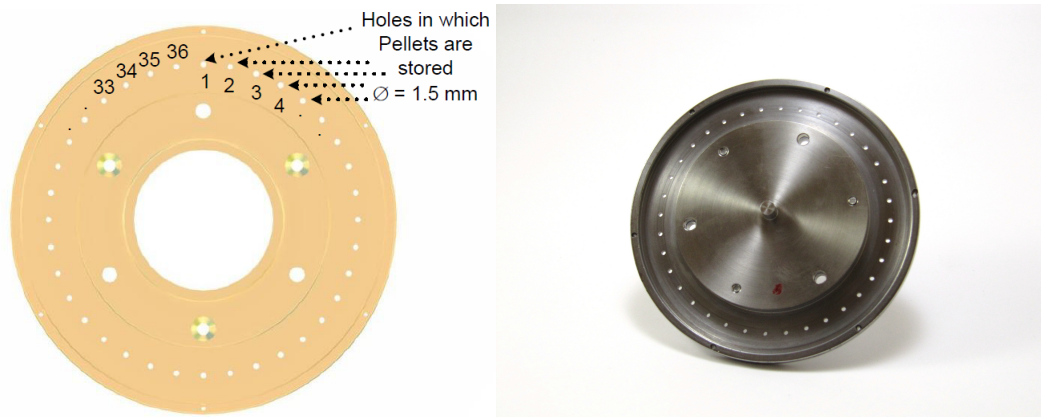


**Figure 3.1:** Lithium injector revolver plate [Ale11]

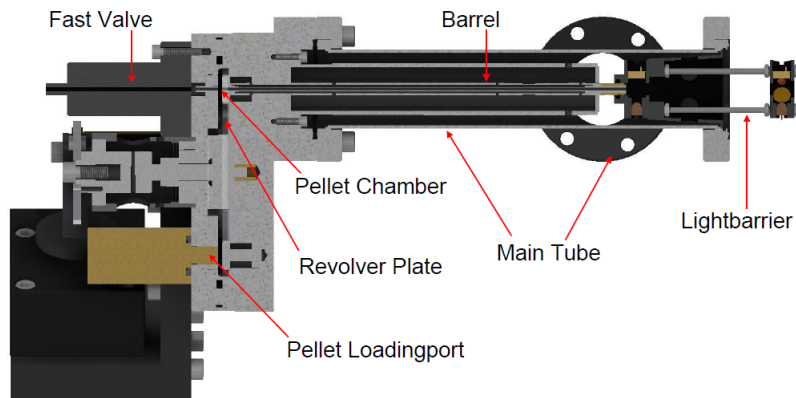


**Figure 3.2:** Lateral cut of the lithium injector [Ale11]

pellet chamber is situated 180°, or 18 positions, from the pellet loading-port. Here the fast valve is attached, which releases a gas pulse, thus propelling the pellet through the barrel and out of the injector. Two arrays of light barriers detect the pellet in flight. These consist on an LED<sup>1</sup> and a photodiode<sup>2</sup>. When a pellet flies through the light barrier, the photodiode is obscured from the light emitted by the LED, thus registering a voltage drop. Lastly, the main tube provides structural support for the injector, creating at the same time a vacuum-tight union (fig. 3.2 and 3.3).

<sup>1</sup>Light Emitting Diode

<sup>2</sup>A diode that generates current when struck by light

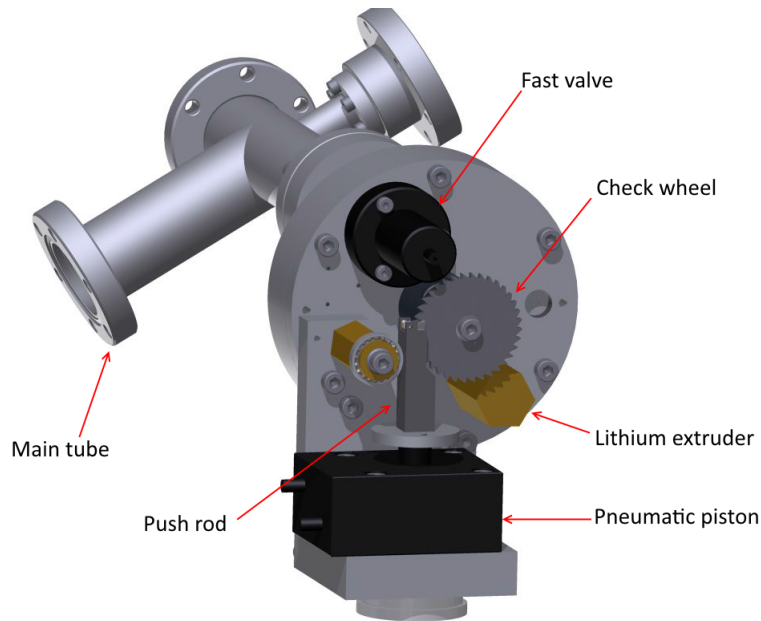


**Figure 3.3:** 3D model of the lithium injector [Ale11]

### 3.1.2 Gas injection system and pneumatics

The propellant gas injection system is shown in figure 3.4.

A pressurized (max. 200 bar) bottle of the propellant gas (in our case deuterium) is used. It is connected to a pressure regulation valve, with which the desired operating pressure can be selected. The Nupro shut-off valve (fig. 3.5) constitutes a safety feature, ensuring that in case of malfunction, the fast valve can only “fire” a limited amount of gas: the volume between the Nupro and fast valve, approximately  $2 \text{ cm}^3$ . This limited gas inventory is also of use during regular pellet shots, having the effect of reducing the propellant gas flux by a factor of 2 [Ale11].

The electronic manometer permits remote verification of the desired propellant gas pressure before injection. Lastly, the fast valve is operated via an electromagnet, reaching fully open position in 0.2 ms and remaining open for 2 ms [Mün01] (fig. 3.6). The maximum designed operating pressure for this valve is 150 bar, this being the upper limit to the propellant gas pressure for the injector.



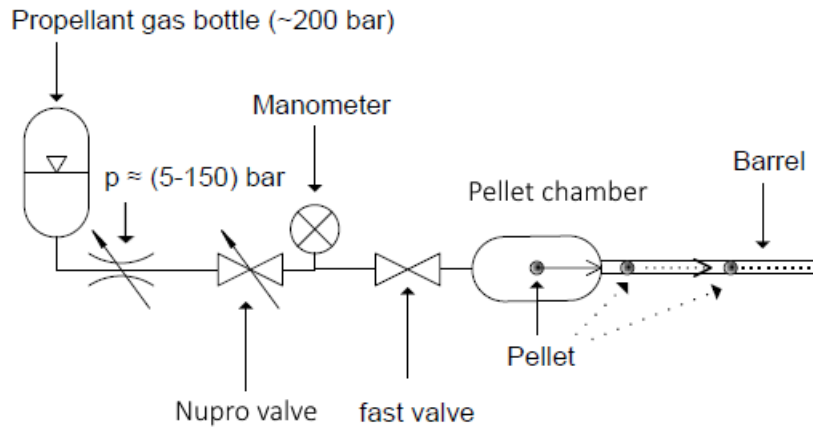


**Figure 3.4:** Propellant gas injection system



**Figure 3.5:** Swangelok Nupro SS-HBS6-C shut-off valve  
[[www.swangelok.com](http://www.swangelok.com)]

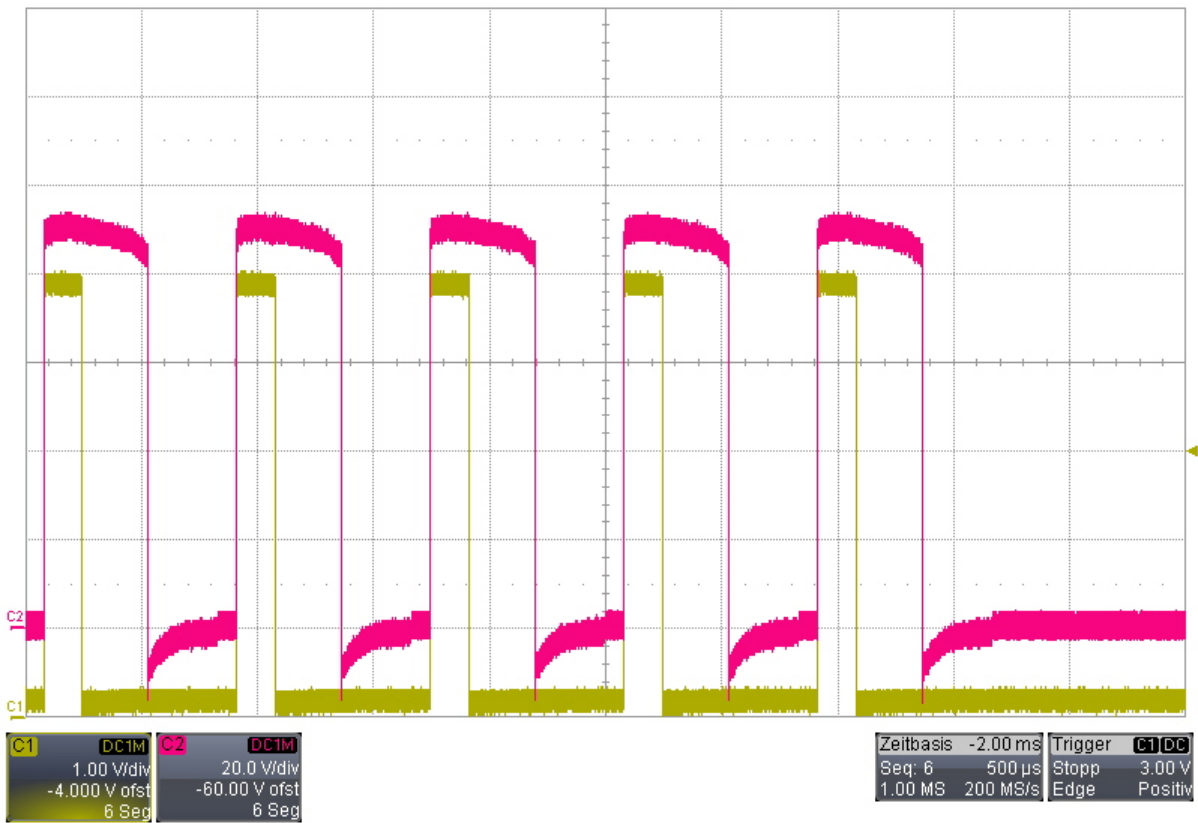


**Figure 3.6:** Power source output and valve opening of a five pellet firing sequence at 2 Hz

The fast valve is a critical component in the injector, essential for its operation and determinant in almost all of its operational parameters (propellant gas flux, pellet flight speed and repetition rate). However, it is not a commercial product and therefore a replacement cannot be bought. Two similar fast valves were found and are meant to serve as emergency replacements in the event that the currently used fast valve malfunctions. The fast valves, labeled A and B have been inspected and could supply spare parts for the current valve if ever a reparation is needed. Additionally, tests have been performed in the lab to compare the operation of the current fast valve to its replacements. The description of these tests can be found in chapter 4, while the results thereof are explained in chapter 5.

The injector pneumatic circuit is fed by a 6 bar pressure line and is operated electronically by a series of electrovalves. Three of these (in the test bed, two for ASDEX Upgrade) actuate the gate valves pertinent to the vacuum system. Another one controls the Nurpo shut-off valve. The last one actuates the switch valve that controls the lithium injector double-action piston which moves the push rod, thereby turning the revolver plate. When this line is pressurized, the push rod lowers. When the line is not pressurized, the switch valve reverts and pressure is used to raise the push rod, setting the check wheel into the next position. A manual valve is also mounted on the pressure valve plate attached to the injector. This manual valve acts upon the switch valve as well. This way, the injector revolver plate can also be rotated locally. This is necessary during lithium pellet reloading, which must be done manually.

The double-action piston stroke is regulated in two places. An Allen screw below the piston controls the stroke's highest point while two screws and bolts on the upper part of the piston determine the stroke's lower point. The highest point directly determines the end check wheel position, and must be adjusted carefully in order to ensure revolver plate hole alignment with the loading port and pellet chamber. This is done by dismantling the fast valve and shining a light through the end of the injector barrel, looking through

the pellet chamber into the barrel while cycling positions on the revolver plate, slightly adjusting the lower Allen screw each time until the light from the barrel end is aligned with the chamber. The lowest point of the piston stroke does not play such a delicate role, as the piston sinks in order to have the push rod come into contact with the next tooth in the check wheel. The injector is therefore insensitive to the lower piston position, and care must only be taken to ensure that the push rod grabs one tooth of the check valve and not two, which would cause the revolver plate to skip every other position, reducing the effective pellet inventory by half.

### **3.1.3 Electronic firing mechanism**

As previously mentioned, pellets are injected by way of a gas pulse, which is released via a gas valve. The fast valve is by default in the closed position, and opens when it receives a strong electric current, causing a relay to switch. For the purpose of the lithium injector, very short electric pulses are desired, since propellant gas flux - and therefore valve opening times - must be minimized. To this effect, a power source and electronic firing circuit are used. The power source allows a maximum current of 7 A, while the electronic circuit, functioning at 115 V, together with an array of capacitors totaling 10 mF, loads and stores the required energy to actuate the electromagnetic valve. The stored energy is released in a period of 3 ms (fig. 3.6). The discharge supplies the fast valve relay coil with a power of 18kW, and a current of up to 7000 A, opening the valve. With said power source, a pellet firing repetition rate of 2Hz is achieved, allowing for 8-10 lithium pellets per plasma discharge, therefore allowing study of the effects of lithium buildup within a discharge. This was hitherto impossible, as the previous power source of 0.25 A did not permit more than one pellet to be fired per plasma discharge.

For operation at ASDEX Upgrade, the power supply is mounted outside of the torus hall, since the powerful magnetic fields present in the torus during operation could lead to induced currents in the sensitive equipment. The

electronic circuit is bolted to a rack close to the injector, and can be activated either manually via a built-in button or at a distance via the remote control electronics.

## **3.2 Experimental test bed set-up**

### **3.2.1 Equivalent expansion volume**

As previously stated, it has been deemed necessary to outfit the lithium injector with an expansion volume, in order to reduce propellant gas fluxes into the plasma vessel. This expansion volume was modeled and calculated in accordance with the available space and geometry of the ASDEX Upgrade entry port where the injector is to be installed. Said model is discussed in more detail in future sections of this thesis, and provides a total expansion volume of 30 l.

The aforementioned model is partly made out of vacuum components that must either be ordered or modified or constructed entirely. To avoid the delay to the injector characterization process that would ensue from waiting for these components, an equivalent expansion volume of similar characteristics was determined necessary. This was accomplished by designing a vacuum system with readily available parts of similar volume. Openings for all necessary pumps, valves and diagnostics must also be provided, along with that for the injector and purge valve.

The designed system (fig. 3.7) provides an expansion volume of 23 l and identical vacuum pumping capacity as that projected for ASDEX Upgrade. It is designed to facilitate tests to determine the speed of fired pellets, their angular scatter, transfer rates and of special importance the new propellant gas outlet fluxes which validate the effect of the expansion vessel.

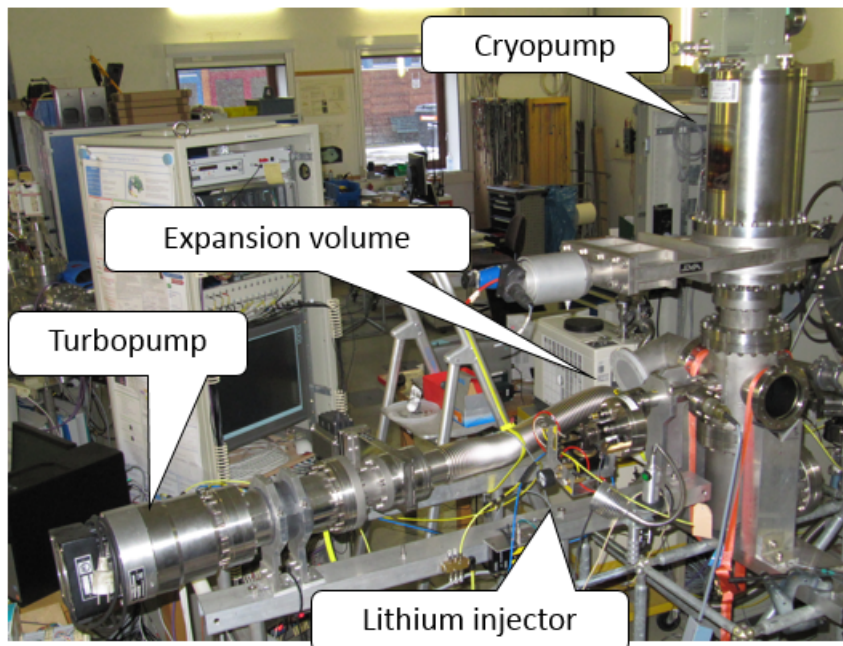
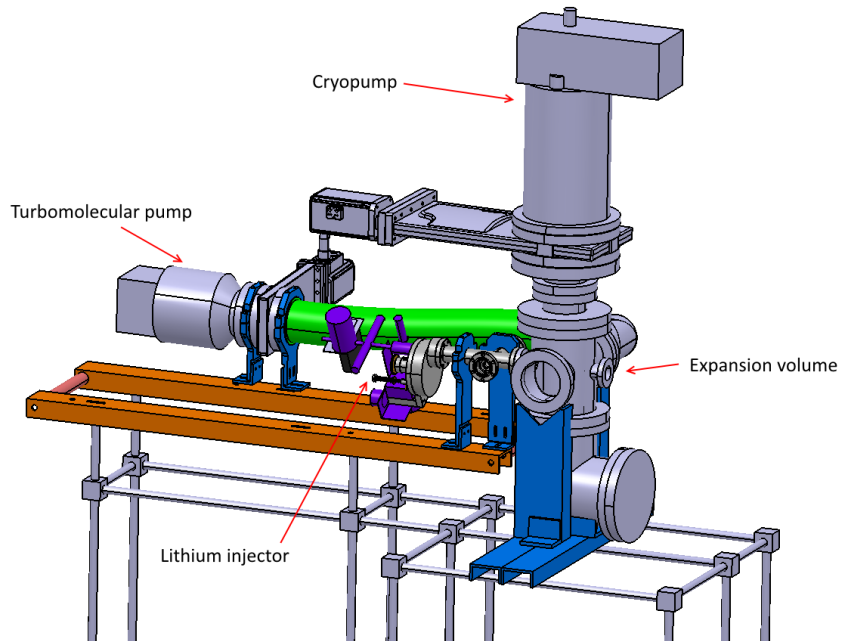


Figure 3.7: Lithium injector test bed

### 3.2.2 Required vacuum pumps and valves

As shown in fig. 3.7, two vacuum pumps are available. A CTI Cryo-Torr 8 High Vacuum cryopump is mounted on the top of the vacuum vessel, together with a CF 200 UHV<sup>3</sup> gate valve from VAT. To the side and behind the injector is a Leybold 360 Turbomolecular pump, together with a CF 100 UHV gate valve, also from VAT. The turbomolecular pump is connected in series to a rough vacuum pump, acting as a booster. First a rough vacuum of the order of  $10^{-2}$  mbar is created, and then the turbomolecular and cryopumps are connected, reaching a vacuum of the order of  $10^{-6}$  mbar.

A cryopump creates and maintains a vacuum by cooling an internal surface to low temperatures inside the vacuum system, where it condenses gases. In the case of the cryopump used, the cold head contains baffles to increase its effective surface and is cooled to temperatures of 5 K by expanding helium in a piston. The expanded helium is then compressed and cooled with the use of a supporting compressor and heat exchanger, which is cooled with water. Since the condensed gasses are retained inside the cryopump, these will with time block the cold surfaces, progressively reducing the pump's effectiveness to zero. The cryopump must then be regenerated by allowing it to reach higher temperatures, until all the condensed gases have evaporated. This can be done at room temperature and pressure, although regeneration is most effective if done while maintaining a vacuum, since boiling and sublimation temperatures decrease with pressure.

In the test bed setup, a valve is needed to not saturate the cryopump prematurely. Since the vacuum in the test bed must be broken frequently (each time the injector magazine is loaded or the pellet catching box is to be examined), it would be necessary to let the cryopump heat up to room temperature every time. Otherwise, the gas that enters the vacuum chamber would immediately freeze in the cryopump, quickly saturating it and forcing a regeneration cycle. By including a valve before the cryopump, the vacuum in the pump could be

---

<sup>3</sup>Ultra High Vacuum

maintained while the vacuum in the rest of the system was broken.

A turbomolecular pump contains multiple rotor/stator pairs in series, providing escalated vacuum power. The rotor revolves at high frequency, and gas molecules are guided towards the pump's exhaust. The turbomolecular pump should not operate for extended periods of time at atmospheric pressure or low vacuum conditions. For this reason, it is only connected once a rough vacuum has been reached with the rough pump.

Lastly, a hand-operated purge valve is also present. This valve is used in order to vent the system in a controlled manner by puffing in nitrogen, which provides an inert atmosphere for the vacuum components.  $N_2$  is preferable to air, since the water molecules present in humid air can be adsorbed on the vacuum components' inner surface. These water molecules would then be slowly released the next time that a vacuum is created, prolonging waiting times until a suitable vacuum regime is reached.

### 3.2.3 Support structure

The lithium injector and turbomolecular pump were previously fitted on a support structure by A. Alexiou in 2011 [Ale11]. Based on this, a similar support structure was assembled out of the standardized parts in order to provide a base for the vacuum system. The structure is made out of metal bars of varying defined lengths with threads at the ends and metal joints known as MERO balls serving as nodes for the structure (fig. 3.8).

The vacuum system structure was screwed to the previously existing one. However, a custom-fit construction was required in order to cushion the vacuum system and ensure it could not pivot or tilt. This structure was made specifically for this configuration out of readily available standard U-profiles (fig. 3.9).





**Figure 3.8:** Standardized bars of length 250, 353, 500, 707 and 1000 *mm* and MERO ball [Ale11]

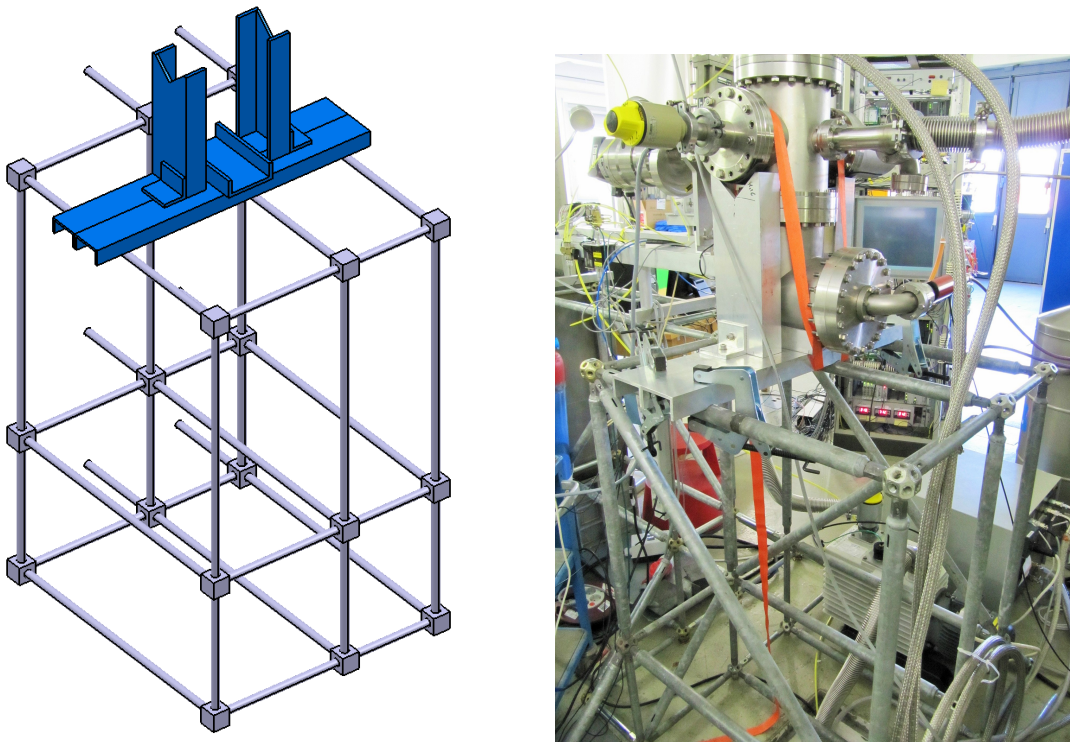


**Figure 3.9:** Complete vacuum system support structure

### 3.2.4 Lithium manipulation & extrusion

Lithium is the lightest metal in the periodic table, with a density of  $534 \text{ kg/m}^3$  and an atomic number of 3, being the first alkali metal. It is soft and has a silver white color, turning gray when oxidized. As with all alkali, lithium reacts strongly with water, producing inflammable gasses. It is also inflammable in solid form, and can cause irritation to the skin and mucous membranes (eyes, respiratory and digestive tract). Because of this, special care must be taken during lithium manipulation. Gloves and protective eye-wear must be worn at all times. Gases or dust must not be breathed and contact with skin or mucous membranes should be treated by washing with water and removing all contaminated articles of clothing. Manipulation must only be performed in a well ventilated room. Lithium also oxidizes in the presence of air, forming a passivized layer or lithium oxide. For this reason lithium should be stored in an inert container whenever not directly in use [Sci].

A  $\phi 6$  mm lithium wire is used to load the injector. Lithium must be extruded into the revolver plate holes via the loading port. This procedure is performed manually with the use of two lithium extruders (fig. 3.10). These extruders work in series. The first one extrudes lithium from  $\phi 6$  mm to  $\phi 2.5$  mm, while the second one extrudes lithium from  $\phi 2.5$  mm to  $\phi 1.5$  mm. This second one is directly screwed to the loading port, ensuring correct alignment with the revolver plate holes once the injector has been correctly calibrated.

The  $\phi 2.5$  mm to  $\phi 1.5$  mm extruder was already present, but the extruder pin had to be designed and manufactured again due to a mechanical failure in a passing pin. The  $\phi 6$  mm to  $\phi 2.5$  mm extruder was made specifically for this project, with a similar but scaled design to that of its counterpart. Additionally, a series of nozzles of varying diameter were made, to be fitted on the end of the  $\phi 2.5$  mm to  $\phi 1.5$  mm extruder. These allow the production of lithium rods of different diameters, necessary for the extrusion of the smaller  $\phi 0.5$  mm and  $\phi 1.0$  mm pellets. Also, an optimized nozzle of  $\phi 1.2$  mm was manufactured, as it was determined that lithium expanded during loading, causing lithium buildup outside of the revolver plate holes when using the

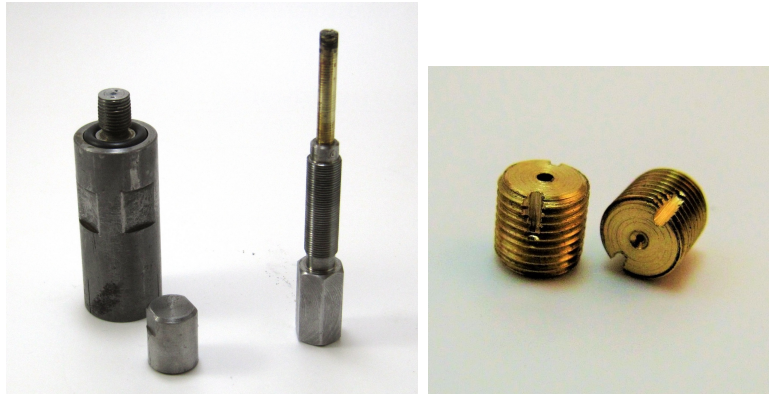


**Figure 3.10:** Lithium extruder and extrusion nozzles.

standard  $\phi 1.5\text{mm}$  nozzle. This buildup would eventually lead to an increased friction between the revolver plate and the lithium injector casing, allowing a progressive misalignment of the revolver plate and the pellet chamber. With the inclusion of a nozzle of smaller diameter than the pellet hole, no lithium buildup occurred (fig. 3.10).

### **3.2.5 Design of the lithium injector characterization tests**

#### **3.2.5.1 Angular scatter measurements**

Pellet flight angular scatter is measured by firing pellets inside a vacuum onto a target that marks the impact position of each pellet. Since pellet speeds can reach  $800\text{ m/s}$  [Mün01], a hard target for the pellets was devised, so that flying pellets would not harm the interior of the vacuum components. The target was also designed to provide storage for the pellets.

The designed system consists on a  $\phi 70\text{mm}$  stainless steel closed cylinder with a  $\phi 35\text{ mm}$  hole. This aperture is aligned with the lithium injector's barrel. Inside the cylinder there is a stainless steel plate at an angle of  $45^\circ$ , onto which a sheet of paper is screwed. The bottom of the cylinder is filled with steel wool. The angled plate and the wool can be manipulated by removing

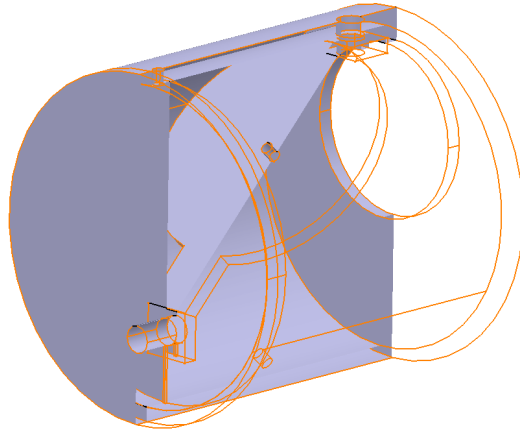


**Figure 3.11:** Lithium pellet catching box design

the back lid of the cylinder, which is secured by three lateral pressure screws. See fig. 3.11.

A flying pellet will enter the box through the  $\phi$  35 mm and impact on the angled plate, perforating the paper and thus leaving a mark. The pellet will be deflected downwards by said plate, penetrating the steel wool, thereby impeding it from exiting the box. Angular scatter will be determined from the relative position of all the marks left by pellets on the paper. A Gaussian distribution is assumed for in-flight pellet scatter. See fig. 3.12.

### 3.2.5.2 Pellet speed and speed scatter measurements

Pellet flight speed and pellet speed scatter will be measured by firing lithium pellets through the light barriers present in the lithium injector main tube into the vacuum chamber. The light barriers are arranged in two arrays in series, with a distance of 72 mm between them. The first array hosts one sensor/LED pair, while the second array holds three of said pairs (see fig. 3.13 and 3.14). It was hoped when the system was constructed that the second light barrier array could provide a limited spatial resolution. This

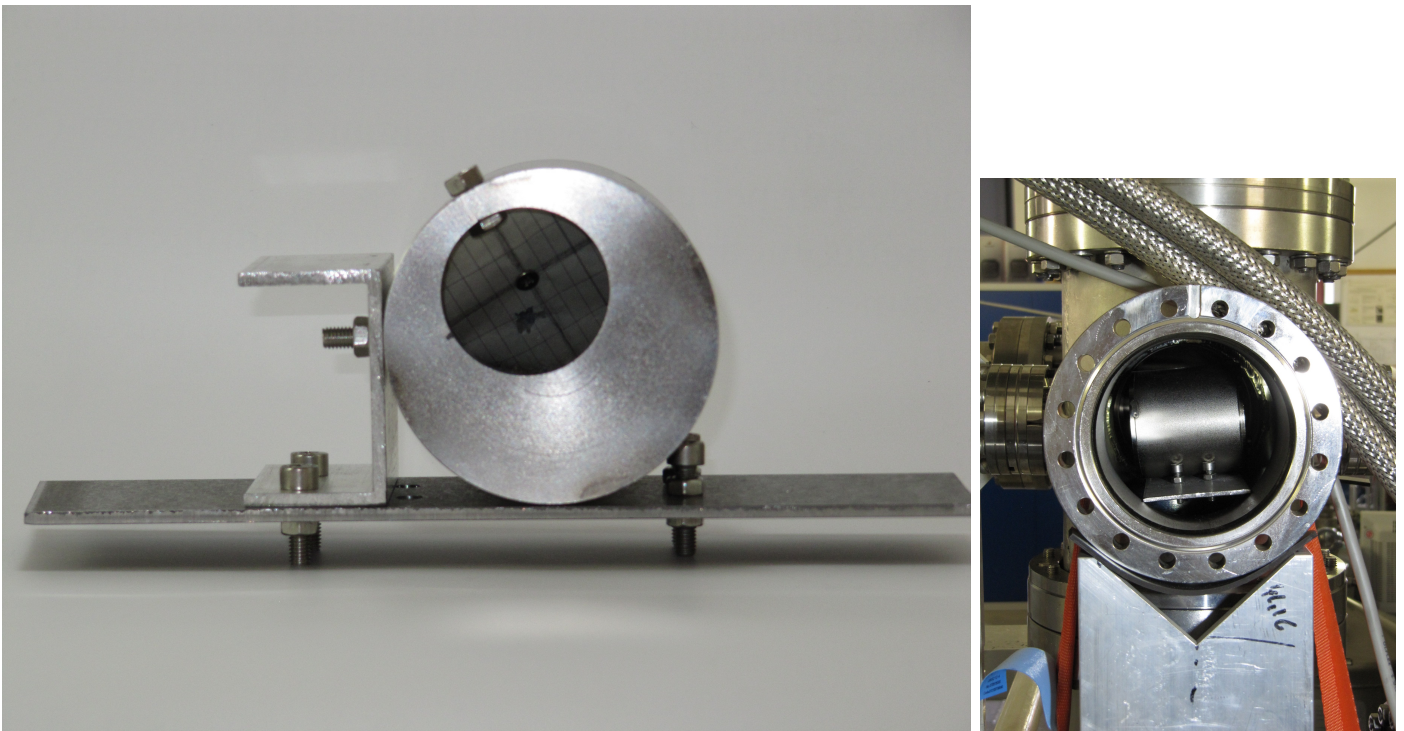


**Figure 3.12:** Catching box with paper for angular scatter measurement and catching box position inside the vacuum system

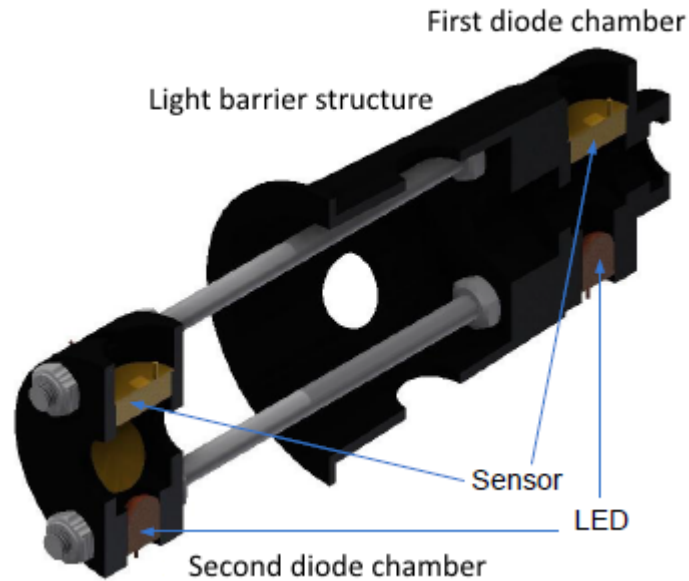


**Figure 3.13:** Light barrier structure [Ale11]

was proven impossible in practice, since the light barriers signal variability is too high for any such measurements to be made reliably.

When the pellet passes through a light barrier, it obstructs the sensor's view of the corresponding LED. This creates a voltage drop in the circuit, which can be measured from the light barrier electronic box attached to the lithium injector main tube (see fig. 3.15).

These signals are read on a LeCroy Waverunner 104Xi-A oscilloscope. The voltage drops are registered as peaks in the signals (fig. 3.16), and can be saved as ASCII files. The time delay between the peaks in the first and second light barrier arrays can be used to determine the speed of the pellet, as the distance traveled is the separation between light barriers. The speed scatter is obtained from the measured speeds of various pellets fired under the same parameters, assuming a Gaussian distribution.





**Figure 3.14:** Light barrier arrays. Left: first diode chamber. Right: Second diode chamber [Ale11]

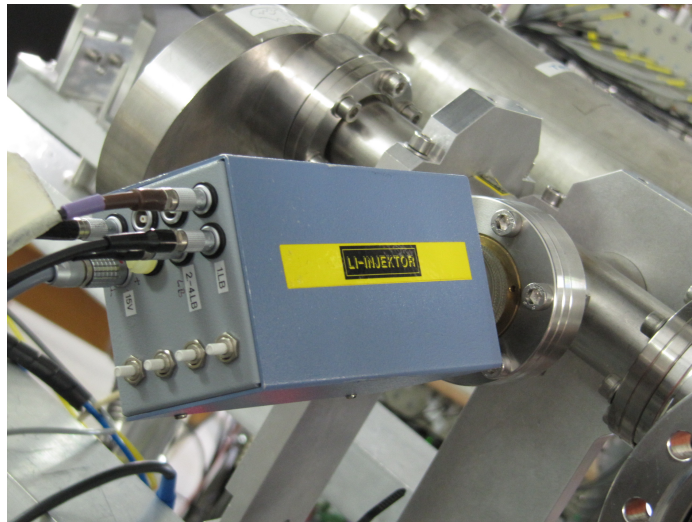


**Figure 3.15:** Light barrier electronic box

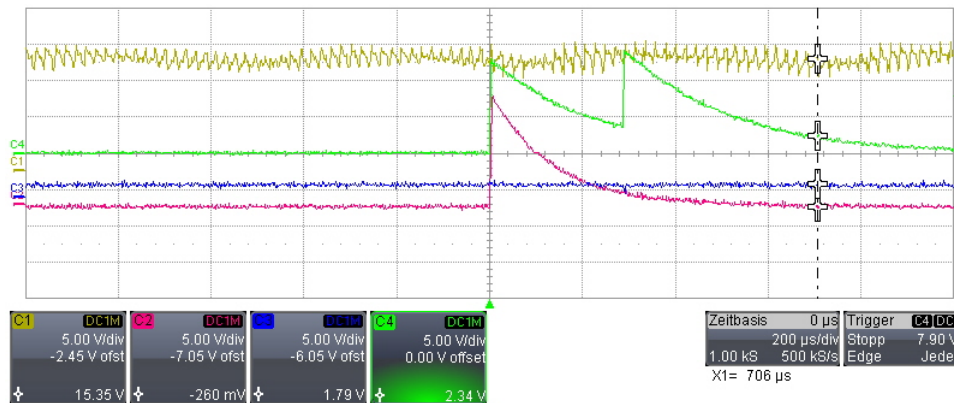


Figure 3.16: Oscilloscope readout of pellet flight

### 3.2.5.3 Pellet transfer rate measurements

Pellet transfer rates<sup>4</sup> are determined by counting the number of pellets that remain in the injector after each series of shots. Once a series has been completed, it can be verified if a pellet was successfully fired by visually inspecting the hole which aligns with the fast valve opening for the magazine plate position correspondent to each shot. If the hole is empty, the pellet was fired successfully. If a pellet remains in the hole, the shot was unsuccessful. Given the lack of room inside the injector and in the barrel ( $\phi$  1.56 mm compared to the  $\phi$  1.5 mm of the pellet), it is believed that every pellet that is fired will exit the injector.

An alternative would be to estimate the number of successfully fired pellets by counting the number of impact points on the paper used for angular scatter measurements. This would provide a similar readout, but with a large number of fired pellets it is very likely that one pellet impacts near a previous impact point, thus leaving no new mark. This leads to higher false negative rates (the pellet may be fired without a signal being received) than when inspecting the revolver plate in the injector, where false negative rates are effectively to be zero (a pellet cannot be fired and yet its corresponding hole remained filled). It could be argued that, since the pellet catching box

<sup>4</sup>Pellets that successfully exit the injector versus total number of pellets



is farther away from the injector, this measurement would be more valuable. It would not require the hypothesis that all fired pellets successfully exit the injector. However, if this were not the case, one pellet would suffice to obstruct the system, causing pellet and gas buildup. Said obstruction has as of yet never been observed.

#### 3.2.5.4 Propellant gas flux measurements

Attached to the vacuum system is a vacuum tank of 160 l. Both systems are connected by a gate valve and a flexible vacuum tube. The role of this vacuum tank is to simulate the ASDEX Upgrade plasma chamber in the lab. Propellant gas fluxes are measured by way of two pressure gauges, location shown in fig. 3.17. One is attached to the exit tube of the vacuum expansion system, while the other is mounted on the 160 l vacuum tank.

Pressure in the system can be measured before and after a propellant gas pulse. The pressure increment between the base value before the pulse and the peak value after it can then be multiplied by the volume of the container to yield an estimate for the amount of gas present (eq. 3.1). Since this can be done for both containers, the amount of gas that has reached each container can be calculated, thus providing the propellant gas flux for each container.

$$(P_{peak} - P_{before}) [\text{mbar}] \cdot Vol [\text{l}] = \text{Amount of gas} [\text{mbar} \cdot \text{l}] \quad (3.1)$$

The pressure gauges in use are MPT 200 Pirani/Cold Cathode combination from Pfeiffer Vacuum. They have a measurement range of  $5 \cdot 10^{-9}$  to 1200 mbar, and are connected via Profibus to the central control computer, where the measured values can be stored, visualized and compared.

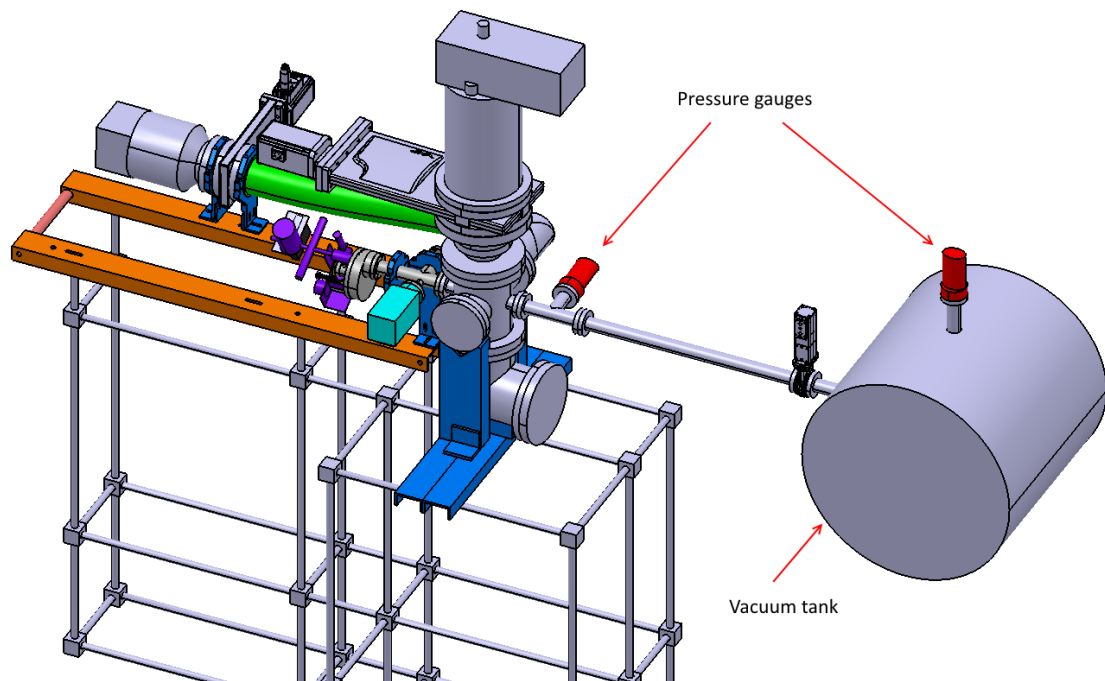


**Figure 3.17:** Complete injector and vacuum system test bed, showing the position of both pressure gauges

## 3.3 Design of the lithium injector installation in ASDEX Upgrade

### 3.3.1 Commissioning of the CAD models

#### 3.3.1.1 Expansion vessel

The Sector 16 Bo port of ASDEX Upgrade was selected for the installation of the lithium injector and associated vacuum system. This constituted a complex technical challenge, as the injector presented itself as a new diagnostic which had to be installed and put into operation within the frame of a mature machine that has been active for over twenty years. Fig. 3.18 shows the spatial limitations of the port prior to the arrival of the lithium injector. Coordination with other diagnostics' teams and the assembly crew of ASDEX Upgrade was necessary at every step. This translated itself into a process of periodical meetings, of re-evaluation of design criteria and of progressively finding technical solutions and compromises to the emerging problems. The nuclear aspect of this cycle is the central expansion vessel, as it had to be designed specifically for this application. Because of this it was the component with longest waiting times, costs and possibilities for modification to fit the design criteria of the system.

As starting conditions, it was determined that the injector must shoot pellets with a direct line of sight of the plasma and be as close to the port as possible, as it was already made clear in Demirtas' thesis that a guiding tube hampers the transmission rates to an unacceptable degree [Dem12]. Additionally, an expansion volume of at least 20 l should be provided, in order to reduce propellant gas fluxes into the plasma chamber. Given the high position of the port with respect to the ceiling structure, and the desired volume of the vacuum system, it was determined that standard vacuum components could not be used, as they would either lead to too small a volume, or directly incur in collisions with the other diagnostics and structure. Therefore, a central expansion vessel was specifically designed for the geometry, maximizing the

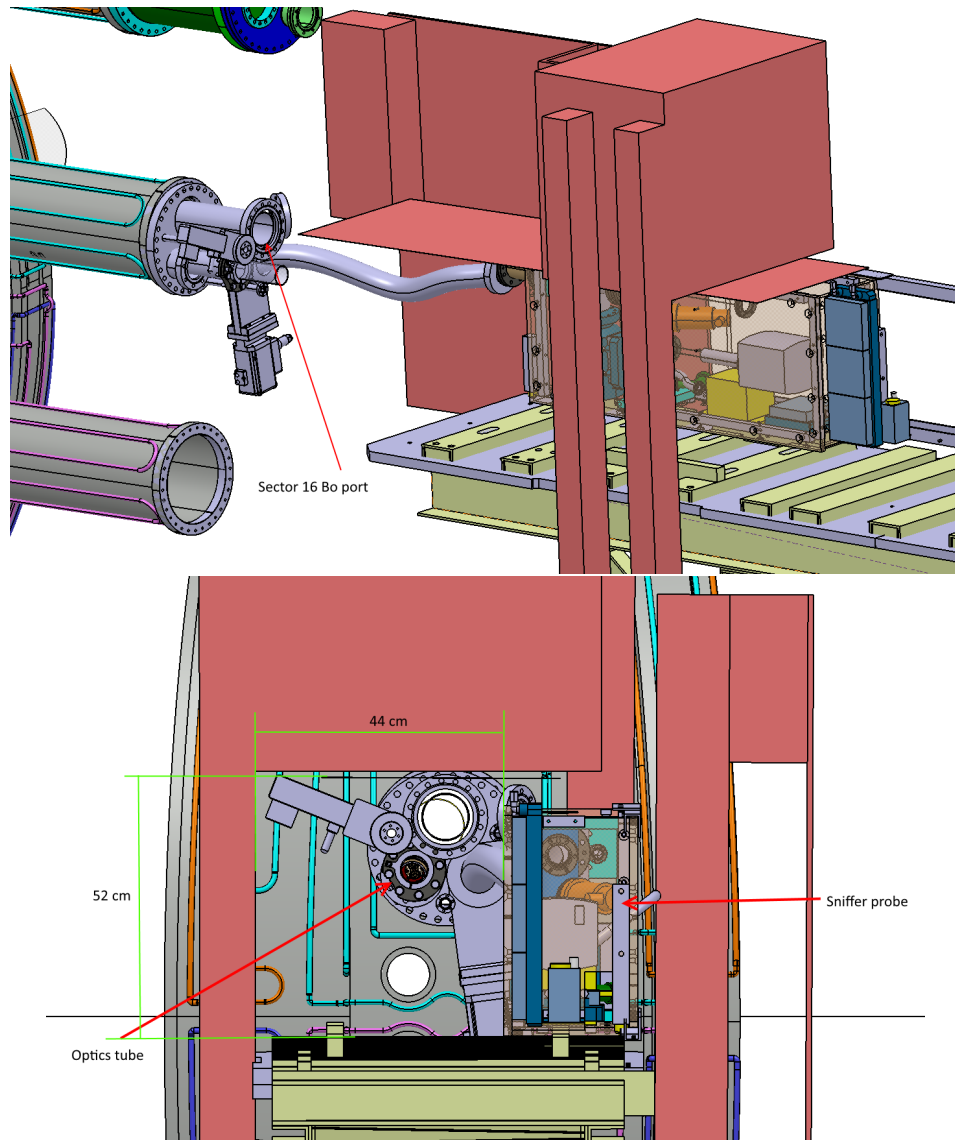


**Figure 3.18:** Space limitations in the S16 Bo port. A window of approx. 52 cm by 44 cm was available for the injector. However, this was further reduced by the entry ports of the optics tube and sniffer probe, two diagnostic systems with which the injector shared the port.

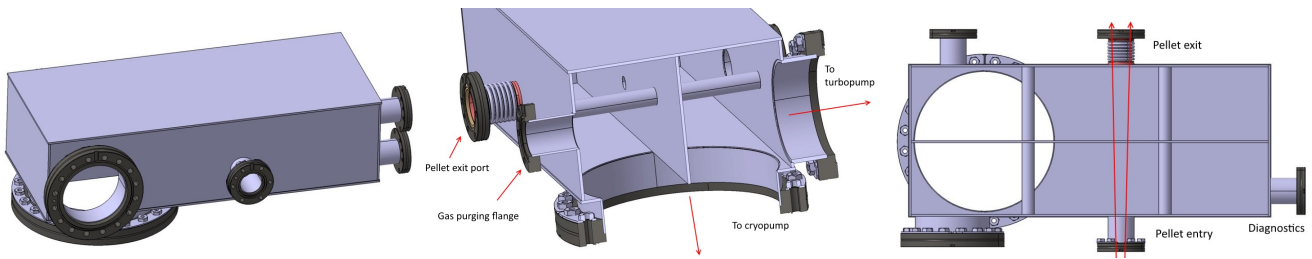


**Figure 3.19:** View of the central expansion vessel

available volume while providing all the necessary couplings for the vacuum system.

The central expansion vessel was made from flat stainless steel plates in order to hold the most possible volume, forming a box of  $525 \times 220 \times 138 \text{ mm}^3$  for a volume of approx. 13l. Rigid bars and an inner metal sheet were added to increase rigidity of the structure, as the pressure difference between the inner vacuum and outer atmospheric pressure leads to strong compressive forces on the structure. The inner sheet is outfitted with a hole for the free flight of the lithium pellets. As an added benefit, this sheet will partially impede the flow of propellant gas through the expansion chamber, providing differential pumping.

The expansion vessel possesses five CF 35 flanges, two of which are the entry and exit ports for the pellets. The other three are intended for diagnostics and vacuum system venting. A CF 200 flange is present to allow connection to the cryopump. Similarly, a CF 100 flange connects to the turbomolecular pump. The expansion vessel is shown in fig. 3.19.

### 3.3.1.2 Shielding tube

To prevent damage to other diagnostics and plasma facing components by stray lithium pellets, a shielding tube was developed. It consists on an electro-polished stainless steel tube of  $\phi 85 \text{ mm}$  outer diameter and  $\phi 81 \text{ mm}$  inner diameter. The tube is placed co-axially with the lithium injector, and extends from the S16 Bo port past the sniffer probe and optics tube, in or-

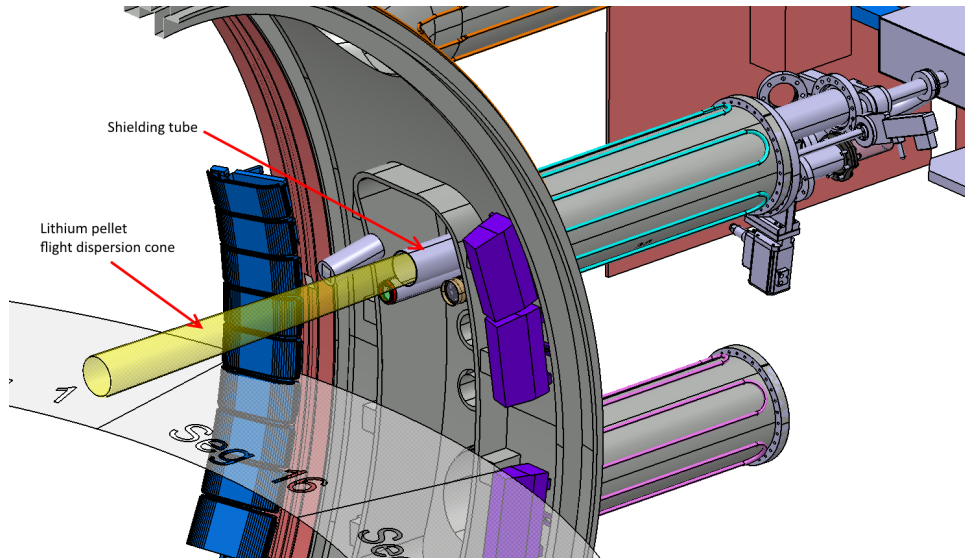


**Figure 3.20:** Lithium pellet flight dispersion cone and shielding tube

der to offer the greatest amount of protection without compromising lithium pellet transmission efficiencies, ensuring that pellets flying with an angular dispersion of  $2\sigma^5$  will reach the plasma. The shielding tube and pellet flight dispersion cone can be seen in figure 3.20.

### 3.3.1.3 Required vacuum pumps and valves

The vacuum pumping power for the lithium injector expansion vessel is provided by the turbomolecular pump and cryopump already installed in the test bed setup.

To provide optimal pumping power, the cryopump is situated as close to the expansion vessel as possible. Still, a  $90^\circ$  elbow is required due to space constraints, as other diagnostics are situated below the base platform, and access to the sector 16 Bo port optics tube must be respected.

The turbomolecular pump is located 1.4 m away from the expansion vessel, connected by a flexible CF 100 tube. This decision was motivated by the

---

<sup>5</sup> $\sigma$  represents the standard deviation of the pellet flight angular scatter with respect to the injector axis, if a normal distribution is assumed

strong magnetic fields at ASDEX Upgrade. Since the pump's rotor is a fast-moving electrical conductor, it will be under strong forces if placed inside a magnetic field above a certain strength and could break. Therefore, it is necessary to distance the pump from these coils. Additionally, the connecting tube effectively increases the expansion volume available for the lithium injector by another 10 l.

As in the test bed installation, a CF 100 gate valve is required to control the turbomolecular pump. Likewise, a CF 35 gate valve controls access to ASDEX Upgrade. This valve may only be opened once synchronization with the control room has been established and the trigger signal has been received, in order to always ensure safety to the torus and plasma facing components. Unlike the test bed installation however, no CF 200 valve is required for the cryopump.

At ASDEX Upgrade a valve before the cryopump is no longer required, since the vacuum can only be broken once each two days, when access to the torus hall is permitted, and there will always be an interval of at least 12 hours until the vacuum is needed again. Therefore, there is sufficient time to allow the cryopump to heat up to room temperature between operational periods of the lithium injector.

#### **3.3.1.4 Standardized connection parts and support structure**

As mentioned, a CF 200, 90° elbow is required to connect the cryopump to the central expansion vessel, as well as a CF 100 flexible tube that connects the expansion vessel to the turbomolecular pump. Additionally, a CF 35 flexible tube of 150 mm of length has been chosen to connect the central expansion vessel to the CF 35 valve which is connected to the torus. This tube has been included to provide the necessary separation between the entrance port and the expansion vessel so as to facilitate assembly and manipulation of other components at the Bo port. The distancing is enough to allow work in the area without compromising pellet transmission efficiencies. A flexible tube allows to compensate for small discrepancies between the real port structure

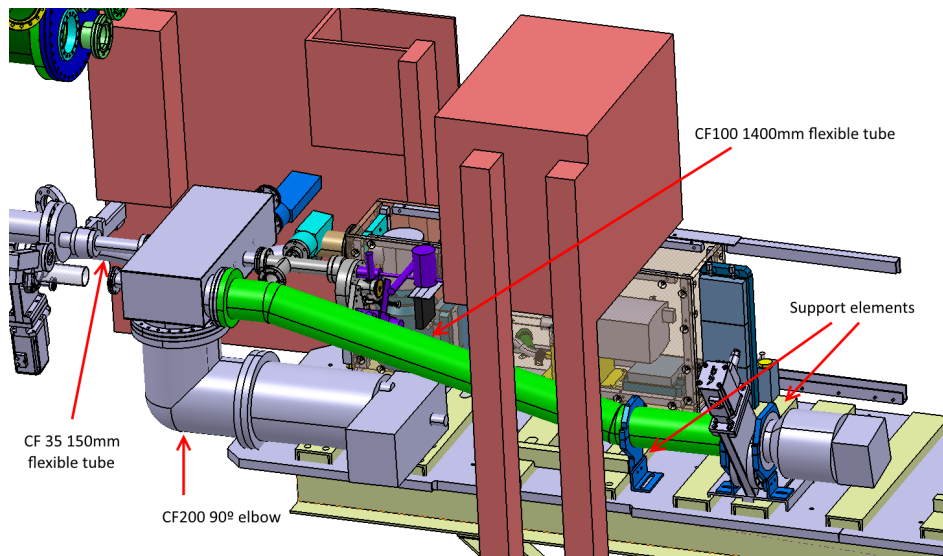


**Figure 3.21:** Lithium pellet injector installation in ASDEX Upgrade

and the model, and protects the system in case of expansions or contractions, which are expected during the scheduled heating phases of the reactor. The short length ensures that tube bending due to gravity or other forces is not an issue. A bent tube could intersect the pellet flight dispersion cone, jeopardizing pellet transmission efficiencies. All these elements are shown in fig. 3.21.

A support structure was designed to hold the turbomolecular pump and pump valve, the connection tube and the shielding tube. These structures can be seen in fig. 3.21, except this last one, which is visible in fig. 3.22.

### 3.3.2 Pressurized gas and cooling water lines

Similarly to the setup in the test bed, the lithium injector must be fed with a pressurized air line of 6 bar, as well as a propellant gas line of variable pressure to shoot the pellets. Similarly, a water line is required to provide cooling for the cryopump compressor. These lines are all available as part of the torus hall infrastructure. Unlike the test bed, no propellant gas bottle is used directly, as the ASDEX Upgrade safety regulations do not allow pressur-



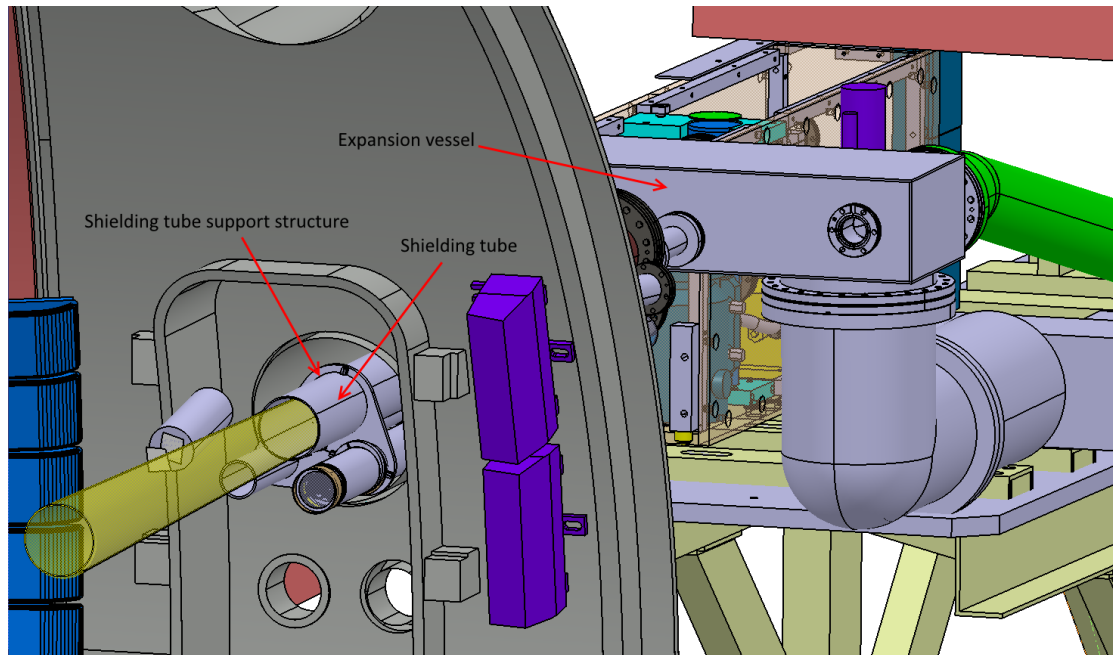


**Figure 3.22:** Shielding tube support structure

ized bottles to be mounted in the torus hall except for in special situations. Instead, the propellant gas bottle is located in a chamber designed to this effect outside of the torus hall, from where a preexisting gas line connects it to the torus hall interior. The lithium injector fast valve is connected to this gas line, which has a maximum operating pressure of 80 bar. This constitutes the maximum pressure for operation of the injector in ASDEX Upgrade.

### 3.3.3 Remote control electronics

Since torus hall access during ASDEX Upgrade operation is prohibited, a remote control system is required, as occurs with all other diagnostic systems. In the case of the lithium injector, a SIMATIC S7 FM 352-5 and WINCC system was chosen. These Siemens products constitute what is known as a SCADA<sup>6</sup> automation system, allowing collection and storage of information from different sensors and programmed control of actuators, facilitating

<sup>6</sup>Supervisory Control And Data Acquisition

conditional and procedural control while working from a given time stamp. This system can therefore be used to control the vacuum pumps in order to achieve a desired level of vacuum, activate and deactivate the electrovalves in order to change the revolver plate's position and keep track of this position, or coordinate a pellet firing sequence at specific times, which may be subject to external triggers and logical or Boolean operations.

Signals from the different systems are connected to labeled entry ports, from where their values can be stored, interpreted, operated upon and used as variables by the SIMATIC system. The man-machine interface is realized via a touchscreen on which a visual representation of the injector prepared by WINCC is running (fig. 3.23). Here, pre-programmed options are available to the user, such as visualizing data, changing revolver plate position or programming a series of pellet shots, being able to specify values such as time between shots, number of pellets injected, etc. Programmed series of shots can then be set to standby, and will be performed once a series of pre-specified conditions have been met, for example opening of the torus port valve and reception of the trigger signal from the ASDEX Upgrade control room.

A Boolean processor is the Siemens SIMATIC-compatible hardware system in charge of receiving the signals from SIMATIC and translating them into signals to be received by the different actuators (electrovalves, etc). It allows for signal processing within a precise time frame, with an internal clock time-frame  $1 \mu s$ .

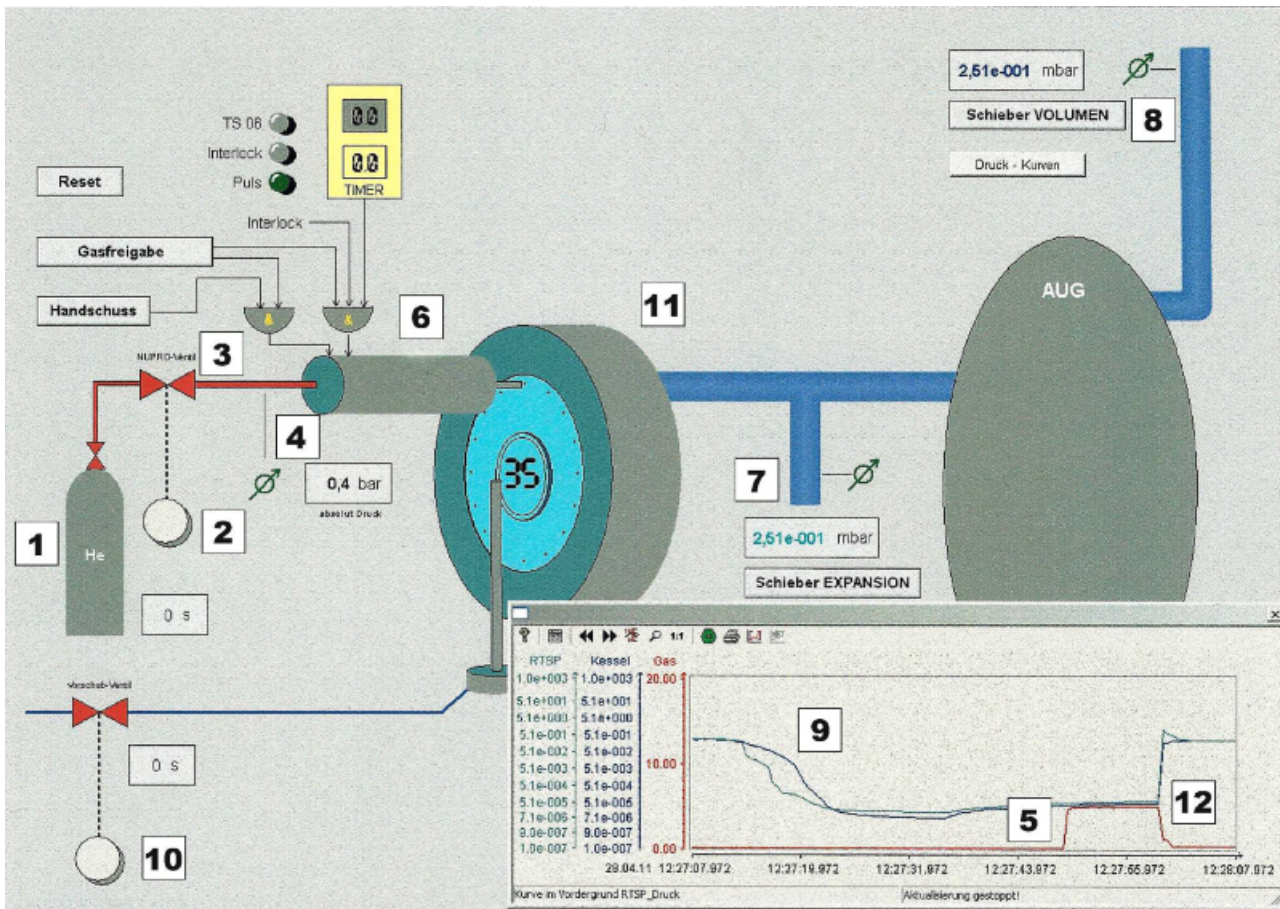


**Figure 3.23:** Visual representation of the lithium injector with the WINCC control program [Dem12]

- 1) Propellant gas bottle
- 2) Nupro safety valve
- 3) Propellant gas loading volume
- 4) Fast valve and pressure in the propellant gas loading volume
- 5) Plot of the propellant gas loading volume pressure
- 6) Visualization of boolean conditions for fast valve trigger
- 7) Pressure in the expansion volume
- 8) Pressure in the expansion tank (in test bed) or ASDEX Upgrade plasma vessel (in torus hall)
- 9) Plot of the pressure in the expansion volume and expansion tank/plasma vessel
- 10) Pneumatic actuation of the injector revolver plate
- 11) Pellet revolver plate showing the current rotation position
- 12) Pressure plot of a possible pellet shot

# Chapter 4

## Experimental procedure

### 4.1 Pellet transfer rate

Pellet transfer rates are recorded for propellant gas pressures of 10, 20, 30, 40, 50, 80 and 110 bar . After each firing series at a certain configuration, the expansion volume is closed and filled with nitrogen gas to atmospheric pressure, as per standard vacuum procedure, providing an inert atmosphere. The injector is subsequently opened, and each position in the revolver plate is checked for pellets. Contrasting with the initial (full) state, the amount of empty positions - and thus fired pellets - is tallied. Each series comprises 36 pellets, except those of 80 and 110 bar, where 18 pellets per gas pressure have been used, since no variation from the results at 50 bar was expected. This is confirmed in chapter 5.

### 4.2 Angular scatter

Similarly to the pellet transfer rate, angular scatter is also measured for different propellant gas pressures. Likewise, series also consist of 36 and 18 pellets for pressures of 10, 20, 30, 40, 50 and 80 and 110 bar respectively. The tests were performed parallel to the pellet transfer rate measurements. After

filling the expansion volume, the lithium pellet catching box is removed, and the marking paper is extracted, replacing it with a new one. The parameters of the test are noted on each paper beforehand.

Clearly outlying points are removed, provided that the number of removed points does not exceed 30% of the population. Since the paper is tilted inside the catching box, it is necessary to correct the influence of the tilt on the data. In the dispersion cloud on the paper, the maximum dispersion length is measured in both the direction of the projection of the flight path on the plane (longitudinal direction) and the direction perpendicular to this one. The latter requires no correction, while the former must be multiplied by  $\sin 45^\circ = \frac{\sqrt{2}}{2}$ . The greatest of the two values is taken as the dispersion length ( $d$ ). The distance from the pellet chamber to the catching box paper is  $l = 303$  mm. With this and the dispersion length, the angular scatter is calculated in equation 4.1, representing the angular scatter with a deviation of  $\sigma$ .

$$\alpha = 2 \cdot \arctan \left( \frac{d/2}{l} \right) \quad (4.1)$$

### 4.3 Pellet speed and speed scatter

Pellet speed and speed scatter are measured for propellant gas pressures of 30, 40, 50, 80 and 110 bar. Six pellets are fired at each pressure. During each shot of the sequence, in-flight pellets are detected by the light barriers, registering two distinct electric signals on the oscilloscope. One signal is the trigger, appearing at time  $t = 0$ . The other signal appears delayed or early. The time difference is the time the pellet has taken to pass from one light barrier array to the other one. The distance between both light barriers is known, 72 mm, and so the pellet flight speed can be taken as  $v = \frac{72 \text{ mm}}{\Delta t}$ . Speed scatter is taken as the standard deviation of all pellets fired with the same propellant gas pressure, assuming a normal distribution. An average speed scatter is calculated as the mean value of the speed scatters for each

propellant gas pressure.

## 4.4 Propellant gas flux

Prior use of the injector in 2011 with helium as propellant gas lead to termination of the plasma, due to excessive propellant gas fluxes. For this reason it was deemed necessary to utilize deuterium as propellant gas<sup>1</sup>, as well as to employ previously mentioned techniques to reduce the incoming gas fluxes to the torus: a larger expansion volume, an aperture and a cryopump.

The aperture consists on a nylon disk with an  $\phi$  14 mm hole. The disk fits in a plastic seal attached to a standard CF 35 coupling (fig. 4.1). It is intended to allow the pellet to continue its flight while providing a reduced cross section for the expanding gas. It is attached between the lithium injector vacuum system and the vacuum tank (which simulates the torus volume), thus hindering the gas from the injector from entering the vacuum tank. Nylon was chosen as the aperture material in the test bed due to its ease of manufacturing and good gas retention rates while still being chemically inert. For the tests at ASDEX Upgrade, the same principle of the aperture is implemented in the dividing plate inside the central expansion vessel, which is outfitted with a  $\phi$  20 mm hole coaxial to the pellet flight path. A larger diameter than in the case of the aperture was necessary, since the aperture was located 65 mm away from the lithium pellet injector port in the test bed, and 120 mm away in the case of the expansion tank at ASDEX Upgrade.

To test the effectiveness of the propellant gas flux reduction methods employed, peak pressure after a gas discharge was measured in both the expansion system and the vacuum tank. This was performed for the following scenarios, with the turbomolecular pump always functioning:

**Normal.** Only the turbomolecular pump is employed. This illustrates the effect of the increased expansion volume.

---

<sup>1</sup>Deuterium, the main plasma species, is less harmful to the plasma in comparison the the heavier helium gas



**Figure 4.1:** Nylon aperture

**Aperture.** The aperture is present between both vacuum systems.

**Cryopump.** The cryopump is employed

**Aperture + Cryopump.** Both the aperture and the cryopump are in operation. This is the intended working regime for use at AUG.

In each configuration, discharges are measured at pressures of 10, 20, 50, 80 and 110 bar (the maximum standard filling pressure of a deuterium gas bottle). Three discharges are measured per pressure. The mean value is used and the standard deviation is represented in the error bars. A normal distribution is assumed. Given the low deviation from the mean value in most cases, three discharges per pressure were considered sufficient.

The data were contrasted to the results obtained in 2011 in the configuration that lead to plasma termination, which serve as reference point [Ale11].

Valve	Electric resistance	Operating voltage
Current	0.9 $\Omega$	114 V
A	2.3 $\Omega$	340 V
B	1.0 $\Omega$	120 V

**Table 4.1:** Resistance and operating voltage of the fast valves

## 4.5 Replacement fast valve characterization

Given the importance of the lithium injector fast valve on important pellet parameters such as propellant gas flux and pellet speed, it was deemed necessary to characterize the two replacement fast valves A and B. The tests have been performed under identical conditions to the Normal scenario for propellant gas flux measurements, with the same expansion volume and turbomolecular pump, and without aperture or cryopump.

Peak gas content is measured in the expansion tank at different pressures. Additionally, gas evacuation times are also noted and compared.

These parameters are deemed sufficient to correctly characterize the three valves for use at ASDEX Upgrade.

Prior to the tests, the electrical resistance of all three valves has also been measured, as this determines the operating voltage of the valve. These are shown in table 4.1.



# Chapter 5

## Evaluation of the experimental results

### 5.1 Pellet transfer rate tests

Fig. 5.1 shows the tallied results of the pellet transfer rate tests. An uncertainty of  $\frac{1}{\sqrt{n}}$  was taken, where  $n$  represents the number of pellets in a sequence.

As shown in fig. 5.1, pellet transfer rates tend to increase with propellant gas pressure, plateauing at 100% approximate transfer rate for pressures of or above 50 bar. The local peak at 20 bar can be explained by the measurement uncertainty, as there is ample overlap between the error bars of the measurements for 20 and 30 bar.

In view of this information and with regard to the future tests at ASDEX Upgrade, propellant gas pressures of or above 50 bar are recommended, as they ensure transfer rates above 90%. Within this region, the choice of propellant gas pressure should be determined by other factors, as no difference in the transfer rate was observed for 50, 80 or 110 bar.

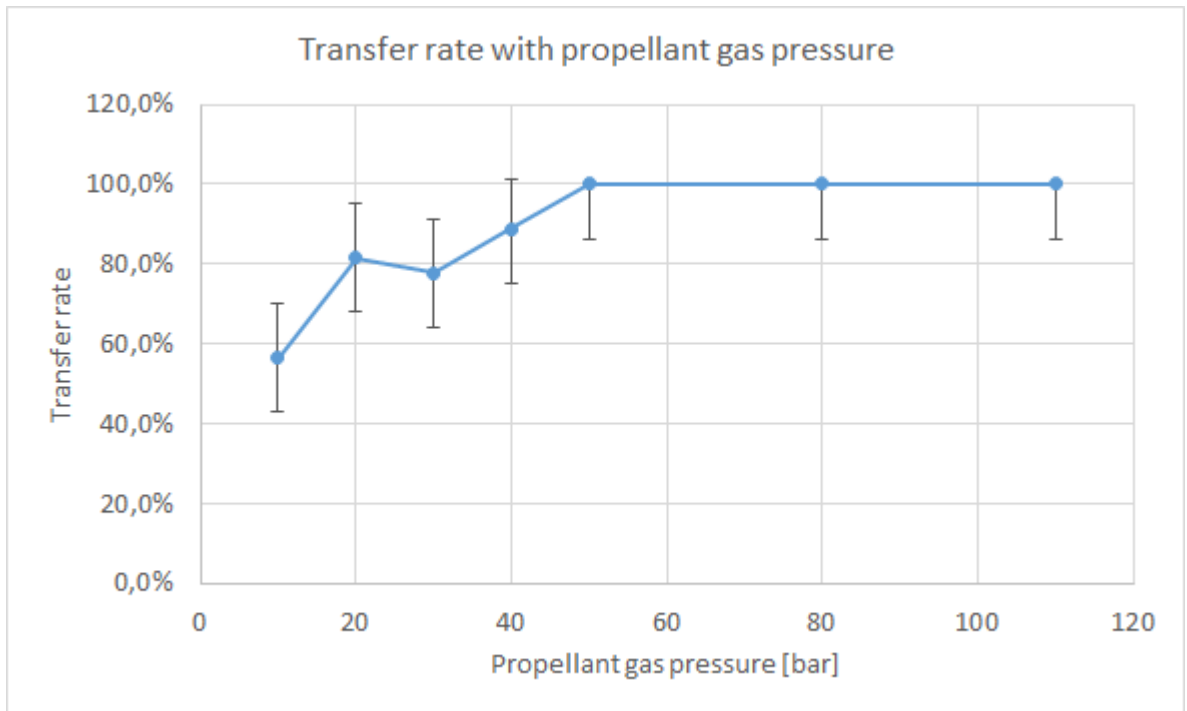


Figure 5.1: Pellet transfer rates with propellant gas pressure

## 5.2 Angular scatter measurements

The full cone scattering angle can be seen for each propellant gas pressure in fig. 5.2. The uncertainty calculations can be found in Appendix B.1, with values of approximately 5% being obtained.

As can be seen in fig. 5.2, pellet scattering angles are kept between  $1.2$  and  $0.95^\circ$  for all pressures, with a trend towards lower angles at higher pressures. Due to overlap between the error bars at low pressures, the peak at 20 and 30 bar is considered non-significant. Based on this information, it is determined that propellant gas pressure has only a slight impact on pellet angular scatter, with higher propellant gas pressures being recommended for use in ASDEX Upgrade.

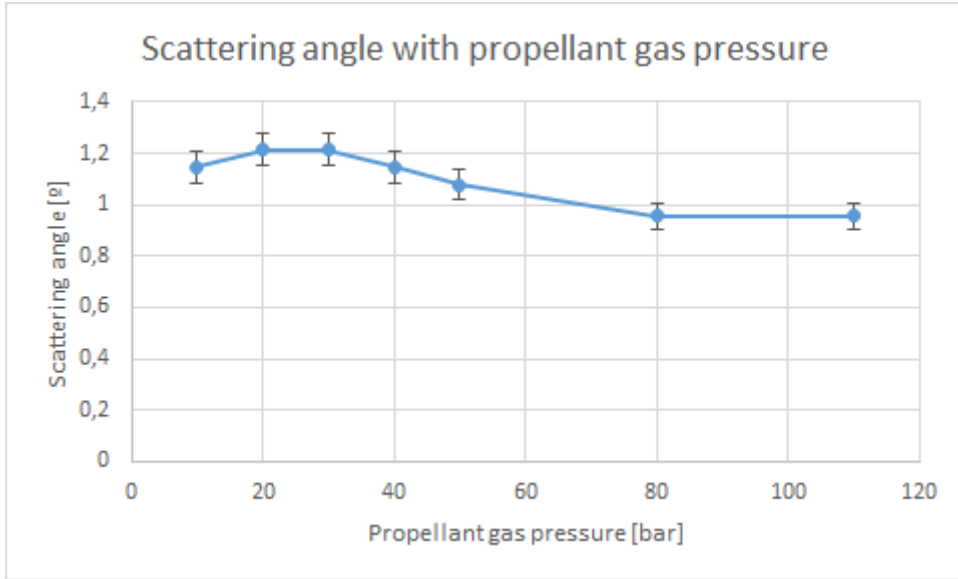


Figure 5.2: Pellet scattering angle with propellant gas pressure

### 5.3 Pellet speed and speed scatter measurements

The average pellet speeds for each propellant gas pressure used are shown in figure 5.3, along with their respective speed scatter.

Pellet flight speeds range from  $\sim 420 \frac{m}{s}$  at 30 bar to  $\sim 700 \frac{m}{s}$  at 110 bar, with an average speed scatter across all propellant gas pressures of  $\sigma = 21 \frac{m}{s}$ . As predicted by the model, higher pressures lead to higher speeds, with a sharp initial increase at low pressures and a flattening of the profile for pressures above 50 bar, since the propellant gas speed (and thus the pellet speed) cannot be greater than the sonic speed of the gas.

With this data in mind, it can be stated that high-speed<sup>1</sup> lithium pellets are available for use at ASDEX Upgrade, with a very low average speed scatter (at or below 5%). While high pellet flight speeds lead to greater penetration into the plasma, pressures in the 50 - 80 bar region are recommended for

<sup>1</sup>In comparison to the lithium injection methods used at other reactors, which typically cap at  $\sim 300 \frac{m}{s}$

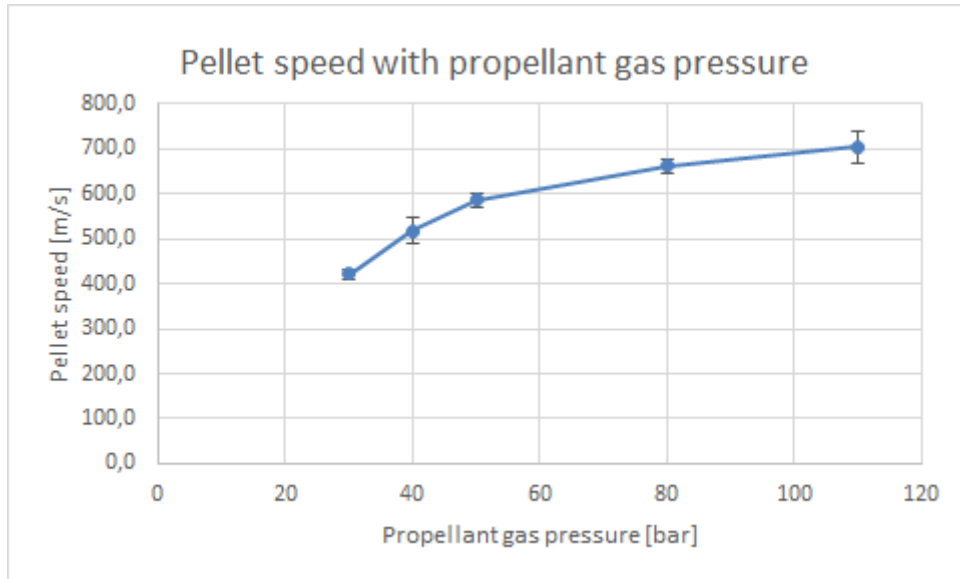


**Figure 5.3:** Pellet flight speed and speed scatter with propellant gas pressure

general deep penetration shots, since the pellet speed increase with pressure has a very limited effect beyond this region.

## 5.4 Propellant gas flux measurements

The peak amount of gas measured in the lithium injector expansion volume for each configuration and pressure is shown in fig. 5.4. Similarly, fig. 5.5 illustrates the peak amount of gas present in the vacuum tank that simulates the plasma vessel, for each configuration and pressure, as well as the reference scenario. It is worth noting the logarithmic scale used in both cases, as the data varied within several orders of magnitude.

In all tests, the lithium pellet catching box was removed in order to provide the gas pulse with a clear line of sight to the vacuum tank. This is similar to the conditions which would be present at ASDEX Upgrade. The presence of the catching box would suppose an obstacle to the gas reaching the tank, facilitating retention in the expansion volume and thus leading to too

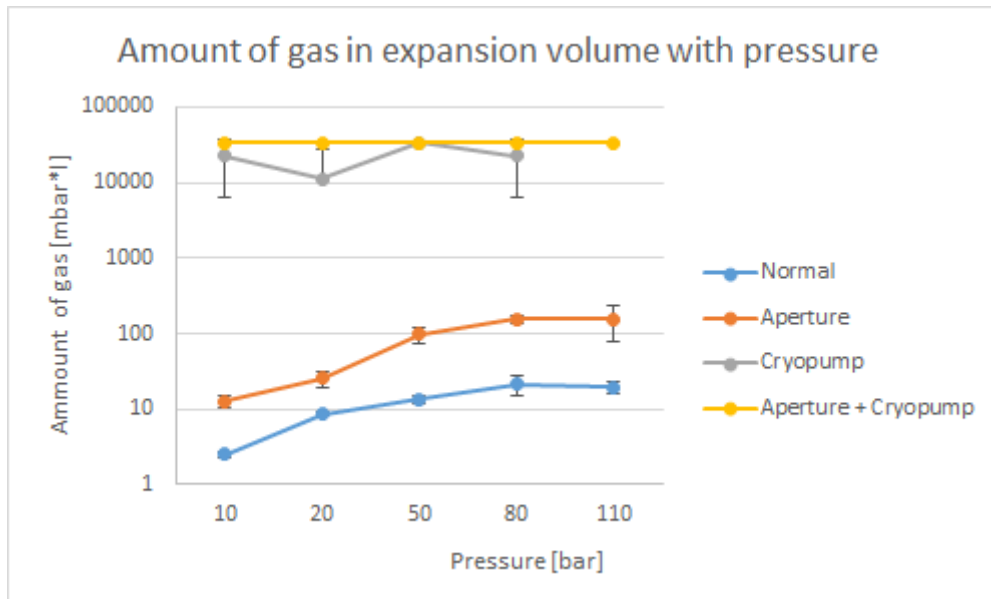


**Figure 5.4:** Peak amount of gas in the lithium injector expansion volume with pressure

optimistic results for the gas suppression.

### 5.4.1 Expansion volume

As was expected, in all scenarios the peak amount of gas measured increases with the operating pressure. Also for all pressures, all configurations show an enhanced gas retention when compared to the normal scenario. This is to be expected. Since the amount of gas ejected by the injector at any given pressure is the same in all cases, any scheme which aims to limit gas inflow to the vacuum tank (or plasma vessel) will invariably lead to an increase in the gas content inside the expansion system.

Of note are the large values obtained when using the cryopump, both with and without the aperture. It was seen during the experiment that gas discharges in these configurations produced a series of steep spikes in the pressure measurement. These spikes are due to warm gas suddenly heating the already frozen gas present on the cryopump surface, sublimating the gas and

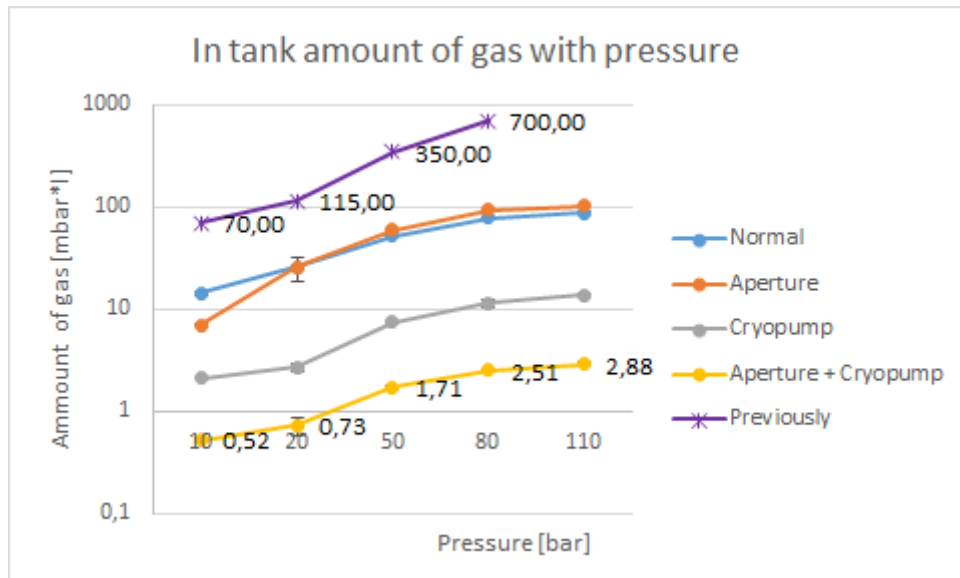


**Figure 5.5:** In tank amount of gas with pressure

producing a pressure spike. The gas is then very quickly once again frozen by the cryopump before it can exit the expansion volume. Due to the short duration of the process, these spikes could not always be measured, leading to a relatively high standard deviation for these scenarios. Nonetheless, the presence of the aforementioned spikes is testimonial to the fast response of the cryopump.

### 5.4.2 Vacuum tank

As occurred in the previous case, for all configurations an increase in pressure is directly linked to an increase of gas content. It is also clearly visible that all configurations offer significantly better results than those prior to the construction of the vacuum system. The lowest values are found with all systems in use (turbomolecular pump, aperture and cryopump), where a maximum reduction factor of 280 times the original values was measured for a propellant gas pressure of 80 bar.

Of note is the inversion of values for the Normal and Aperture scenarios for pressures of 20 bar and beyond. The data show that in this region the use

of an aperture hinders gas retention in the expansion volume, rather than facilitate it. The reason for this can be found in the operational regime of the turbomolecular pump. With the aperture in place (and without a cryopump), the expansion volume is subjected to a rough vacuum in the mbar range for a period of seconds. The turbomolecular pump cannot work under these conditions, thus hampering the effective pumping speed of the expansion volume. Consequently, more gas is allowed into the vacuum tank. This does not occur when the cryopump is in operation however, since in this case no lengthy low-level vacuum is achieved and the turbomolecular pump is allowed to function practically unhindered. With a cryopump, the inclusion of an aperture is beneficial, reducing gas content by a factor of 10 compared to when it is not in place.

At expected operating pressures of between 20 and 110 bar, with an expansion volume of 30 l, turbomolecular pump, cryopump and a separating plate with an aperture, the designed system will be able to provide a propellant gas flux reduction of 150 to 280 times the previously measured values.

## **5.5 Replacement fast valve characterization tests**

The peak gas content in the expansion tank with pressure for each fast valve is shown in fig. 5.6, while the average gas evacuation time can be seen for each fast valve and pressure in fig. 5.7.

### **5.5.1 Amount of gas**

As can be seen in the graph, valves A and B operate similarly, providing a gas output approximately 10 to 100 times greater than the original valve for propellant gas pressures of 10 and 20 bar, and reaching a maximum of just over 100000 mbar · l at higher pressures. This jump occurs between 20 and 50 bar for valve A, and between 20 and 30 bar for valve B. This is due to

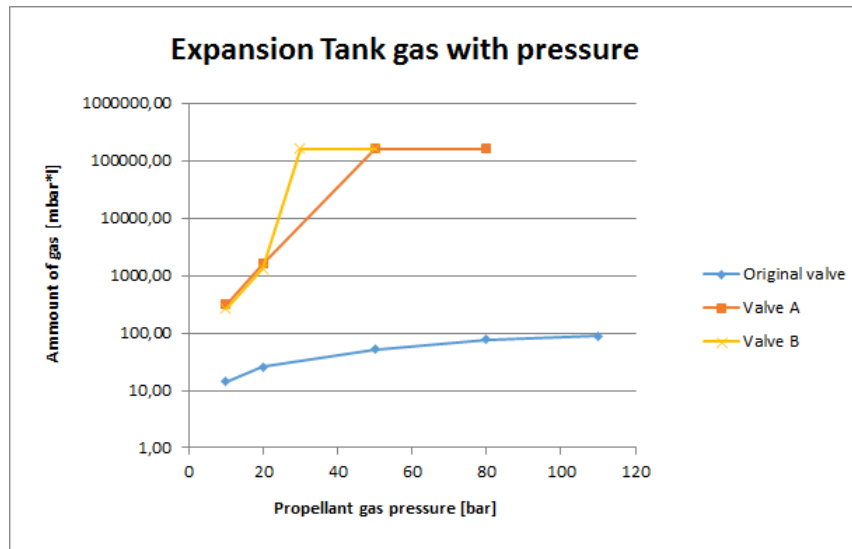


**Figure 5.6:** Expansion tank gas with pressure

the springs present within the valves offering less resistance than the spring present in the original valve. This spring counteracts the effect of the gas pressure and closes the valve once the electromagnet has been switched off. In the case of valves A and B, this spring is unable to overcome the force exerted by the gas at higher pressures.

Said maximum values would prove deadly for the plasma. For said reason, the replacement valves can only be used in AUG for low velocity pellets, using propellant gas pressures of maximum 20 bar.

### 5.5.2 Gas evacuation time

Gas evacuation times were measured without the use of cryopump or aperture, as these have an important effect on the gas evacuation times. The measured times are consistently of the order of 2-3 times higher with the replacement valves than with the original valve. This is linked to the valves' opening times, and helps to explain the large peak gas content values that were measured, since as already mentioned long exposure to rough vacuum inhibits the effect of the turbomolecular pump, further hindering gas evac-



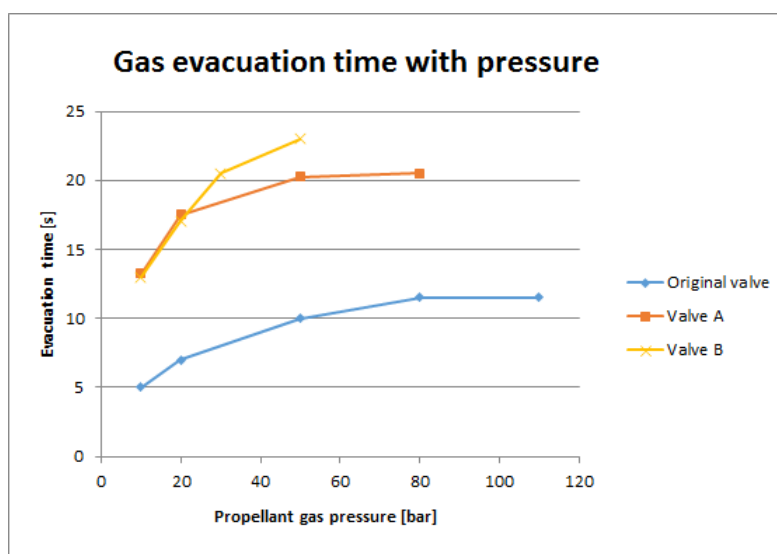


**Figure 5.7:** Gas evacuation time with pressure

uation. It is worth noting that gas evacuation times with the use of the cryopump are considerably shorter, and so the values shown here are not those expected during normal operation at ASDEX Upgrade. Thanks to this, no significant gas accumulation effects are expected while operating at 2 Hz.

Given these results, it has been determined that in the event of a fast valve malfunction, parts should be used from valves A and B to attempt to repair the fast valve currently in use. If this is impossible, the replacement valves can be used, albeit only in the lower operating pressure range.

# Chapter 6

## Conclusion

The goal of this project was to characterize and condition the lithium injector for use at ASDEX Upgrade. For this purpose it was necessary to design and model a vacuum system to be used in the installation, as well as construct and test the complete system in a test bed. The injector was characterized in its whole range of operating conditions, for pressures ranging from 10 to 110 bar.

As a conclusion of this project, it can be stated that the lithium pellet injector is capable of reliably firing high-speed pellets of  $\phi$  1.5 mm with frequencies of up to 2 Hz with low angular scatter. It was seen that transfer rates remained above 90% for all pressures of or above 50 bar. Likewise, it was determined that angular scatter is approximately at or below  $1^\circ$  within this same propellant gas pressure interval.

Speeds ranging from  $420\text{ m/s}$  (at 30 bar) to  $700\text{ m/s}$  (at 110 bar) have been measured, with an average speed scatter of  $\sigma = 21\text{ m/s}$ . These are consistent with a deep pellet penetration in the plasma, capable of reaching the plasma center.

Propellant gas flow rates have been successfully reduced by a factor of 100-200 for the envisioned operating regime, thus eliminating major risks for the plasma.

Lithium pellet injection experiments are planned at ASDEX Upgrade for

---

June and July. In view of these, it is recommended to use propellant gas pressures in the 50-80 bar range, according to desired pellet speed and penetration. In this region, the optimums in transfer rate and angular scatter are achieved, while higher pressures produce no direct benefits aside from a slight increase in pellet speed and slightly increase the propellant gas flow rates into the plasma. The repetition rate of 2 Hz is believed sufficient to study lithium pellet and lithium accumulation effects, and potentially reach the envisioned optimal injection rate. Pedestal broadening is expected, thus enhancing the operational space for pedestal studies, allowing for new scenarios to be tested.

If lithium injection is shown to be a useful experimental tool, future projects can be planned. A new lithium injection system may be developed to suit the current and future needs of ASDEX Upgrade and other tokamaks.

# Appendix A

## Test results

### A.1 Propellant gas flux tests

Propellant gas pressure	10	20	50	80	110
Pressure (exp) [mbar]	8.90E-02	3.07E-01	4.77E-01	7.67E-01	7.00E-01
Standard deviation [mbar]	9.43E-03	1.25E-02	6.34E-02	2.45E-01	1.28E-01
Pressure (tank) [mbar]	8.90E-02	1.60E-01	3.27E-01	4.87E-01	5.53E-01
Standard deviation [mbar]	4.50E-03	8.16E-03	4.71E-03	1.70E-02	9.43E-03
Gas (exp)[mbar · l]	2.49	8.59	13.35	21.47	19.60
Standard deviation [mbar · l]	0.26	0.35	1.78	6.85	3.59
Gas (tank) [mbar · l]	14.24	25.60	52.27	77.87	88.53
Standard deviation [mbar · l]	0.72	1.31	0.75	2.72	1.51

**Table A.1:** Propellant gas flux results for the “Normal” scenario

Propellant gas pressure	10	20	50	80	110
Pressure (exp) [mbar]	4.53E-01	9.10E-01	3.50E+00	5.47E+00	5.57E+00
Standard deviation [mbar]	7.85E-02	2.12E-01	8.83E-01	7.59E-01	2.74E+00
Pressure (tank) [mbar]	4.40E-02	1.60E-01	3.73E-01	5.87E-01	6.47E-01
Standard deviation [mbar]	8.16E-04	4.15E-02	4.71E-03	4.71E-03	4.71E-03
Gas (exp)[mbar · l]	12.69	25.48	98	153.07	155.87
Standard deviation [mbar · l]	2.20	5.93	24.73	21.24	76.83
Gas (tank) [mbar · l]	7.04	25.60	59.73	93.87	103.47
Standard deviation [mbar · l]	0.13	6.64	0.75	0.75	0.75

**Table A.2:** Propellant gas flux results for the “Aperture” scenario

Propellant gas pressure	10	20	50	80	110
Pressure (exp) [mbar]	8.00E+02	4.00E+02	1.20E+03	8.00E+02	1.20E+03
Standard deviation [mbar]	5.66E+02	5.66E+02	0.00E+00	5.66E+02	0.00E+00
Pressure (tank) [mbar]	1.30E-02	1.67E-02	4.70E-02	7.13E-02	8.57E-02
Standard deviation [mbar]	0.00E+00	1.70E-03	8.16E-04	6.02E-03	1.70E-03
Gas (exp)[mbar · l]	22400.12	11200.04	33600	22400.02	33600
Standard deviation [mbar · l]	15839.02	15839.17	0.00	15839.17	0.00
Gas (tank) [mbar · l]	2.08	2.67	7.52	11.41	13.71
Standard deviation [mbar · l]	0.00	0.27	0.13	0.96	0.27

**Table A.3:** Propellant gas flux results for the “Cryopump” scenario

Propellant gas pressure	10	20	50	80	110
Pressure (exp) [mbar]	1.20E+03	1.20E+03	1.20E+03	1.20E+03	1.20E+03
Standard deviation [mbar]	0.00E+00	0.00E+00	0.00E+00	0.00E+00	0.00E+00
Pressure (tank) [mbar]	3.27E-03	4.53E-03	1.07E-02	1.57E-02	1.80E-02
Standard deviation [mbar]	1.25E-04	9.18E-04	4.71E-04	4.71E-04	8.16E-04
Gas (exp)[mbar · l]	33600	33600	33600	33600	33600
Standard deviation [mbar · l]	0.00	0.00	0.00	0.00	0.00
Gas (tank) [mbar · l]	0.52	0.73	1.71	2.51	2.88
Standard deviation [mbar · l]	0.02	0.15	0.08	0.08	0.13

**Table A.4:** Propellant gas flux results for the “Aperture + Cryopump” scenario

Propellant gas pressure	10	20	50	80
Gas (tank) [mbar · l]	70	115	350	700

**Table A.5:** Propellant gas flux results for the “Previously” scenario

## A.2 Replacement fast valve characterization tests

Propellant gas pressure	10	20	50	80	110
Evacuation time [s]	5	7	10	11.5	11.5
Pressure (tank) [mbar]	8.90E-02	1.60E-01	3.27E-01	4.87E-01	5.53E-01
Gas (tank) [mbar · l]	14.24	25.60	52.27	77.87	88.53

**Table A.6:** Results for the fast valve currently in use

Propellant gas pressure	10	20	50	80
Evacuation time [s]	13.25	17.5	20.25	20.5
Pressure (tank) [mbar]	1.95	9.95	1000	1000
Gas (tank) [mbar · l]	312	1592	160000	160000

**Table A.7:** Results for the replacement valve A

Propellant gas pressure	10	20	30	50
Evacuation time [s]	13	17.075	20.5	23
Pressure (tank) [mbar]	1.65	8.2	1000	1000
Gas (tank) [mbar · l]	264	1312	160000	160000

**Table A.8:** Results for the replacement valve B

Pressure [bar]	Transfer rate [%]	Uncertainty [%]
10	57%	14%
20	82%	14%
30	78%	14%
40	89%	14%
50	100%	14%
80	100%	14%
110	100%	14%

**Table A.9:** Transfer rate results

Pressure [bar]	Scatter d [m]	Angle [°]
10	6	1.15
20	6.36	1.22
30	6.36	1.22
40	6	1.15
50	5.65	1.08
80	5	0.96
110	5	0.96

**Table A.10:** Angular scatter results

Pressure [bar]	Speed [ $\frac{m}{s}$ ]	Speed scatter [ $\frac{m}{s}$ ]
30	421	10
40	517	29
50	587	17
80	663	15
110	705	35
Average		21

**Table A.11:** Speed and speed scatter results

### **A.3 Transfer rate**

### **A.4 Angular scatter**

### **A.5 Speed and speed scatter**



# Appendix B

## Calculation of uncertainty

### B.1 Angular scatter

Pellet flight angular scatter is determined through the impact position left on the catching box plate. It is calculated from the scatter diameter on the plate  $d$  and the distance from the lithium injector pellet chamber to the plate  $l = 303$  mm through equation 4.1. The measurement uncertainty in this test is thereby dependent on both of these values, as well as their respective measurement uncertainties. These are taken to be the minimum measuring unit of the instrument (in this case 1 mm, using a standard ruler) or 5% of the total measurement, whichever may prove greatest of the two, thus providing a conservative approximation.

$$\Delta\alpha = \left| \frac{\partial\alpha}{\partial d} \right| \cdot \Delta d + \left| \frac{\partial\alpha}{\partial l} \right| \cdot \Delta l = \left| \frac{l}{d^2 + l^2} \right| \cdot \Delta d + \left| -\frac{d}{d^2 + l^2} \right| \cdot \Delta l \quad (\text{B.1})$$

Where:

$$l = 0.303 \text{ m}$$

Angle [°]	d [m]	Error [°]	Relative error (%)
0.9	0.0048	0.048	5.32
0.95	0.0050	0.050	5.30
1	0.0053	0.053	5.28
1.05	0.0056	0.055	5.26
1.1	0.0058	0.058	5.25
1.15	0.0061	0.060	5.23
1.2	0.0063	0.062	5.22

**Table B.1:** Angular scatter uncertainty

$$\Delta l = 0.05 \cdot s = 0.015 \text{ m}$$

$$\Delta d = 1 \cdot 10^{-3} \text{ m}$$

## B.2 Pellet speed

The pellet flight speed is measured through a set of two light barrier arrays.

These have a separation of  $s = 72 \text{ mm}$ . These light barriers produce an electrical signal which is recorded on an oscilloscope with negligible delay.

The uncertainty in the pellet speed will therefore be dependent of the time

it takes the pellet to pass by the light barriers, the time division of the oscilloscope and the uncertainty regarding the position of the light barriers.

This last one is measured with a standard ruler, with a minimum division of 1 mm.

$$\Delta v_p = \left| \frac{\partial v_p}{\partial s} \right| \cdot \Delta s + \left| \frac{\partial v_p}{\partial t} \right| \cdot \Delta t = \left| \frac{1}{t} \right| \cdot \Delta s + \left| -\frac{s}{t^2} \right| \cdot \Delta t \quad (\text{B.2})$$

Where:

$$s = 0.072 \text{ m}$$

$$\Delta s = 1 \cdot 10^{-3} \text{ m}$$

$$\Delta t = 1 \cdot 10^{-6} \text{ s}$$

Table B.2 shows the uncertainty in the pellet speed measurement.

Speed [m/s]	Time [s]	Error [m/s]	Relative error (%)
400	0.00018	8	1.9
450	0.00016	9	2
500	0.00014	10	2.1
550	0.00013	12	2.2
600	0.00012	13	2.2
650	0.00011	15	2.3
700	0.00010	17	2.4
750	0.000096	18	2.4
800	0.00009	20	2.5

**Table B.2:** Pellet speed uncertainty

# Appendix C

## Lithium loading procedure

During the operation of the lithium injector it was seen that care must be placed on the lithium loading procedure. Failure to do so lead to a decalibrated revolver plate and possible lithium buildup inside the machine, leading to severely reduced transfer efficiencies (20%-50%). To avoid this, a guideline was elaborated.

1. The injector must be loaded while open at its middle section, so as to be able to verify the revolver plate position.
2. The  $\phi$  6 mm to  $\phi$  2.5 mm extruder is loaded with one pre-cut lithium bar ( $\phi$  6 mm by 30 mm).
3. An approximately 50 mm long section is extruded, with the tip of the section being removed. The rod is folded once and coiled around itself, and the extrusion pin is unscrewed two complete turns, so that the lithium inside is no longer in contact with the pin.
4. The coiled rod is inserted into the  $\phi$  2.5 mm to  $\phi$  1.5 mm extruder, with the extrusion nozzle on level screwed in and on level with the injector. A nut or cylinder of min. 8 mm in height is fitted into the extrusion pin in order to act as an end mark.

- 
5. The extrusion pin is turned until lithium starts to exit the nozzle. The tip is cut and discarded.
  6. The alignment of the revolver plate and general cleanliness of the injector is checked. All surfaces in contact with the revolver plate (as well as the revolver plate itself) must be clean. If lithium is seen on the inner side of the revolver plate (extrusion side), the plate must be completely removed, cleaned, and reinserted with new passing pins. In this case, the injector must be fully loaded and a full sequence is needed for calibration, since the passing pins tend to deform slightly in the first sequence after they are inserted.
  7. The revolver plate position aligned with the fast valve is used for calibration (optically). The brass cone and rod are used for calibration on the revolver plate position aligned with the extruder (pass - no pass).
  8. The extruder is screwed with O-ring onto the injector. Lithium is extruded into the revolver plate holes, checking that the extruder exit aligns with the hole before extrusion. During extrusion, a conical pin is pressed against the other side of the hole to ensure that the lithium pellet does not extend beyond the hole.
  9. The extrusion into a hole must be done relatively quickly if possible, so that the lithium does not have a chance to over expand. Per hole, a turn of  $60^\circ - 90^\circ$  is needed.
  10. After extrusion of the last hole, one more revolver plate position must be turned, so that the lithium rod is broken. Otherwise the lithium rod from the last pellet will continue attached to the extruder, and will exit the hole if the extruder is removed.
  11. The extruder is removed and the brass plug with O-ring is screwed onto the injector extrusion hole.

- 
12. Very slowly, the injector is closed, avoiding that any pellet falls out of the hole and remains inside the injector, as it would smear and possibly block the pellet chamber opening.
  13. The nozzle and extrusion pin of the  $\phi$  2.5 mm to  $\phi$  1.5 mm extruder are removed, and the extruder is cleaned in water. The extruder is dried with paper towels and pressurized air.

# Appendix D

## Vacuum

### D.1 Vacuum system at ASDEX Upgrade





## D.2 pump specifications

Pump rate $\left[\frac{l}{s}\right]$	12.67
Minimum vacuum pressure [mbar]	$\approx 4 \cdot 10^{-4}$
Minimum vacuum pressure with gas ballast [mbar]	$\approx 4 \cdot 10^{-3}$
Rotation speed [rpm]	1725
Power consumption [kW]	1.12
Connection flange	KF40
Weight [kg]	73.94
Maximum operating temperature [K]	313

**Table D.1:** Specifications of the Leybold Trivac D30A vacuum pump [Vac]

Pump rate $\left[\frac{l}{s}\right]$	345
Minimum vacuum pressure [mbar]	$< 10^{-10}$
Forevacuum pressure [mbar]	$10^{-2} - 10^{-3}$
Rotation speed [rpm]	45000
Startup time [s]	180
High vacuum port	CF100
Weight [kg]	11
Maximum operating temperature [K]	328

**Table D.2:** Specifications of the Leybold Turbovac 360 turbopump [Vac04]

Pumping speeds (hydrogen) $\left[\frac{l}{s}\right]$	2500
Throughput (Argon) $\left[\frac{mbar \cdot l}{s}\right]$	11.86
Capacity (hydrogen at $6.67 \cdot 10^{-8}$ mbar) [l]	12
Cooldown time [hours]	1.5
Connection flange	CF200
Weight [kg]	20.4

**Table D.3:** Specifications of the Cryo-Torr 8 cryopump [CC]

# Appendix E

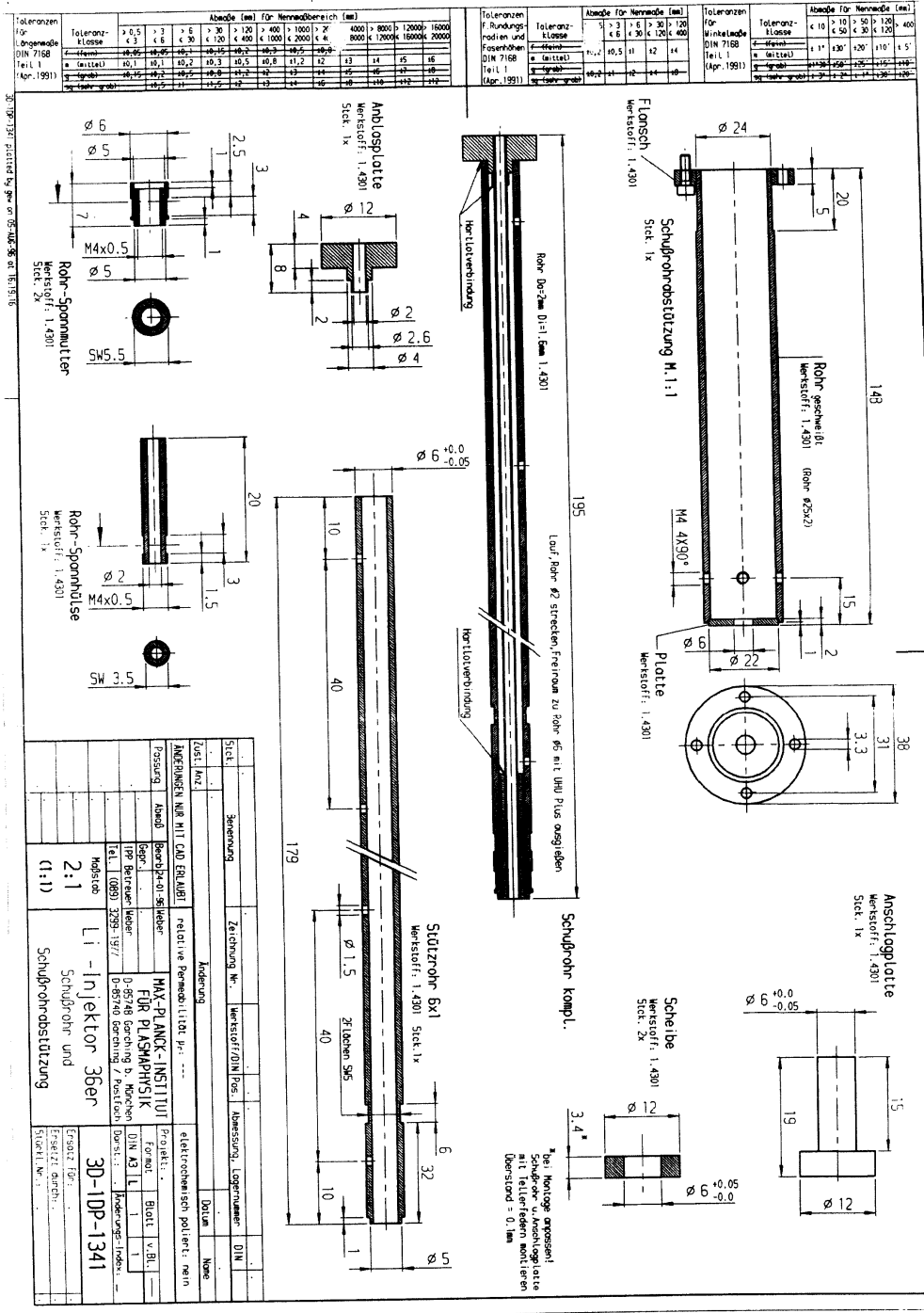
## Lithium injector drafts

E.1 Injector

E.2 Pneumatics

E.3 Diagnostics

E.4 Extrusion



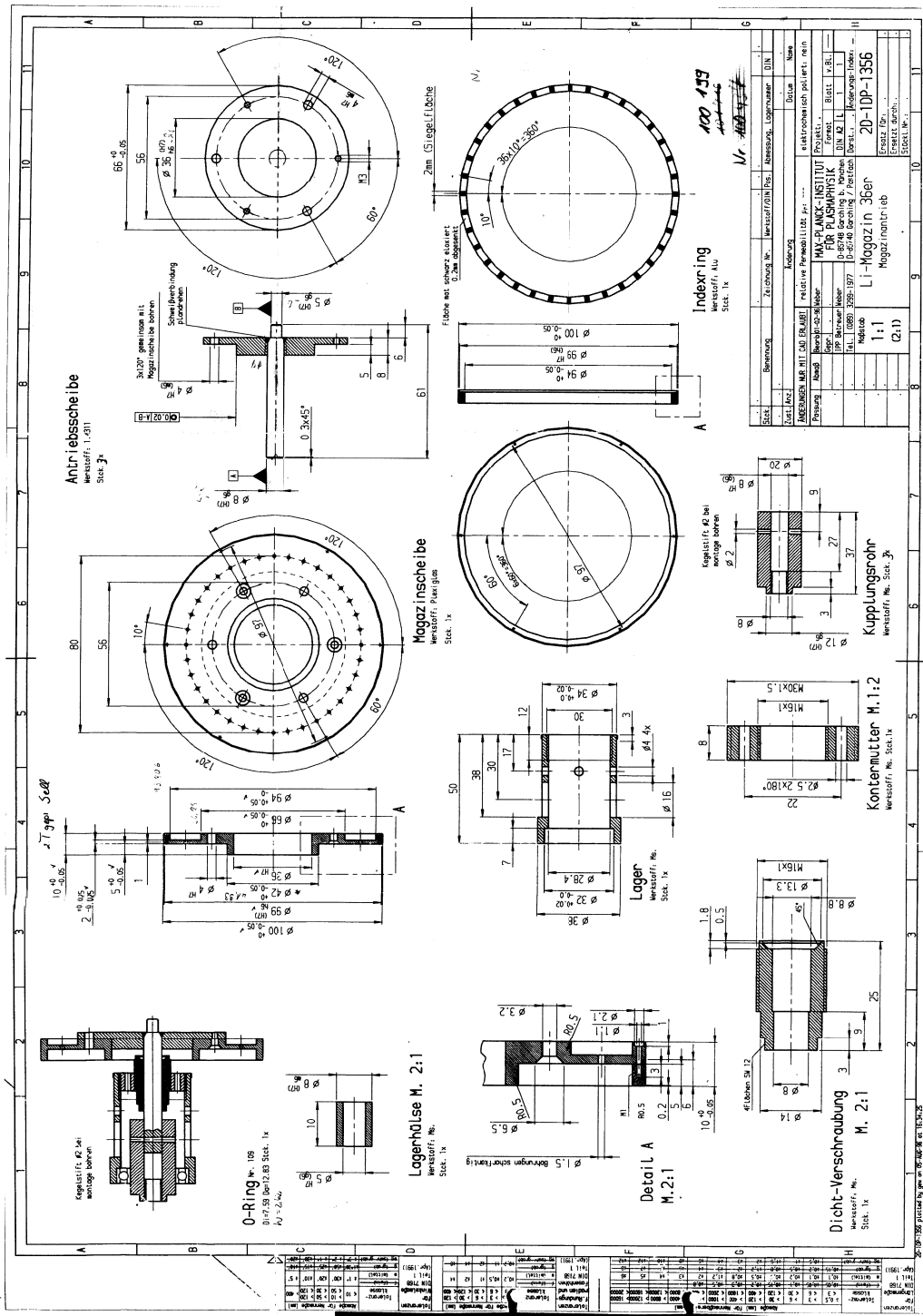


Figure E.2: Lithium injector revolver plate draft [MPIFP]

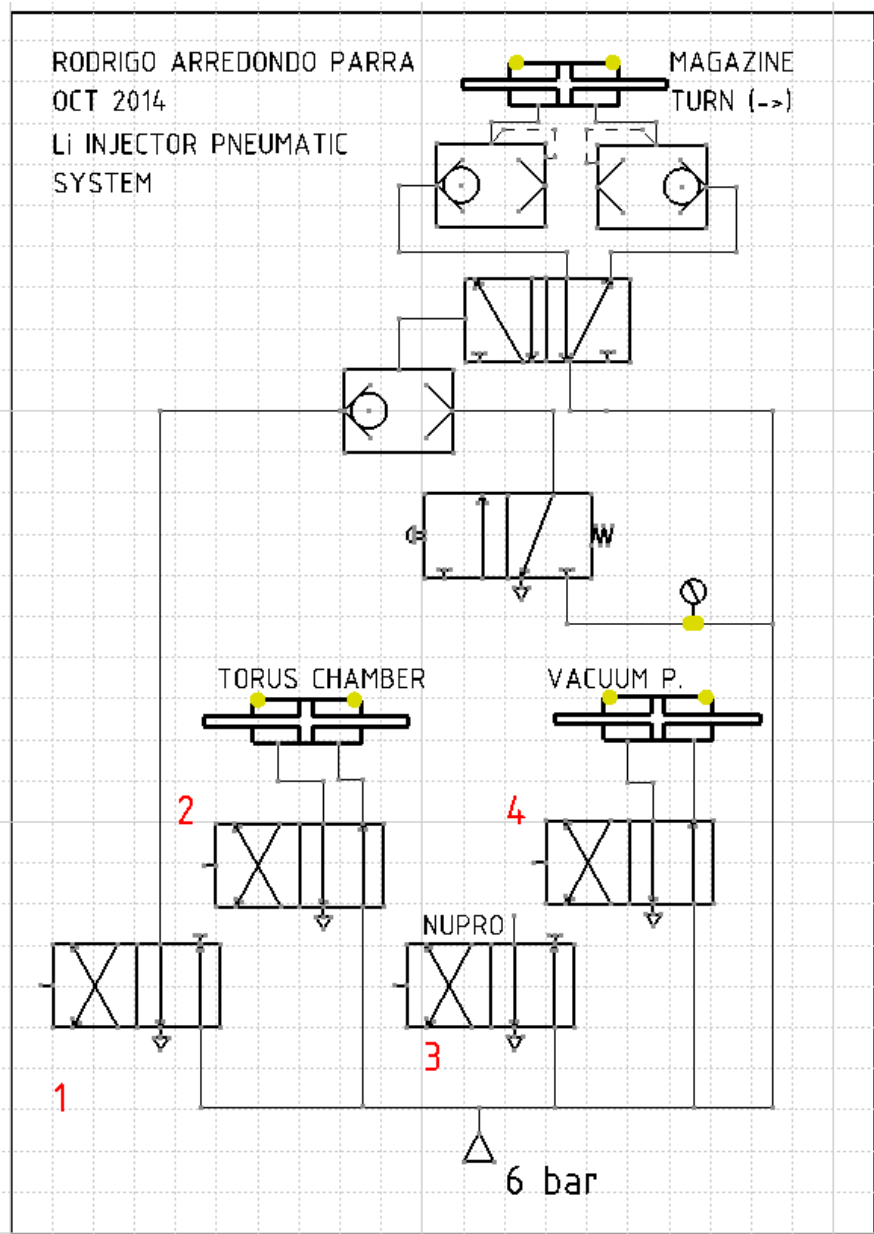


Figure E.3: Lithium injector pneumatic system



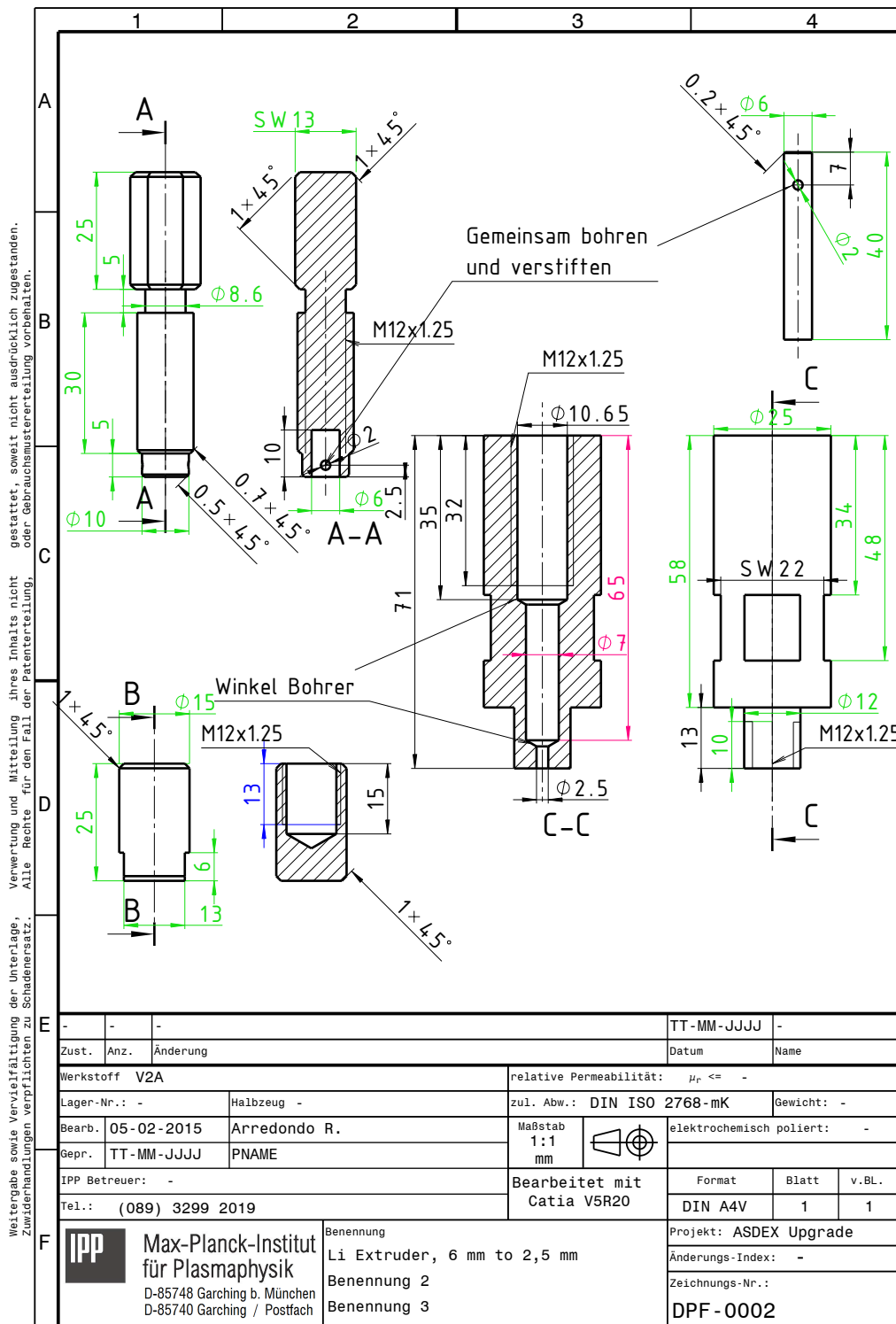


Figure E.5: Lithium injector extruder,  $\phi$  6 mm to  $\phi$  2.5 mm





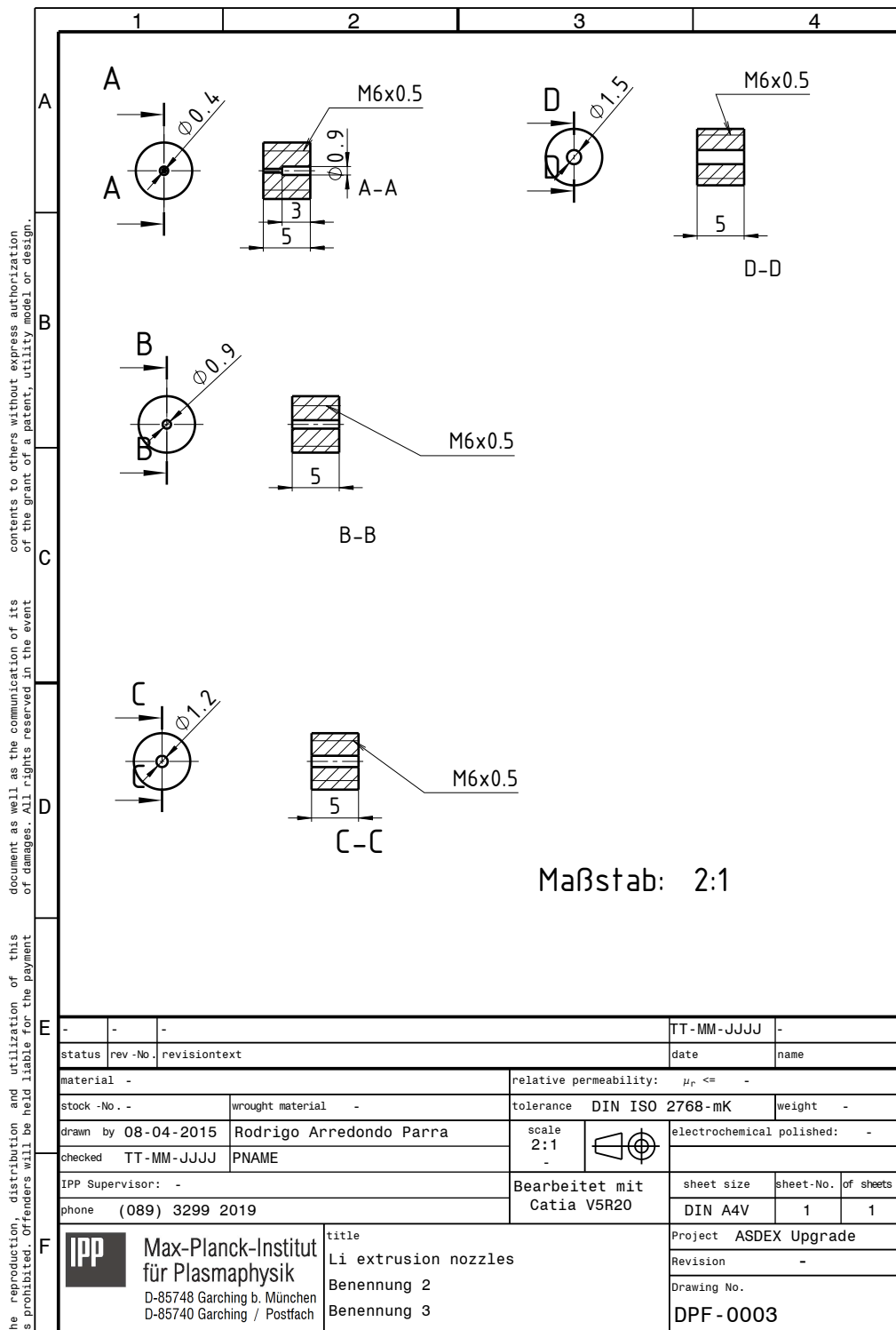


Figure E.7: Lithium injector extrusion nozzles,  $\phi$  1.5 mm to  $\phi$  0.4 mm

# Appendix F

## Electronics

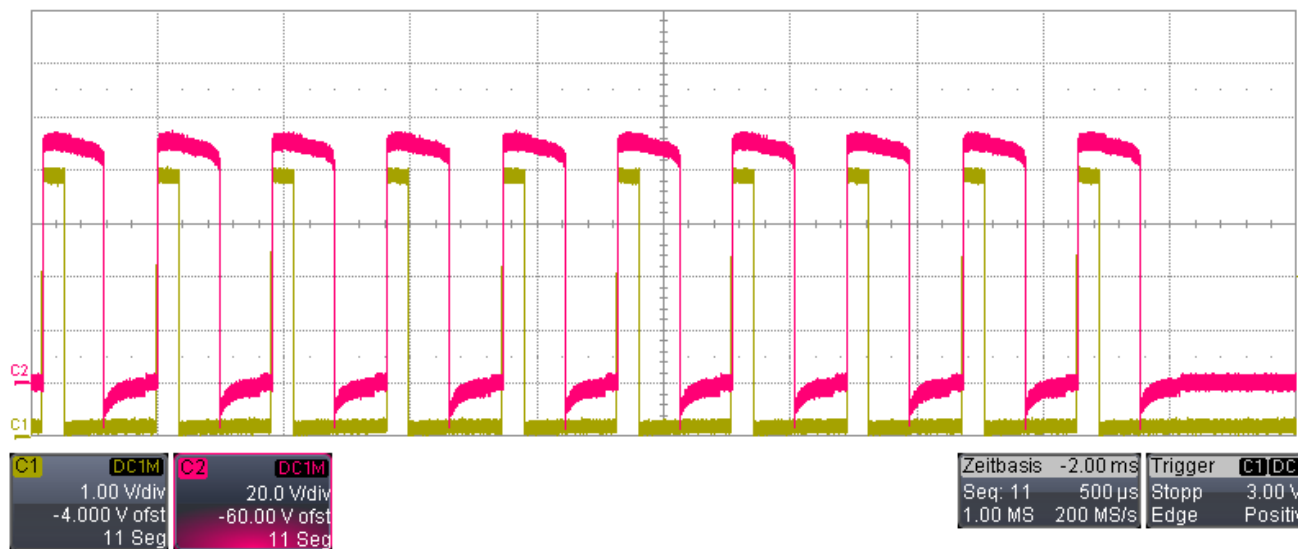
### F.1 Fast valve trigger sequence

Lab Notebook Entry from LeCroy DSO  
 DSO S/N: LCRY0616N50688  
 User: LeCroyUser  
 Time: 4/8/2015 2:32:15 PM

4/8/2015 2:32:15 PM



Valve Test mit 10 Pulse u. Kniel Netzteil 120V 7A  
 Ch1: Trigger  
 Ch2: Spannung am Ventil (Teiler 1:10)



**Channel Status**

	C1	C2
<b>Vertical</b>		
V / Div	1.00 V	20.0 V
Offset	-4.000 V	-60.00 V
Coupling	DC1M*	DC1M*
BW-Limit	Full	Full
Probe	1.000000	10.0000
Sweeps	1 #	1 #

**Acquisition Status**

<b>Horizontal</b>	Time / Div	500 µs	Sampling Rate	200 MS/s	Segments	11
	Time / Pt	5.000 ns	Sampling Mode	Sequence		
	Pts / Div	100.0000 kS	Trigger Delay	-2.00 ms		
	Mode	Stop	Slope	Positive		
<b>Trigger</b>	Type	Edge	Level	3.00 V		
	Source	C1	Coupling	DC		

## **F.2 Lithium Injector SIMATIC control system**

# LPI

( Lithium - Pellet - Injektor)

(Pelletgruppe)

Kostenstelle 20916

Steuerung mit  
Simatic S7 und WinCC

( Betriebssteuerung im Pelletlabor - L2 )


Wolfgang Weisbart  
Telefon 2022

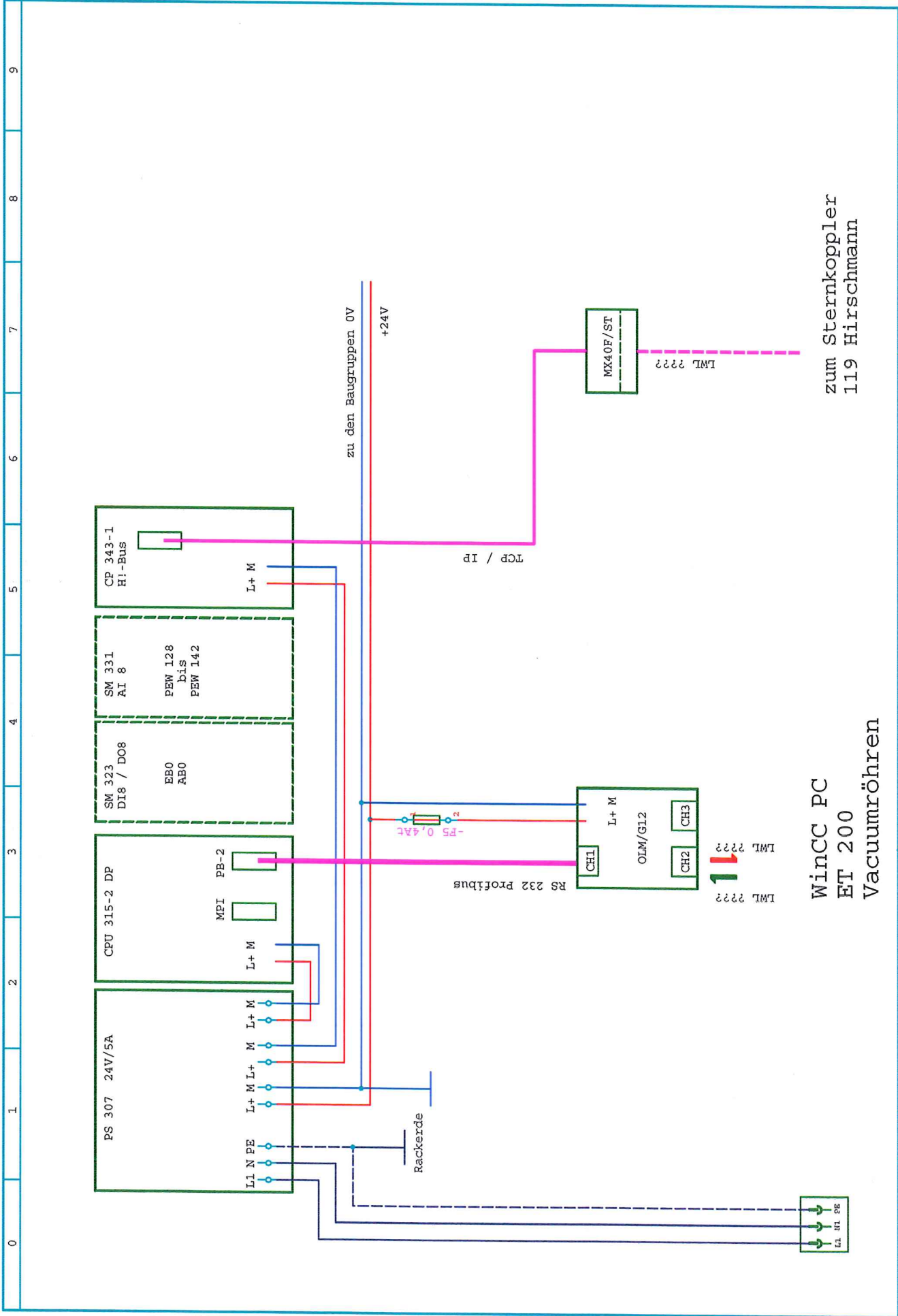
Max-Planck-Institut für Plasmaphysik		ASDEX Upgrade	
Bearb.	Weisbart	C:\WSCAD55\PROJEKTE\Lithium-Injektor\LIP-Deck	Blatt 1
Datum	18.11.14		von 1 Bl.

# Inhalt von: Lithium - Pellet - Injektor

Seite : 1

Nr.	Datei	Projektseite	Kommentar	Datum
1	LPI_I.0001		Inhaltsangabe	12.02.2015
2	LIP.0001		Übersicht Zentralgerät	10.02.2015
3	LIP.0002		Digitale Eingänge EB0	11.02.2015
4	LIP.0003		Digitale Ausgänge AB0	10.02.2015
5	LIP.0004		Anloge Eingänge PEW128-PEW134	11.02.2015
6	LIP.0005		Anloge Eingänge PEW136-PEW142	11.02.2015
7	LIP.0006		Übersicht Erweiterungsgerät	11.02.2015
8	LIP.0007		Digitaleingänge E21-E22	11.02.2015
9	LIP.0008		Digitaleingänge E23	11.02.2015
10	LIP.0009		Digitalausgänge A21-A22	11.02.2015
11	LIP.0010		Anloge Eingänge PEW50-PEW56	12.02.2015
12	LIP.0011		Anloge Ausgänge PAM50-PAM52	11.02.2015
13	LIP.0012		Digitalausgänge Ventilinsel	10.02.2015
14	RTSP_ST.0001		Steckerplan	04.02.2015
15	RTSP_ST.0002		Steckerplan	04.02.2015
16	RTSP_FG.0001		Pneumatic	20.11.2014

Datum	12.02.2015	 Max-Planck-Institut für Plasmaphysik	Lithium - Pellet - Injektor	Inhaltsangabe	Blatt	1
Bearb.	MS/ENST				=	von
					C:\WSCAD55\PROJEKTE\Lithium-Injektor\LPI_I	



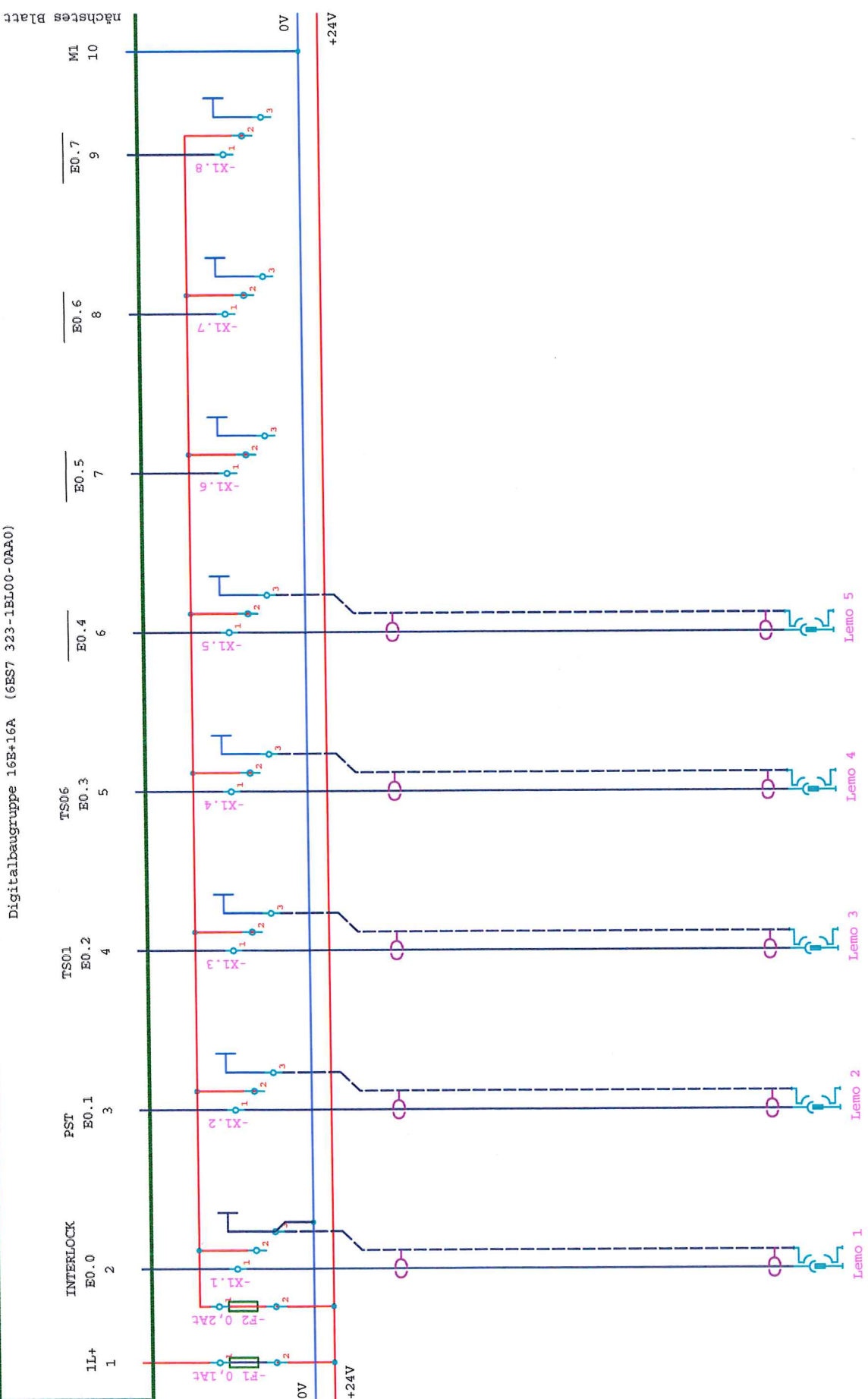
WinCC PC  
ET 200  
Vacuumröhren

zum Sternkoppler  
119 Hirschmann

Zust.	Änderung	Datum	Name	Norm	Gepr.	Beisbart	15.04.2015	ASDEX Upgrade Pellet	IPP Max-Planck-Institut für Plasmaphysik	Lithium - Pellet - Injektor LPI - Lithium - Pellet - Injektor	Übersicht Zentralgerät
								C:\MSCAD55\PROJEKTE\Lithium-Injektor\IIP			Projektseite
										von Seiten	Blatt 1 von 12 Bl.

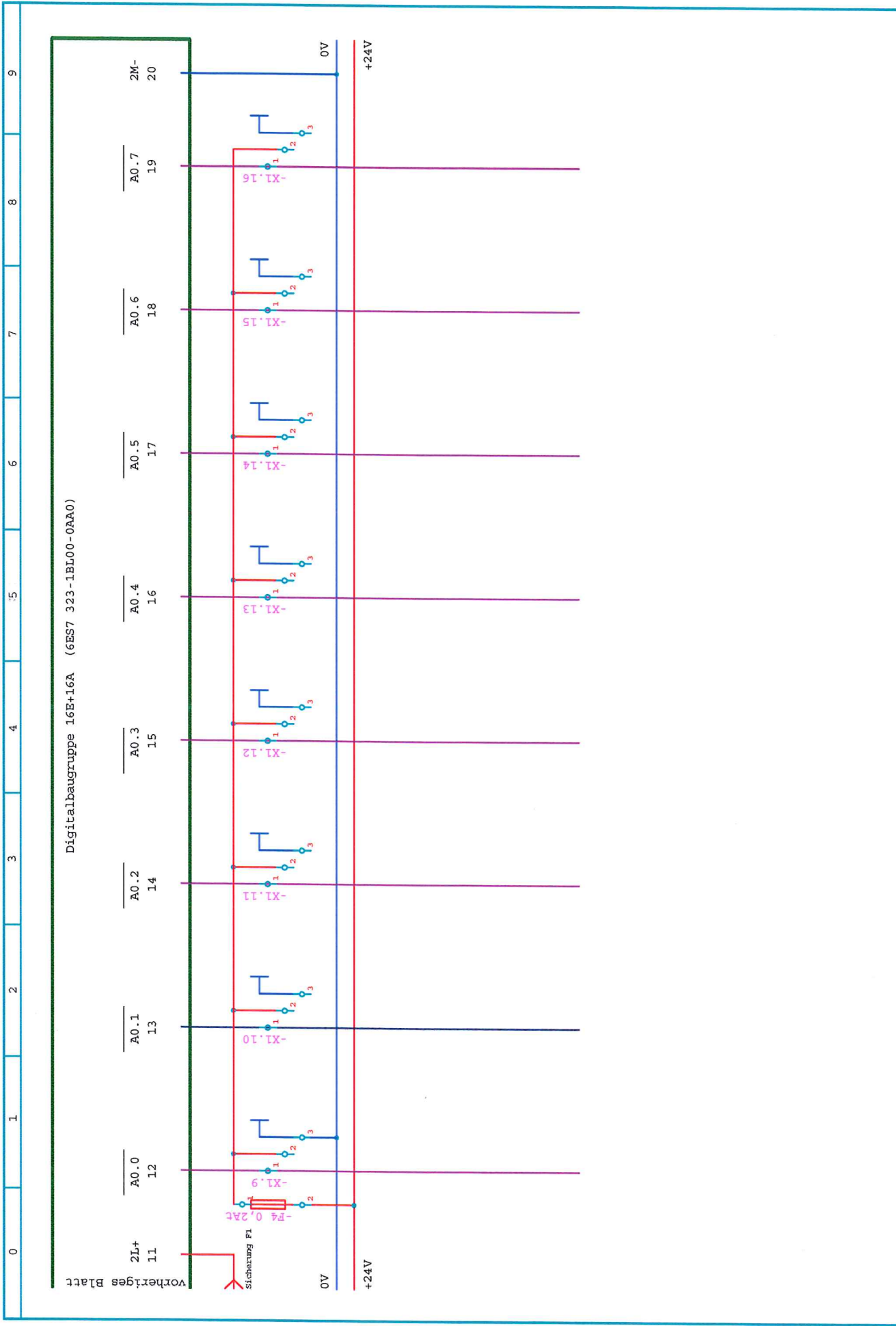


Digitalbaugruppe 16E+16A (6ES7 323-1BL00-0AA0)

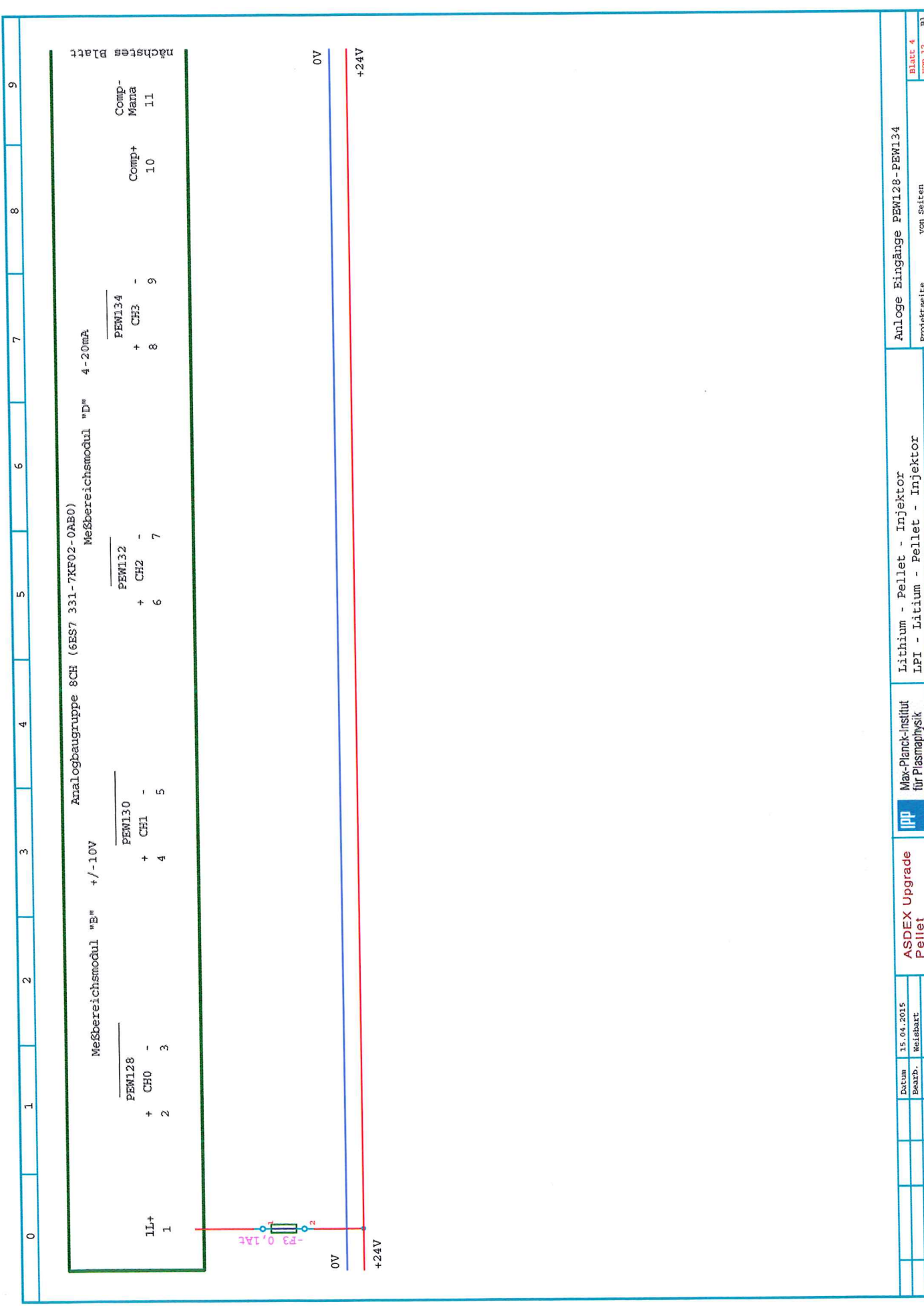


nächstes Blatt

AUG-Interlock		AUG-Pulsstop		TIMER TS01		TIMER TS06		Digitale Engänge		EBO	
15.04.2015		15.04.2015		Max-Planck-Institut für Plasmaphysik		Lithium - Pellet - Injektor		Projektseite		von Seiten	
Weißbart		Weißbart		ASDEX Upgrade Pellet		Lithium - Pellet - Injektor		Blatt 2		von 12 Bl.	
Gepr.		Gepr.		C:\WSCAD55\PROJEKTE\Lithium-Injektor\LIP		LPI - Lithium - Pellet - Injektor					
Änderung		Änderung		Datum		Name					
Datum		Name									



Zust.		Änderung		Datum		Name		Gepr.		Beisbart		15.04.2015		ASDEX Upgrade Pellet		IPP Max-Planck-Institut für Plasmaphysik		Lithium - Pellet - Injektor LPI - Lithium - Pellet - Injektor		Digitale Ausgänge ABO		Blatt 3 von 12 Bl.	
														C:\WScAD55\PROJEKTE\Lithium-Injektor\LIP				Projektseite von Seiten					



nächsteres Blatt

Comp- Mana 11

Comp+ 10

PEWI34

+ CH3 - 9

+ CH2 - 7

+ CH1 - 5

+ CH0 - 3

PEWI32

+ CH3 - 9

+ CH2 - 7

+ CH1 - 5

+ CH0 - 3

PEWI30

+ CH3 - 9

+ CH2 - 7

+ CH1 - 5

+ CH0 - 3

PEWI28 +/- 10V

+ CH3 - 9

+ CH2 - 7

+ CH1 - 5

+ CH0 - 3

PEWI34

+ CH3 - 9

+ CH2 - 7

+ CH1 - 5

+ CH0 - 3

PEWI32

+ CH3 - 9

+ CH2 - 7

+ CH1 - 5

+ CH0 - 3

PEWI30

+ CH3 - 9

+ CH2 - 7

+ CH1 - 5

+ CH0 - 3

PEWI28 +/- 10V

+ CH3 - 9

+ CH2 - 7

+ CH1 - 5

+ CH0 - 3

PEWI34

+ CH3 - 9

+ CH2 - 7

+ CH1 - 5

+ CH0 - 3

PEWI32

+ CH3 - 9

+ CH2 - 7

+ CH1 - 5

+ CH0 - 3

PEWI30

+ CH3 - 9

+ CH2 - 7

+ CH1 - 5

+ CH0 - 3

PEWI28 +/- 10V

+ CH3 - 9

+ CH2 - 7

+ CH1 - 5

+ CH0 - 3

PEWI34

+ CH3 - 9

+ CH2 - 7

+ CH1 - 5

+ CH0 - 3

PEWI32

+ CH3 - 9

+ CH2 - 7

+ CH1 - 5

+ CH0 - 3

PEWI30

+ CH3 - 9

+ CH2 - 7

+ CH1 - 5

+ CH0 - 3

PEWI28 +/- 10V

+ CH3 - 9

+ CH2 - 7

+ CH1 - 5

+ CH0 - 3

PEWI34

+ CH3 - 9

+ CH2 - 7

+ CH1 - 5

+ CH0 - 3

PEWI32

+ CH3 - 9

+ CH2 - 7

+ CH1 - 5

+ CH0 - 3

PEWI30

+ CH3 - 9

+ CH2 - 7

+ CH1 - 5

+ CH0 - 3

PEWI28 +/- 10V

+ CH3 - 9

+ CH2 - 7

+ CH1 - 5

+ CH0 - 3

PEWI34

+ CH3 - 9

+ CH2 - 7

+ CH1 - 5

+ CH0 - 3

PEWI32

+ CH3 - 9

+ CH2 - 7

+ CH1 - 5

+ CH0 - 3

PEWI30

+ CH3 - 9

+ CH2 - 7

+ CH1 - 5

+ CH0 - 3

PEWI28 +/- 10V

+ CH3 - 9

+ CH2 - 7

+ CH1 - 5

+ CH0 - 3

PEWI34

+ CH3 - 9

+ CH2 - 7

+ CH1 - 5

+ CH0 - 3

PEWI32

+ CH3 - 9

+ CH2 - 7

+ CH1 - 5

+ CH0 - 3

PEWI30

+ CH3 - 9

+ CH2 - 7

+ CH1 - 5

+ CH0 - 3

PEWI28 +/- 10V

+ CH3 - 9

+ CH2 - 7

+ CH1 - 5

+ CH0 - 3

PEWI34

+ CH3 - 9

+ CH2 - 7

+ CH1 - 5

+ CH0 - 3

PEWI32

+ CH3 - 9

+ CH2 - 7

+ CH1 - 5

+ CH0 - 3

PEWI30

+ CH3 - 9

+ CH2 - 7

+ CH1 - 5

+ CH0 - 3

PEWI28 +/- 10V

+ CH3 - 9

+ CH2 - 7

+ CH1 - 5

+ CH0 - 3

PEWI34

+ CH3 - 9

+ CH2 - 7

+ CH1 - 5

+ CH0 - 3

PEWI32

+ CH3 - 9

+ CH2 - 7

+ CH1 - 5

+ CH0 - 3

PEWI30

+ CH3 - 9

+ CH2 - 7

+ CH1 - 5

+ CH0 - 3

PEWI28 +/- 10V

+ CH3 - 9

+ CH2 - 7

+ CH1 - 5

+ CH0 - 3

PEWI34

+ CH3 - 9

+ CH2 - 7

+ CH1 - 5

+ CH0 - 3

PEWI32

+ CH3 - 9

+ CH2 - 7

+ CH1 - 5

+ CH0 - 3

PEWI30

+ CH3 - 9

+ CH2 - 7

+ CH1 - 5

+ CH0 - 3

PEWI28 +/- 10V

+ CH3 - 9

+ CH2 - 7

+ CH1 - 5

+ CH0 - 3

PEWI34

+ CH3 - 9

+ CH2 - 7

+ CH1 - 5

+ CH0 - 3

PEWI32

+ CH3 - 9

+ CH2 - 7

+ CH1 - 5

+ CH0 - 3

PEWI30

+ CH3 - 9

+ CH2 - 7

+ CH1 - 5

+ CH0 - 3

PEWI28 +/- 10V

+ CH3 - 9

+ CH2 - 7

+ CH1 - 5

+ CH0 - 3

PEWI34

+ CH3 - 9

+ CH2 - 7

+ CH1 - 5

+ CH0 - 3

PEWI32

+ CH3 - 9

+ CH2 - 7

+ CH1 - 5

+ CH0 - 3

PEWI30

+ CH3 - 9

+ CH2 - 7

+ CH1 - 5

+ CH0 - 3

PEWI28 +/- 10V

+ CH3 - 9

+ CH2 - 7

+ CH1 - 5

+ CH0 - 3

PEWI34

+ CH3 - 9

+ CH2 - 7

+ CH1 - 5

+ CH0 - 3

PEWI32

+ CH3 - 9

+ CH2 - 7

+ CH1 - 5

+ CH0 - 3

PEWI30

+ CH3 - 9

+ CH2 - 7

+ CH1 - 5

+ CH0 - 3

PEWI28 +/- 10V

+ CH3 - 9

+ CH2 - 7

+ CH1 - 5

+ CH0 - 3

PEWI34

+ CH3 - 9

+ CH2 - 7

+ CH1 - 5

+ CH0 - 3

PEWI32

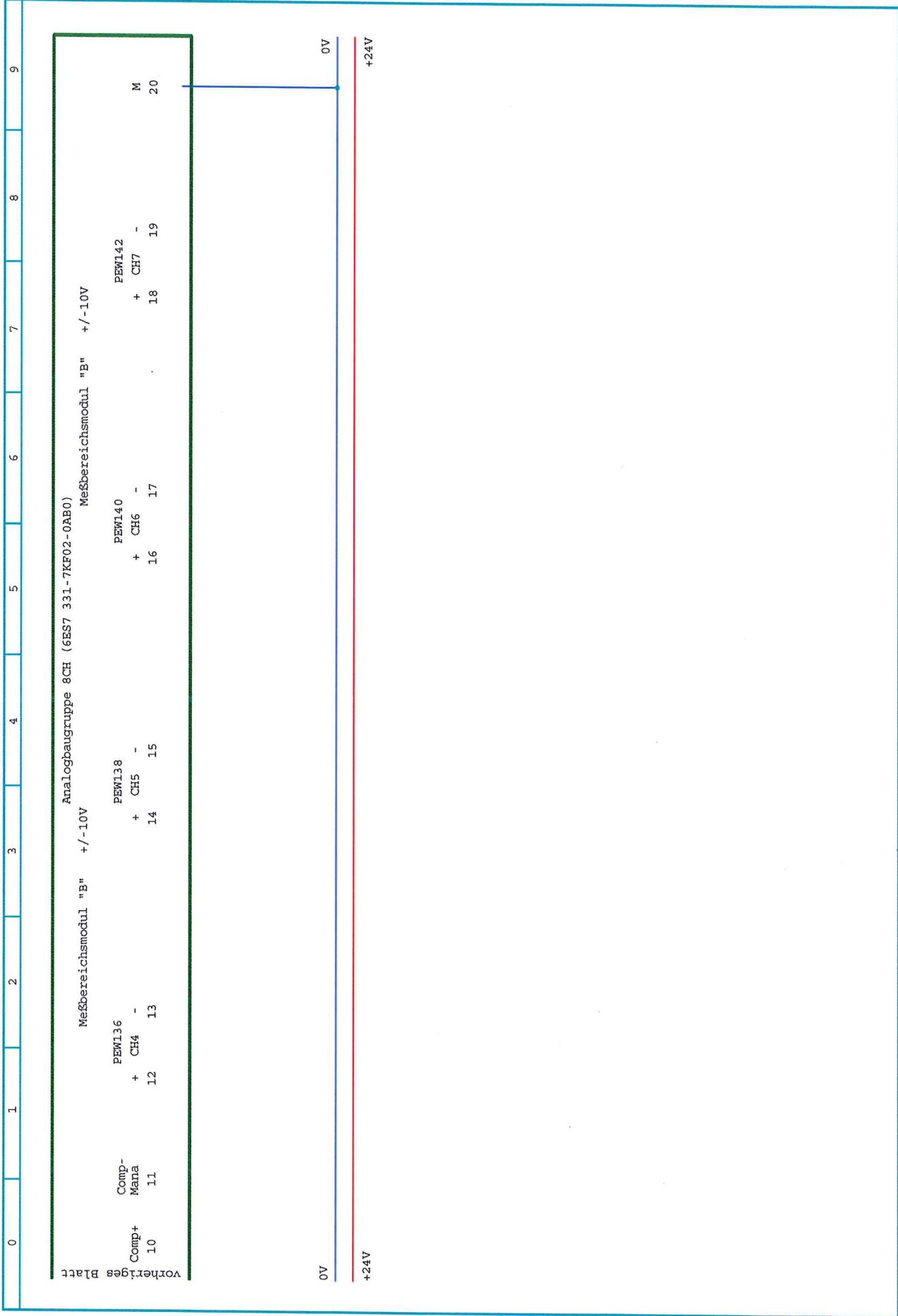
+ CH3 - 9

+ CH2 - 7

+ CH1 - 5

+ CH0 - 3

PEWI30



vorheriges Blatt

Comp+ 10

Comp- Mana 11

PEW136

+ CH4 12

+ CH5 14

+ CH6 16

PEW140

+ CH7 18

+ CH8 19

M 20

0V

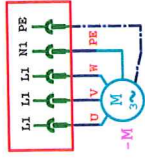
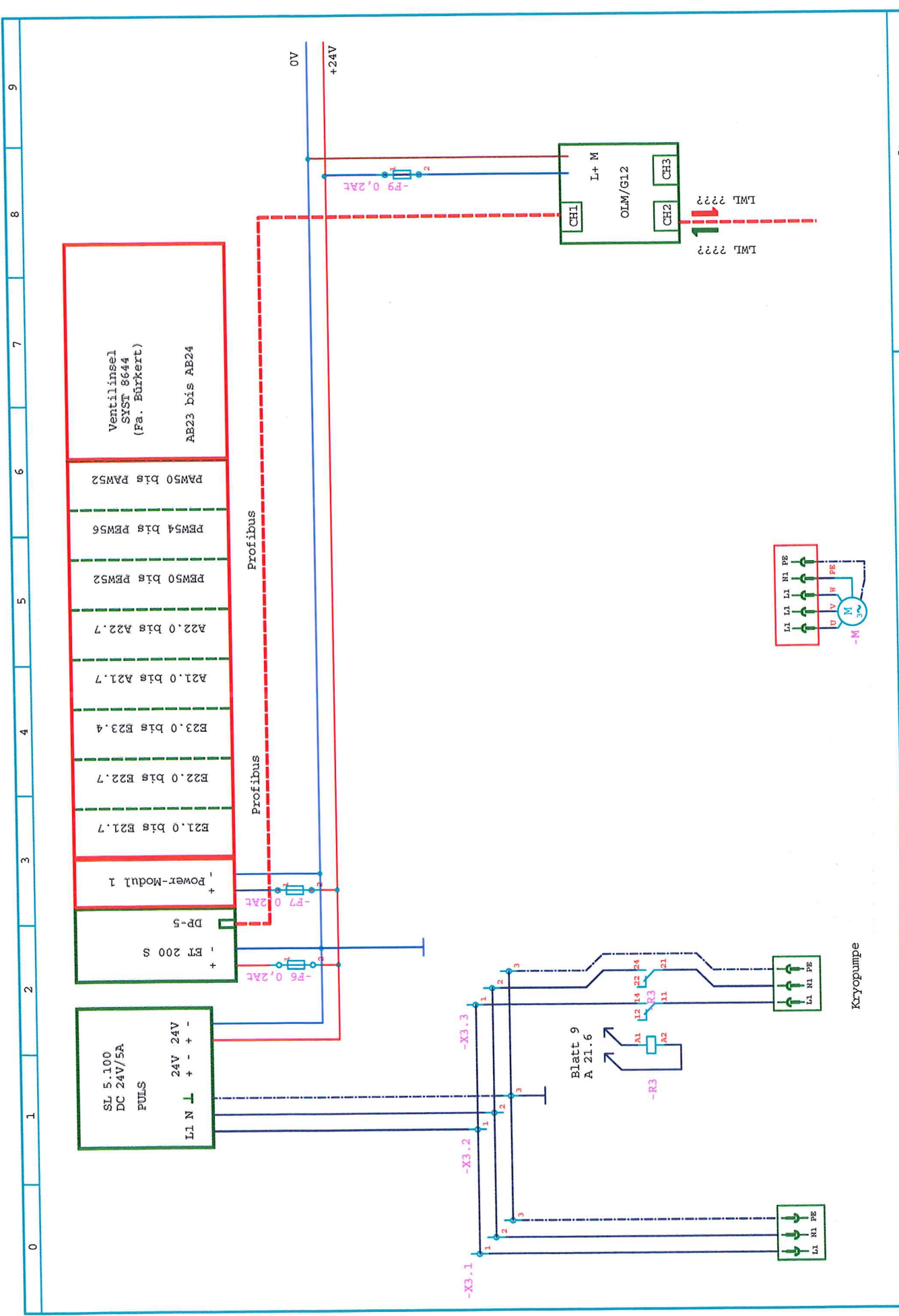
+24V

Analogbaugruppe 8CH (SES7 331-7KF02-0AB0)

Messbereichsmodul "B" +/-10V

Messbereichsmodul "B" +/-10V

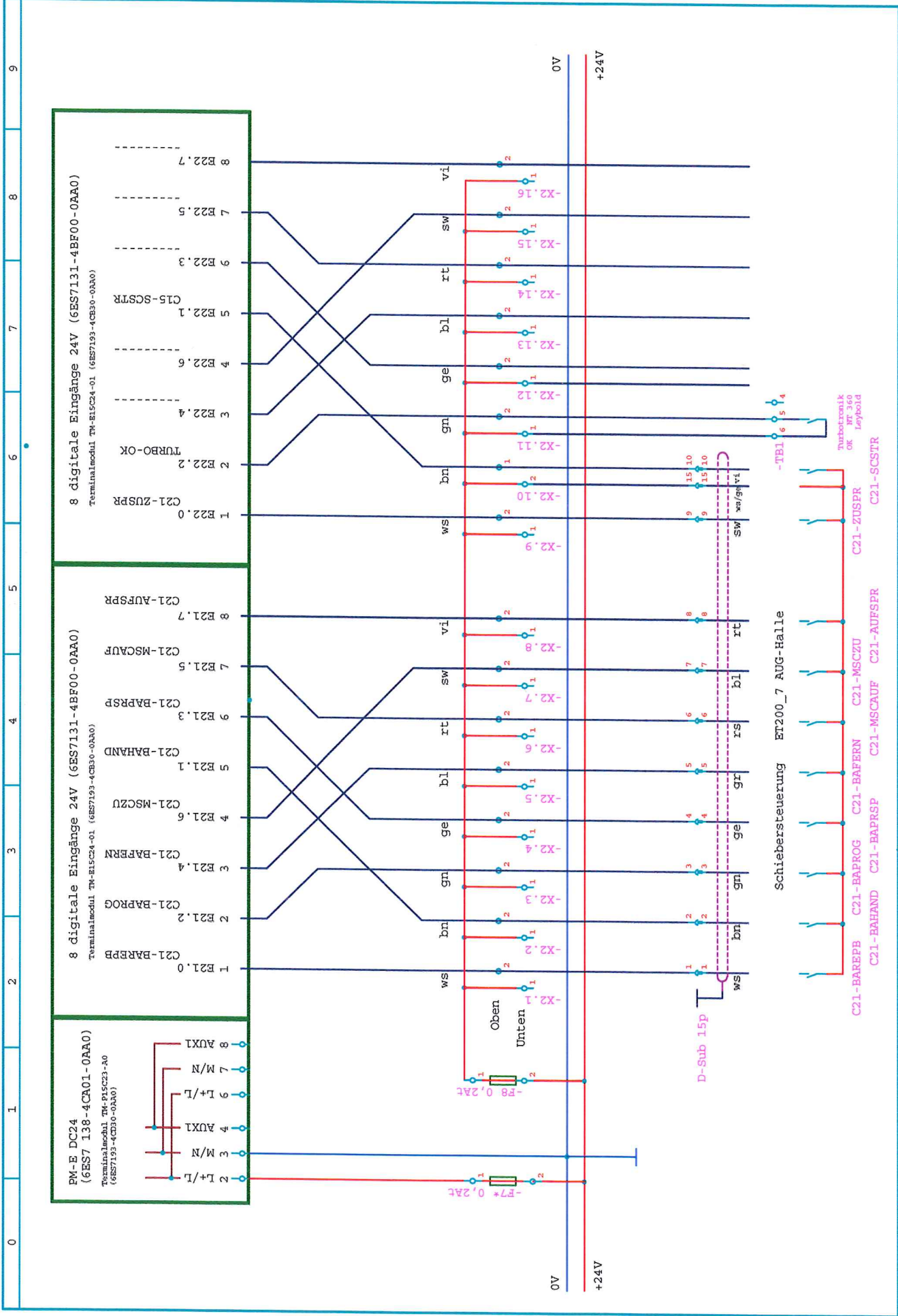
Zust.	Änderung	Datum	Name	Datum	15.04.2015	Reisbart	ASDEX Upgrade Pellet	IPP Max-Planck-Institut für Plasmaphysik	Lithium - Pellet - Injektor LPI - Lithium - Pellet - Injektor	Anlage Eingänge PEW136-PEW142	Blatt 5 von 12
							C:\WSCAD55\PROJEKTE\Lithium-Injektor\IIP			Projektseite von Seiten	Bl.



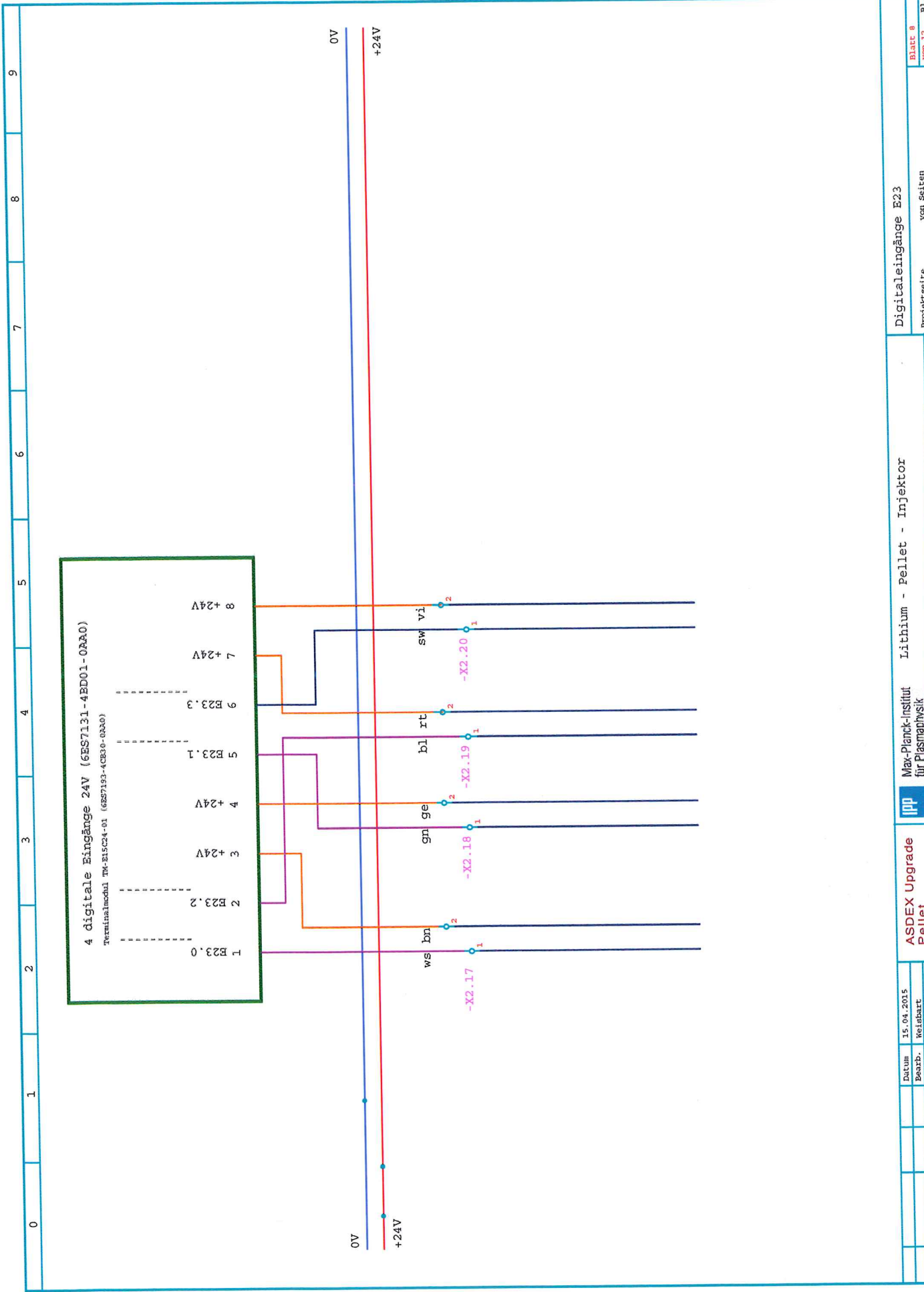
Kryopumpe

Zust.	Änderung	Datum	Name	Norm	Gepf.	Datum	15.04.2015	ASDEX Upgrade Pellet	Max-Planck-Institut für Plasmaphysik	Lithium - Pellet - Injektor	Übersicht Erweiterungsgerät	Blatt 6
								Pellet	LPI - Lithium - Pellet - Injektor	Lithium - Pellet - Injektor	Projektseite	Von 12
									C:\WSCAD55\PROJEKT\Lithium-Injektor\LIP		von Seiten	Bl.

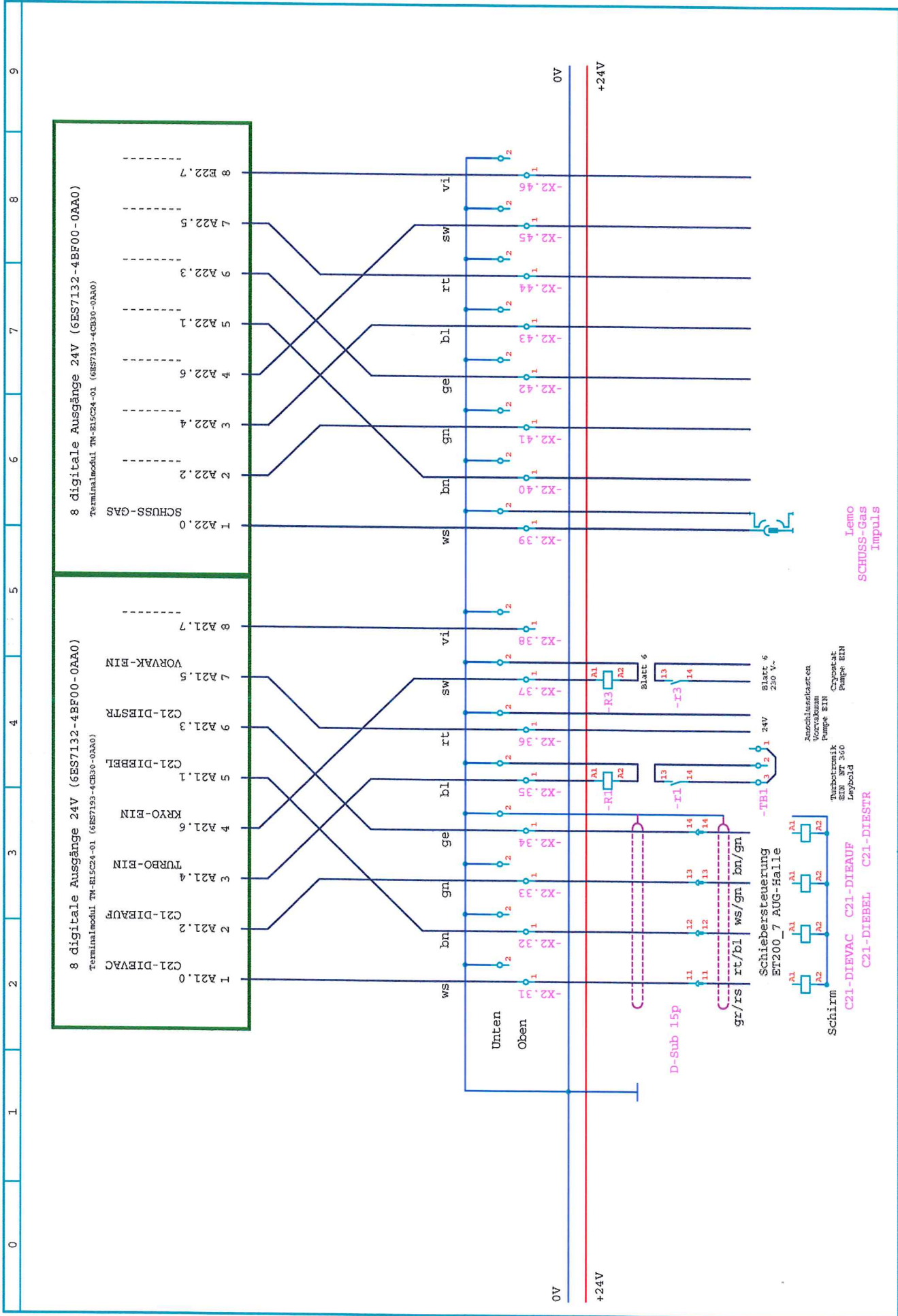




Zust.	Änderung	Datum	Name	Datum	Gepr.	Beisbart	15.04.2015
<b>ASDEX Upgrade</b> Pellet Max-Planck-Institut für Plasmaphysik C:\MSCAD55\PROJEKTE\Lithium-Injektor\LIP							
<b>IPP</b> Lithium - pellet - Injektor							
Digitaleingänge E21-E22 Projektseite von Seiten							
Blatt 7 von 12 Bl.							

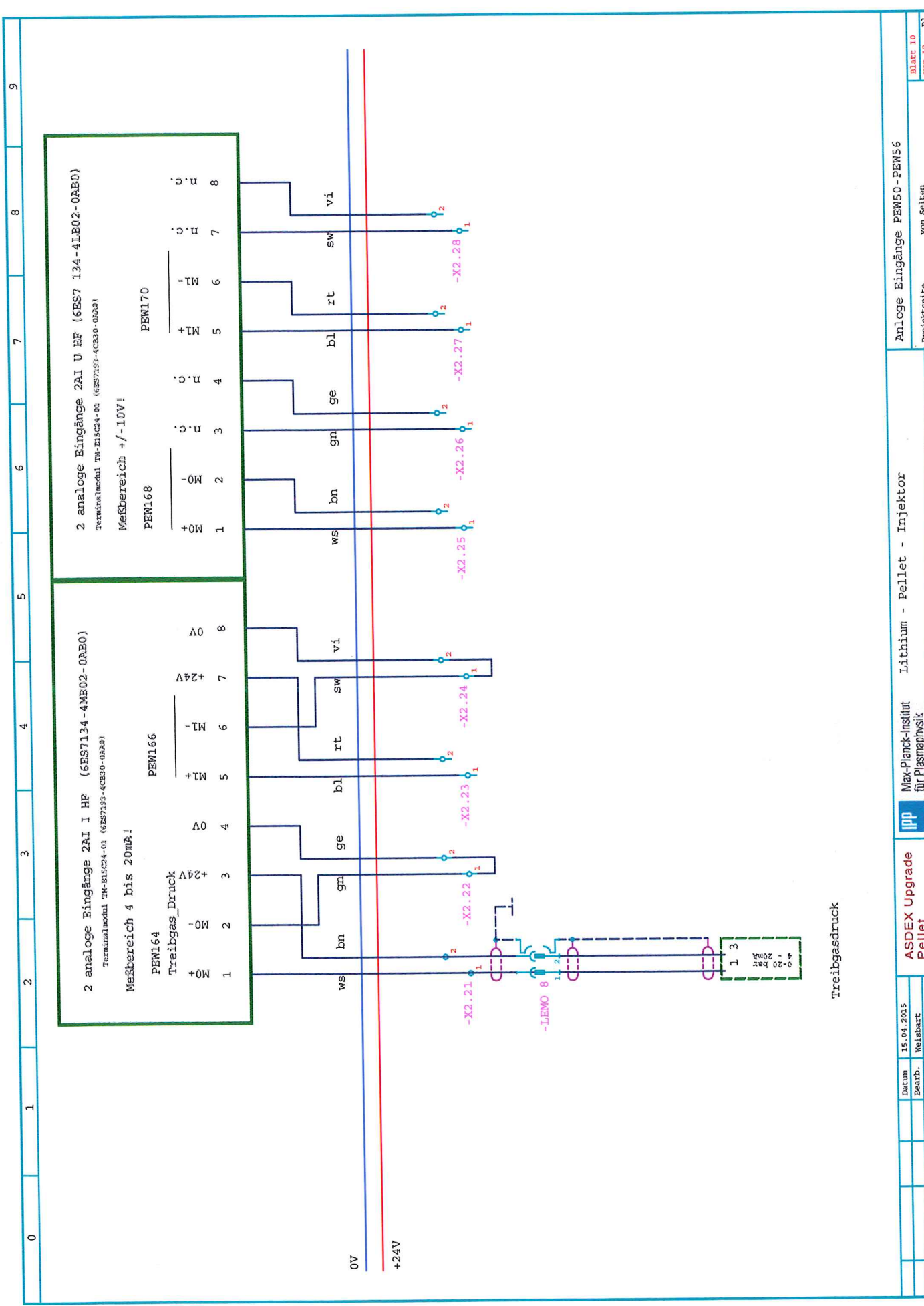


Zust.	Änderung	Datum	Name	Datum	Bearb.	Gepr.	Norm	ASDEX Upgrade Pellet		Max-Planck-Institut für Plasmaphysik		Lithium - Pellet - Injektor		Digitaleingänge E23		Blatt: 8
		15.04.2015	Weisbart					ASDEX Upgrade Pellet		Max-Planck-Institut für Plasmaphysik		Lithium - Pellet - Injektor		Digitaleingänge E23		Von 12
								C:\WSCAD55\PROJEKTE\Lithium-Injektor\LIP		ipp		Lithium - Pellet - Injektor		Projektseite		Bl.
														von 12		



Zust.	Änderung	Datum	Name	Gepr.	Hocm	Datum	15.04.2015	Reisbart
<p>ASDEX Upgrade Pellet</p> <p>Max-Planck-Institut für Plasmaphysik</p> <p>Lithium - Pellet - Injektor</p> <p>Digitalausgänge A21-A22</p>								
<p>C:\MSCAD55\PROJEKTE\Lithium-Injektor\IIP</p>								
<p>Schirm</p> <p>C21-DIEVAC C21-DIEAUF C21-DIEBEL C21-DIESTR</p> <p>Turbotronik EBN NT 360 Layboard</p> <p>Anschlussetreten</p> <p>Pumpe EBN</p> <p>Cryostat</p> <p>Pumpe EBN</p> <p>Blatt 6</p> <p>250 V</p> <p>-TB1</p> <p>Blatt 6</p> <p>-R3</p> <p>-R1</p> <p>-I3</p> <p>D-Sub 15p</p> <p>gr/rs rt/bl ws/gn bn/gn ge bl rt sw vi</p> <p>-X2.31 -X2.32 -X2.33 -X2.34 -X2.35 -X2.36 -X2.37 -X2.38</p> <p>-X2.39 -X2.40 -X2.41 -X2.42 -X2.43 -X2.44 -X2.45 -X2.46</p> <p>0V +24V</p> <p>0V +24V</p>								
<p>Projektseite von Seiten</p>								
<p>Blatt 9 von 12 Bl.</p>								



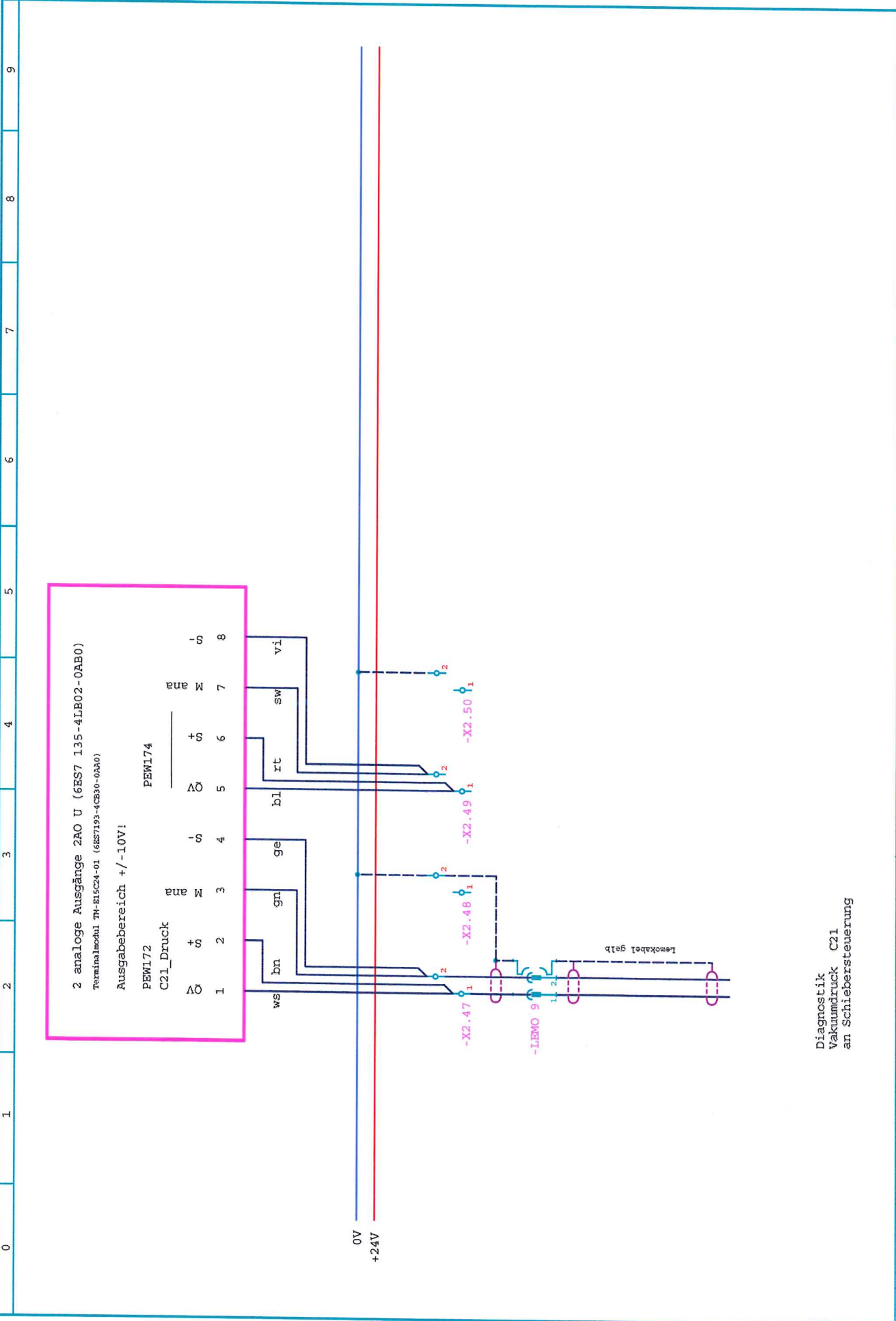


Treibgasdruck

2 analoge Eingänge 2AI I HF (6ES7134-4MB02-0AB0)  
 Terminalmodul TM-215CA4-01 (6ES7193-4CB30-0AA0)  
 Meßbereich 4 bis 20mPa!  
 PEW164  
 Treibgas\_Druck

2 analoge Eingänge 2AI I HF (6ES7134-4MB02-0AB0)  
 Terminalmodul TM-215CA4-01 (6ES7193-4CB30-0AA0)  
 Meßbereich +/- 10V!  
 PEW168

2 analoge Eingänge 2AI U HF (6ES7 134-4LS02-0AB0)  
 Terminalmodul TM-215CA4-03 (6ES7193-4CB30-0AA0)  
 Meßbereich +/- 10V!  
 PEW170

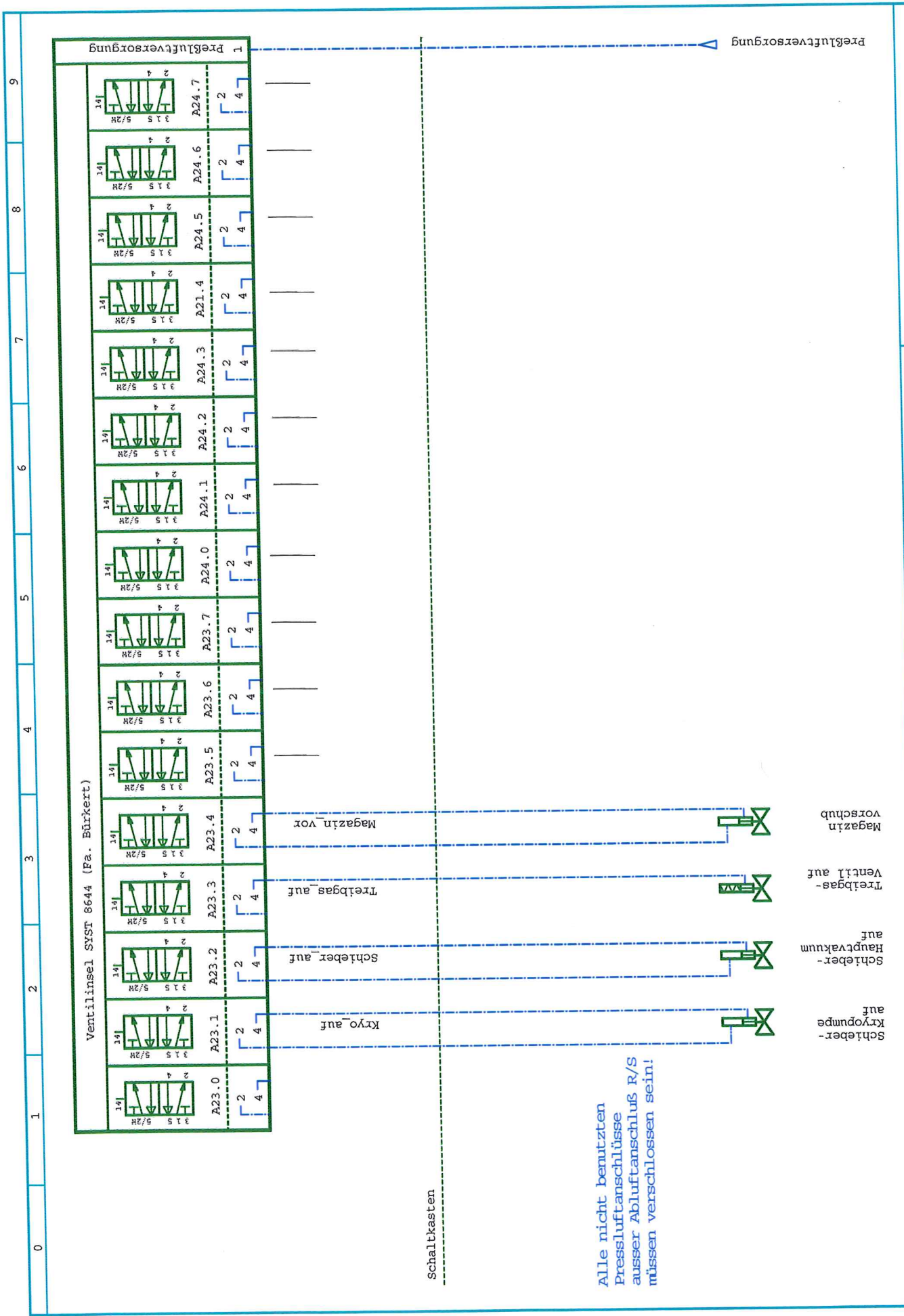


2 analoge Ausgänge 2AO U (6ES7 135-4IB02-0AB0)  
 Terminalmodul TM-815C24-01 (6ES7133-4CB30-0AA0)  
 Ausgabebereich +/-10V!

PEWL174  
 C21\_Druck

0V	1	2	3	4	5	6	7	8
	ws	bn	gn	ge	bl	rt	sw	vi
		ana	ana					

Diagnostik  
 Vakuumdruck C21  
 an Schiebersteuerung

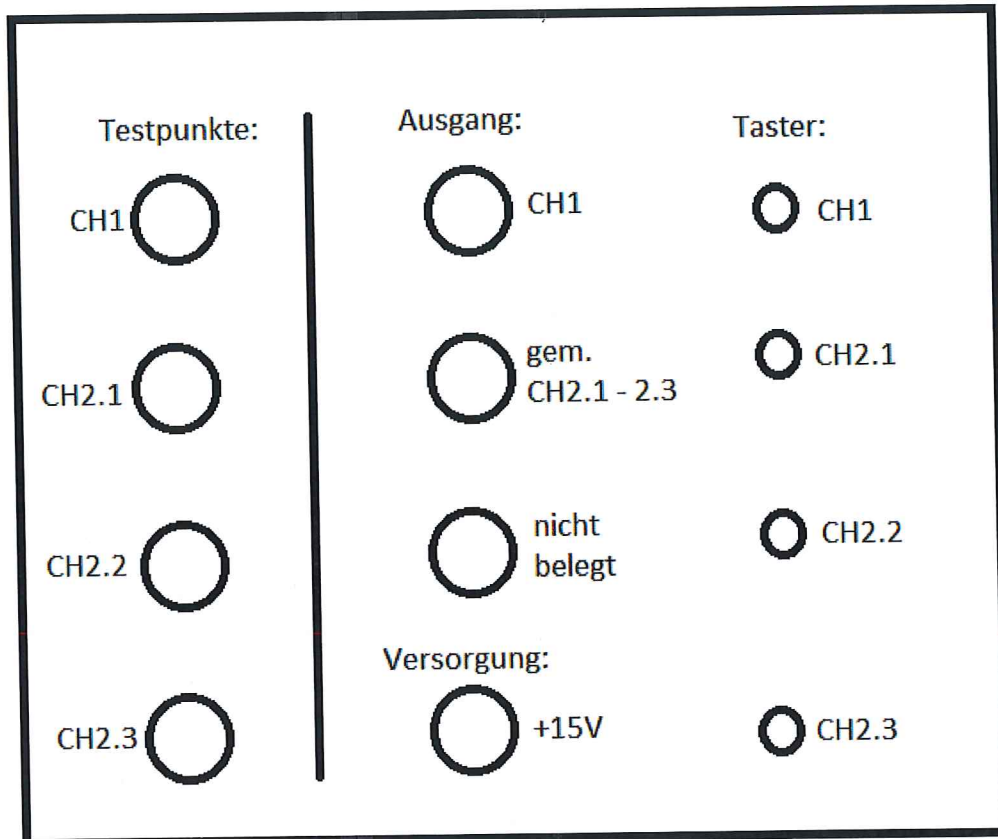


## **F.3 Light barrier electronics**





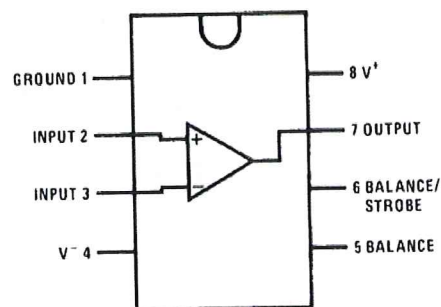
## Frontplatte



gemeinsamer Ausgang: Channel 2.1 bis Channel 2.3 sind miteinander verodert

### Achtung bei LM311:

#### Dual-In-Line Package



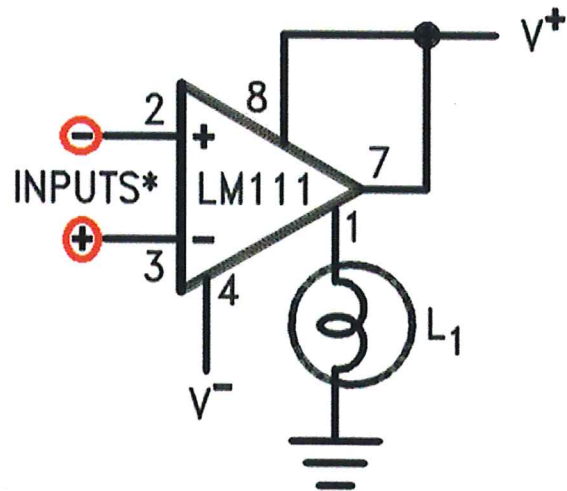
00570434

#### Top View

Order Number LM111J-8, LM111J-8/883(Note 21),  
LM311M, LM311MX or LM311N  
See NS Package Number J08A, M08A or N08E



# Driving Ground-Referred Load



00570416

\*Input polarity is reversed when using pin 1 as output.

Voltage comparator

LM111/211/311/311B

## EQUIVALENT SCHEMATIC

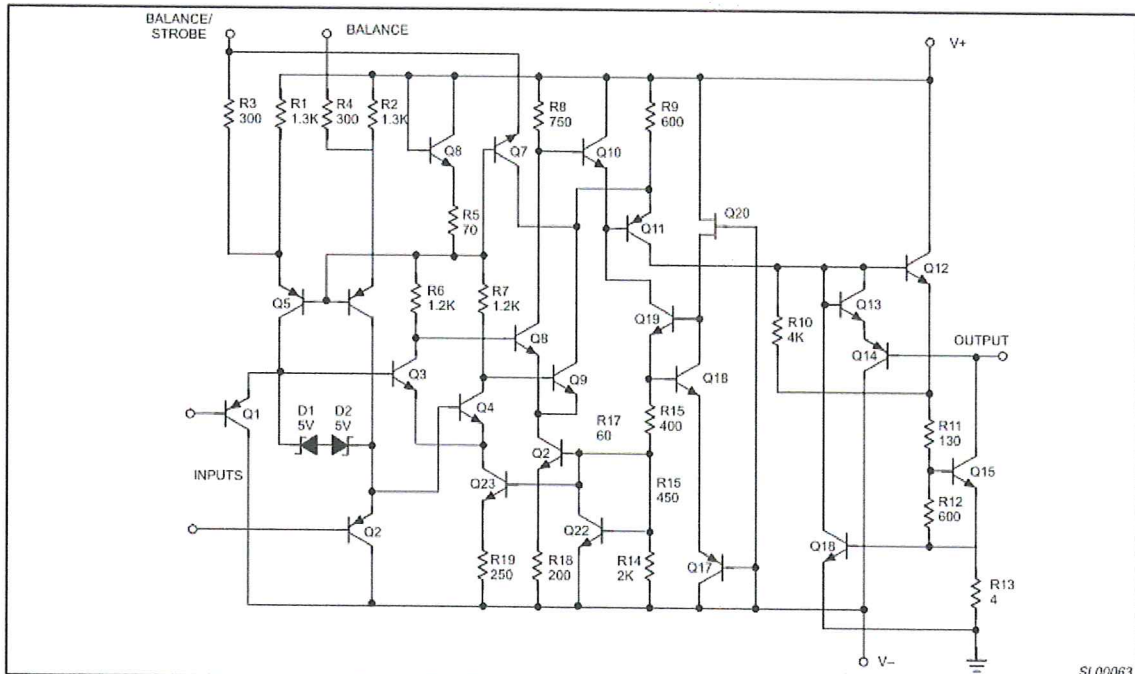
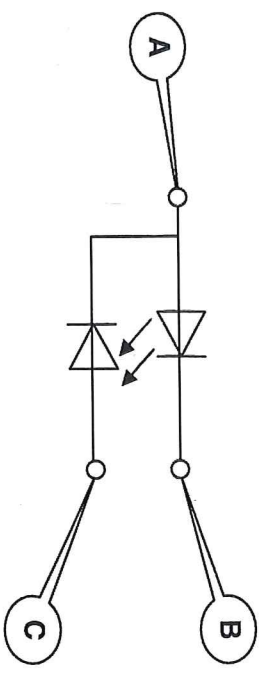
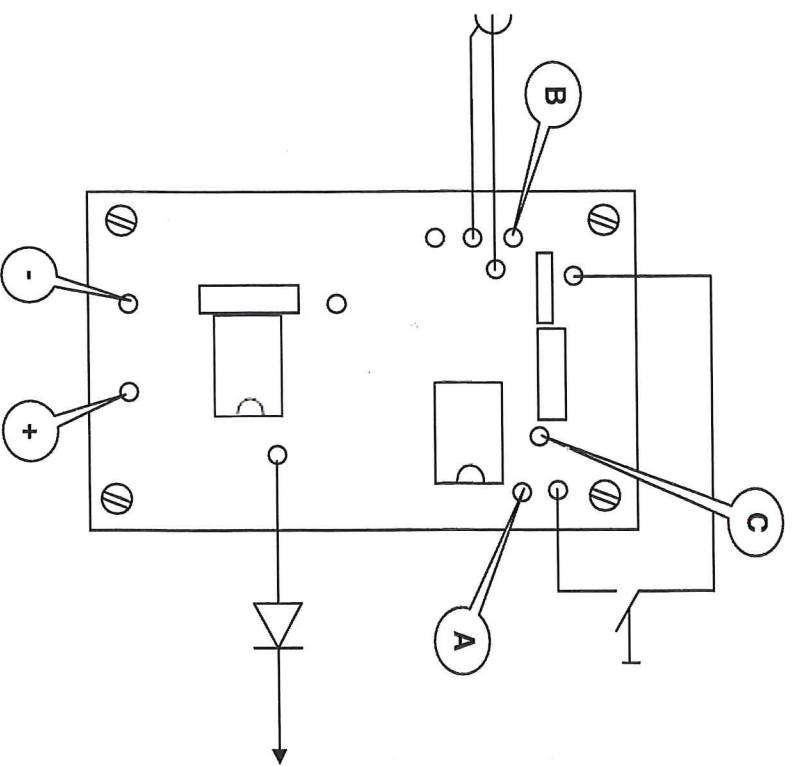


Figure 2. Equivalent Schematic

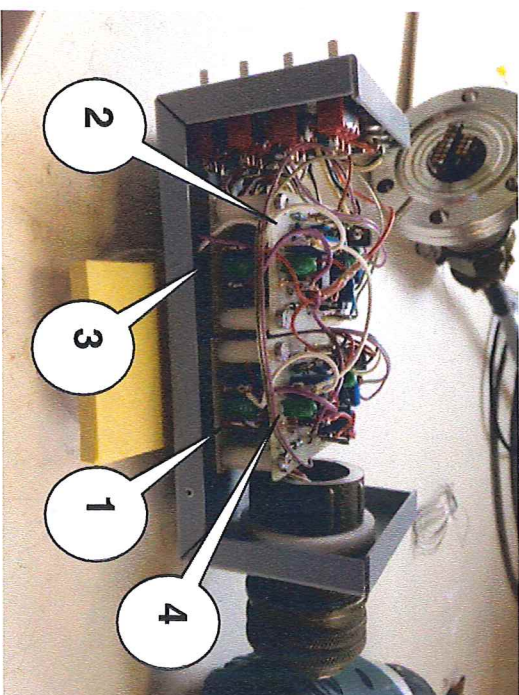
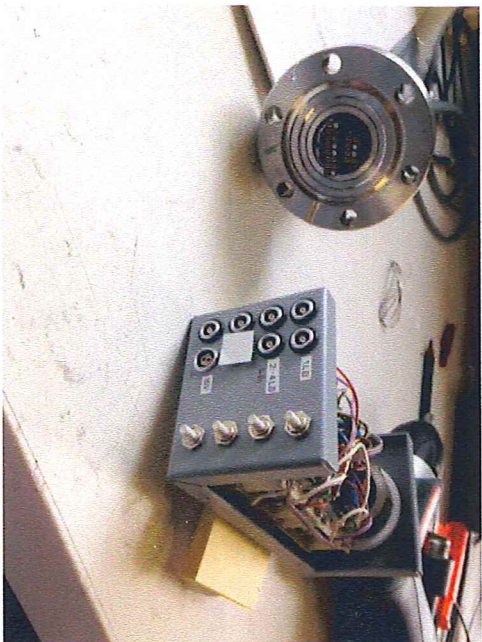
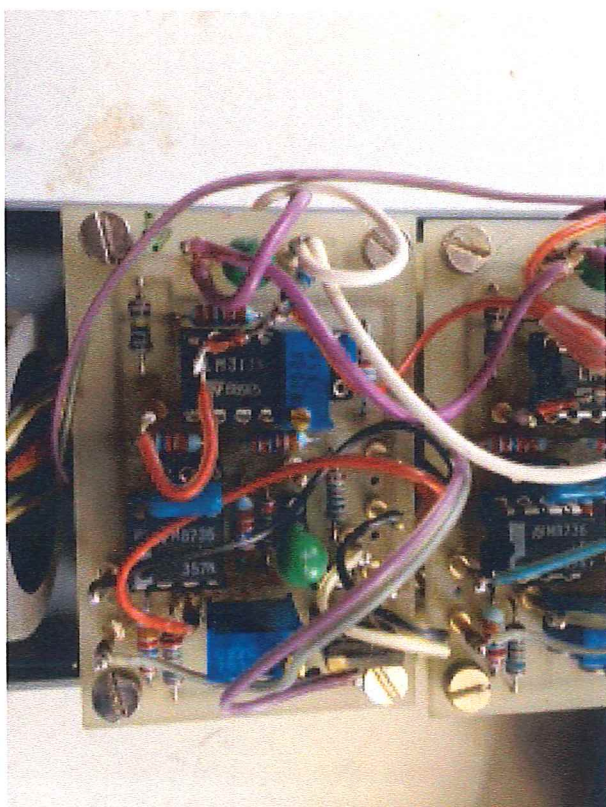
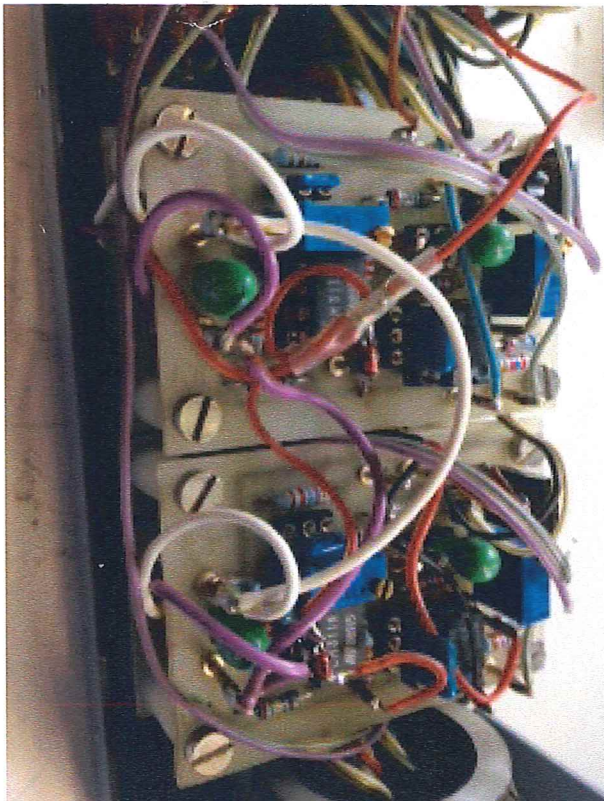
SI.00063





# RTSP — Pelletgruppe

Lichtschränke



# Bibliography

- [AA12] OECD Nuclear Energy Agency and International Atomic Energy Agency. *Uranium 2011: Resources, Production and Demand*. OECD, 2012.
- [Age07] International Energy Agency. Contribution of renewables to energy security. *IEA Information Paper*, page 5, 2007.
- [Age12] International Energy Agency. *Key World Energy Statistics 2012*. 2012.
- [Age15] International Energy Agency. Plasma wall interaction - keeping cool under the blanket. <http://www.iea.org/techinitiatives/fusionpower/plasmawallinteraction/>, January 2015.
- [Ale11] A. Alexiou. Konditionierung und charakterisierung eines modifizierten raumtemperatur - festkörper pellet injektors. Master's thesis, Munich University of Applied Sciences, 2011.
- [AMBF10] T. Hamacher A. M. Bradshaw and U. Fischer. Is nuclear fusion a sustainable energy form? *Fusion Engineering and Design*, 86(2770), 2010.
- [Bod06] David Bodansky. The status of nuclear waste disposal. *American Physical Society*, 35(1), January 2006.

- [CC] Helix Technology Corporation CTI-Cryogenics. *Cryo-Torr High Vacuum Pump System. Installation, Operation and Servicing Instructions*.
- [CIE15] CIEMAT. Sketch of h-mode profile and pedestal. <http://fusionwiki.ciemat.es/wiki/File:H-mode.png>, January 2015.
- [Dem12] C. Demirtas. Modifikation des rtsp-injektors zur abschwächung potentiell elm-triggernder gasflüsse in tokamak h-mode plasmen. Master's thesis, Fachhochschule München, 2012.
- [Dul09] Krista Dulon. Who is afraid of iter? <http://www.iter.org/newsline/107/1489>, November 2009.
- [Ein05] A. Einstein. Ist die Trägheit eines Körpers von seinem Energieinhalt abhängig? *Annalen der Physik*, 323:639–641, 1905.
- [fP14] Max Planck Institut für Plasmaphysik. Ignition conditions. <https://www.ipp.mpg.de/15144/zuendbedingungen>, December 2014. Copyright of IPP.
- [G<sup>+</sup>06] J. Gale et al. *IPCC Special Report on Carbon dioxide Capture and Storage*. IPCC, 2006.
- [Gar14] B. Garland. Binding energy. [http://www.nuceng.ca/igna/binding\\_energy.htm](http://www.nuceng.ca/igna/binding_energy.htm), December 2014.
- [GGR13] R. J. Goldston, A. Glaser, and A. F. Ross. Proliferation risks of fusion energy: Clandestine production, covert production, and breakout. *9th IAEA Technical Meeting on Fusion Power Plant Safety*, 2013.

- [GSUA14] Department of Physics Georgia State University and Astronomy. Coulomb barrier for fusion. <http://hyperphysics.phy-astr.gsu.edu/hbase/nucene/coubar.html>, December 2014.
- [H<sup>+</sup>00] A. A. Harms et al. *Principles of Fusion Energy*. Allied Publishers, 2000.
- [IPP14] IPP. Does fusion involve radioactive waste? <https://www.ipp.mpg.de/2769068/faq9>, December 2014.
- [ITE14a] ITER. Facts and figures. <http://www.iter.org/factsfigures>, December 2014.
- [ITE14b] ITER. How fritz wagner "discovered" the h-mode. <http://www.iter.org/newsline/86/659>, December 2014.
- [ITE14c] ITER. Iter and beyond. <http://www.iter.org/proj/iterandbeyond>, December 2014.
- [ITE14d] ITER. The iter tokamak. [https://www.iter.org/doc/all/content/com/gallery/Media/7%20-%20Technical/2009\\_04\\_29%20MACHINE.jpg](https://www.iter.org/doc/all/content/com/gallery/Media/7%20-%20Technical/2009_04_29%20MACHINE.jpg), December 2014.
- [ITE14e] ITER. Kstar announces successful elm suppression. <http://www.iter.org/newsline/198/950>, December 2014.
- [J<sup>+</sup>14] Maingi R. Jackson, G.L. et al. Calming the plasma edge: The tail that wags the dog lithium injections show promise for optimizing the performance of fusion plasmas. *American Physical Society*, 56, October 2014.
- [Kei87] M. Keilhacker. H-mode confinement in tokamaks. *Plasma Physics and Controlled Fusion*, 29(10A), 1987.

- [Lab14] Laurence Livermore National Laboratory. About nif & photon science. <https://lasers.llnl.gov/about/>, December 2014.
- [lis14] List of fusion experiments, tokamak. [http://en.wikipedia.org/wiki/List\\_of\\_fusion\\_experiments#Tokamak](http://en.wikipedia.org/wiki/List_of_fusion_experiments#Tokamak), December 2014.
- [LS94] Cierpka P. Lang R.S. Egorov S.M. Kuteev B.V. Reznichenko P.V. Lang, P.T. and V. Yu. Sergeev. Compact gas gun injection system for variable sized solid pellets. *Review of Scientific Instruments*, 65(2316), 1994.
- [Mai14] R. Maingi. The effect of lithium on diii-d, nstx, and east. In *AUG Seminar, Garching, Germany*. DIII-D, PPPL, October 2014.
- [Mar15] E. Marmor. Tokamak parameter comparisons. [www.psfc.mit.edu/~marmor/5year\\_2008/06\\_tokamak\\_parameter\\_comparisons.xls](http://www.psfc.mit.edu/~marmor/5year_2008/06_tokamak_parameter_comparisons.xls), January 2015.
- [Mün01] C. Münther. Der repetierende kompaktlithiuminjektor für thermonukleare fusionsreaktoren. Master's thesis, Technische Universität München, 2001.
- [MPIfP] Garching Max Planck Institut für Plasmaphysik.
- [MS12] G. McCracken and P. Stott. Fusion: The energy of the universe. *Academic Press*, pages 198–199, June 2012.
- [oNSWSOP14] University of New South Wales School of Physics.  $E = mc^2$  and binding energies in the nucleus (and in molecules.). [http://newt.phys.unsw.edu.au/einsteinlight/jw/module5\\_binding.htm](http://newt.phys.unsw.edu.au/einsteinlight/jw/module5_binding.htm), December 2014.

- [OVO00] J. Ongena and G. Van Oost. Energy for future centuries. Technical report, Laboratorium voor Plasmafysica - Laboratoire de Physique des Plasmas, 2000.
- [Pen04] R. Penrose. *The Road to Reality: A Complete Guide to the Laws of the Universe*. The Road to Reality: A Complete Guide to the Laws of the Universe, 2004.
- [Pfa06] S. Pfalzner. *An Introduction to Inertial Confinement Fusion*. Taylor & Francis, 2006.
- [S<sup>+</sup>09] S. Shafiee et al. When will fossil fuel reserves be diminished. *Energy policy*, 37(1), 2009.
- [Sci] Fisher Scientific. Material safety data sheet lithium. <http://avogadro.chem.iastate.edu/MSDS/Li.htm>.
- [Stu94] P. A. Sturrock. *Plasma Physics: An Introduction to the Theory of Astrophysical, Geophysical & Laboratory Plasmas*. Number ISBN 978-0-521-44810-9. Cambridge University Press, 1994.
- [TB46] G. P. Thomson and M. Blackman. Improvements in or relating to gas discharge apparatus for producing thermonuclear reactions, 1946.
- [Tea89] ASDEX Team. The h-mode of asdex. *Nuclear Fusion*, 29(11), 1989.
- [UEIA11] EIA U.S. Energy Information Administration. Annual Energy Outlook. <http://www.eia.gov/forecasts/archive/aeo11/>, 2011.
- [Upg14] ASDEX Upgrade. View of the asdex upgrade plasma experiment. [https://www.ipp.mpg.de/87653/standard\\_full.jpg](https://www.ipp.mpg.de/87653/standard_full.jpg), December 2014.

- [Vac] Leybold Vacuum. *Trivac A Dual Stage Rotary Vane Pump Manual*.
- [Vac04] Leybold Vacuum. *Turbovac Operating Instructions*, 2004.
- [Wad09] M.R. Wade. Physics and engineering issues associated with edge localized mode control in {ITER}. *Fusion Engineering and Design*, 84(2-6):178 – 185, 2009. Proceeding of the 25th Symposium on Fusion Technology (SOFT-25).
- [WM87] A. C. Williams and T. W. Moorhead. Double layers in astrophysics. In *NASA Conference Publication 2469*, number NASA CP-2469, 1987.
- [WNN14] WNN World Nuclear News. China plans for nuclear growth. <http://www.world-nuclear-news.org/NP-China-plans-for-nuclear-growth-2011144.html>, November 2014.
- [Zoh96] H. Zohm. Edge localized modes (elms). *Plasma Physics and Controlled Fusion*, 38(2):105, 1996.